Chapter 7

Accelerator and Muon Delivery

In order to achieve a statistical uncertainty of 0.1 ppm, the total $(g-2)$ data set must contain at least 1.8×10^{11} detected positrons with energy greater than 1.8 GeV, and arrival time greater than 30 μs after injection into the storage ring. This is expected to require 4×10^{20} protons on target including commissioning time and systematic studies. For optimal detector performance, the number of protons in a single pulse to the target should be no more than 10^{12} and the number of secondary protons transported into the muon storage ring should be as small as possible. Data acquisition limits the time between pulses to be at least 10 ms. The revolution time of muons around the storage ring is 149 ns, and therefore the experiment requires the bunch length to be no more than ∼100 ns. Systematic effects on muon polarization limit the momentum spread dp/p of the secondary beam. Requirements and general accelerator parameters are given in Table 7.1.

Parameter	Design Value	Requirement	Unit
Total protons on target	2.3×10^{20}/year	4×10^{20}	protons
Interval between beam pulses	10	≥ 10	ms
Max bunch length (full width)	120 (95%)	< 149	ns
Intensity of single pulse on target	10^{12}	10^{12}	protons
Max Pulse to Pulse intensity variation	± 10	± 50	%
$\lvert dp/p \rvert$ of pions accepted in decay line	2-5	2	%
Momentum of muon beam	3.094	3.094	GeV/c
Muons to ring per 10^{12} protons on target	$(0.5 - 1.0) \times 10^5$	≥ 6000 stored	muons

Table 7.1: General beam requirements and design parameters.

7.1 Overall Strategy

The $(g-2)$ experiment at Fermilab is designed to take advantage of the infrastructure of the former Antiproton Source, as well as improvements to the Proton Source and the conversion of the Recycler to a proton-delivery machine. It is also designed to share as much infrastructure as possible with the Mu2e experiment in order to keep overall costs low.

The Antiproton Accumulator will no longer be in use, and many of its components will be reused for the new and redesigned Muon beamlines. Stochastic cooling components and other infrastructure no longer needed in the Debuncher ring will be removed in order to improve the aperture, proton abort functionality will be added, and the ring will be renamed the Delivery Ring (DR). The former AP1, AP2, and AP3 beamlines will be modified and renamed M1, M2, and M3. The DR Accelerator Improvement Project (AIP) will provide upgrades to the Delivery Ring. The Beam Transport AIP will provide aperture improvements to the P1, P2, and M1 lines needed for future muon experiments using 8 GeV protons, including $(g-2)$. The layout of the beamlines is shown in Fig. 7.1.

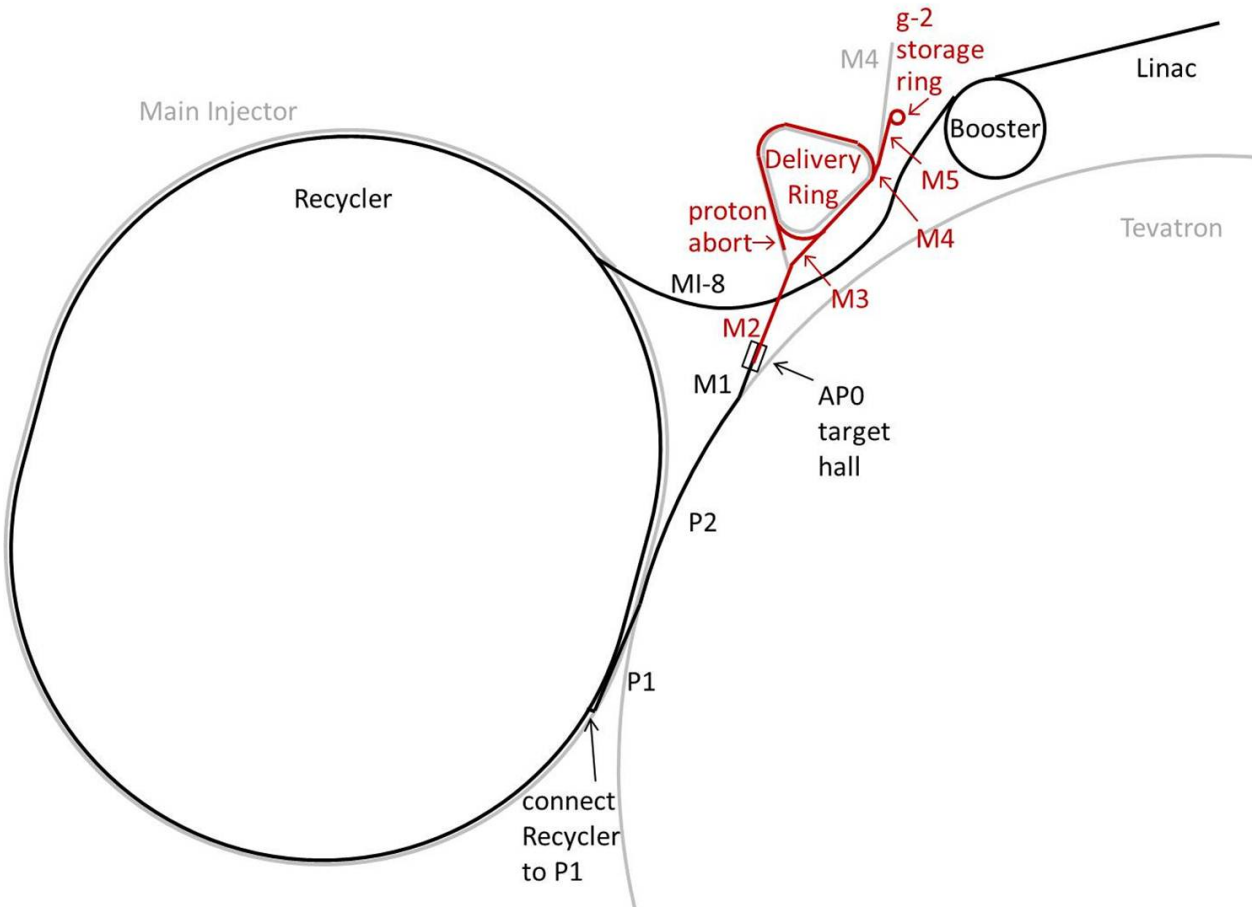

Figure 7.1: Path of the beam to $(g-2)$. Protons (black) are accelerated in the Linac and Booster, are re-bunched in the Recycler, and then travel through the P1, P2, and M1 lines to the AP0 target hall. Secondary beam (red) then travels through the M2 and M3 lines, around the Delivery Ring, and then through the M4 and M5 lines to the muon storage ring.

The Proton Improvement Plan [1], currently underway, will allow the Booster to run at 15 Hz, at intensities of 4×10^{12} protons per Booster batch. The Main Injector (MI) will run with a 1.333 s cycle time for its neutrino program (NOνA), with twelve batches of beam from the Booster being accumulated in the Recycler and single-turn injected into the MI at the beginning of the cycle. While the NOνA beam is being accelerated in the MI, eight Booster

batches will be available for experimental programs such as $(g-2)$ which use 8 GeV protons. Extraction from the Recycler to the P1 beamline, required for $(g-2)$, will be implemented in the Beam Transport AIP.

Protons from the Booster with 8 GeV kinetic energy will be re-bunched into four bunches in the Recycler and transported one at a time through the P1, P2, and M1 beamlines to a target at AP0. Secondary beam from the target will be collected using a lithium lens, and positively-charged particles with a momentum of 3.11 GeV/c ($\pm \sim 10\%$) will be selected using a bending magnet. Secondary beam leaving the Target Station will travel through the M2 and M3 lines which are designed to capture as many muons with momentum 3.094 GeV/c from pion decay as possible. The beam will then be injected into the Delivery Ring. After several revolutions around the DR, essentially all of the pions will have decayed into muons, and the muons will have separated in time from the heavier protons. A kicker will then be used to abort the protons, and the muon beam will be extracted into the new M4 line, and finally into the new M5 beamline which leads to the $(g-2)$ storage ring. Note that the M3 line, Delivery Ring, and M4 line are also designed to be used for 8 GeV proton transport by the Mu2e experiment.

The expected number of muons transported to the storage ring per 10^12 protons on target, based on target-yield simulations using the antiproton-production target and simple acceptance assumptions, is $(0.5-1.0)\times 10^5$. Beam tests were conducted using the existing Antiproton-Source configuration with total charged-particle intensities measured at various points in the beamline leading to the Debuncher, which confirmed the predicted yields to within a factor of two [2]. More details are given in Sec. 7.4.1.

7.2 Protons from Booster

During the period when $(g-2)$ will take data, the Booster is expected to run with present intensities of 4×10^{12} protons per batch, and with a repetition rate of 15 Hz. In a 1.333 s Main-Injector NOνA cycle, twelve Booster batches are slip-stacked in the Recycler and then accelerated in the MI and sent to NOνA. While the Main Injector is ramping, the Recycler is free for a period of seven Booster cycles to send 8 GeV (kinetic energy) protons to $(g-2)$. The RF manipulations of beam for $(g-2)$ in the Recycler (Sec. 7.3.1) allow $(g-2)$ to take three Booster batches in a 1.33 s NOνA cycle, or four in a 1.40 s cycle. Figure 7.2 shows a possible time structure of beam pulses to $(g-2)$.

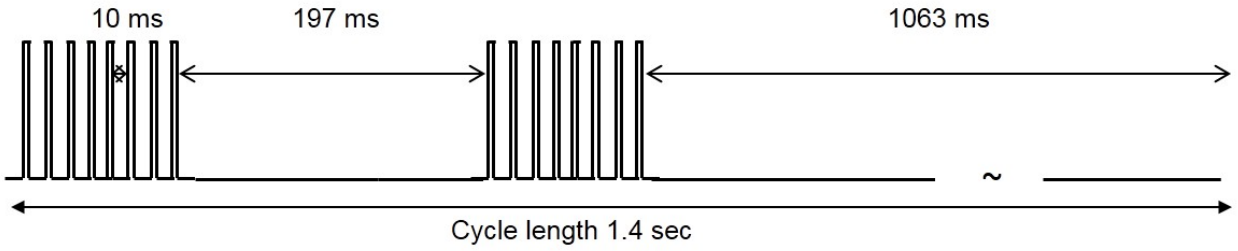

Figure 7.2: Possible time structure of beam pulses to $(g-2)$.

The following section describes improvements needed to run the proton source reliably at 15 Hz.

7.2.1 Proton Improvement Plan

The Fermilab Accelerator Division has undertaken a Proton Improvement Plan (PIP) [1] with the goals of maintaining viable and reliable operation of the Linac and Booster through 2025, increasing the Booster RF pulse repetition rate, and doubling the proton flux without increasing residual activation levels.

The replacement of the Cockroft-Walton pre-accelerator with a radio-frequency quadrupole (RFQ) to increase reliability of the pre-accelerator and to improve beam quality was completed in 2012.

The Booster RF solid-state upgrade necessary for reliable 15 Hz RF operations involved the replacement of 40-year-old electronics that are either obsolete, difficult to find, or unable to run at the required higher cycle-rate of 15 Hz, and allows for easier maintenance, shorter repair times, and less radiation exposure to personnel. The solid-state upgrade was completed in 2013.

Refurbishment of the Booster RF cavities and tuners, in particular, cooling, is also necessary in order to operate at a repetition rate of 15 Hz and is expected to be complete in 2015.

Other upgrades, replacements, and infrastructure improvements are needed for viable and reliable operation. Efforts to reduce beam loss and thereby lower radiation activation include improved methods for existing processes, and beam studies, e.g., aimed at finding and correcting aperture restrictions due to misalignment of components.

The proton flux through the Booster over the past two decades and projected into 2016 based on expected PIP improvements is shown in Fig. 7.3.

The new PIP flux goal will double recent achievements and needs to be completed within five years. The goal of doubling the proton flux will be achieved by increasing the number of cycles with beam. The intensity per cycle is not planned to increase.

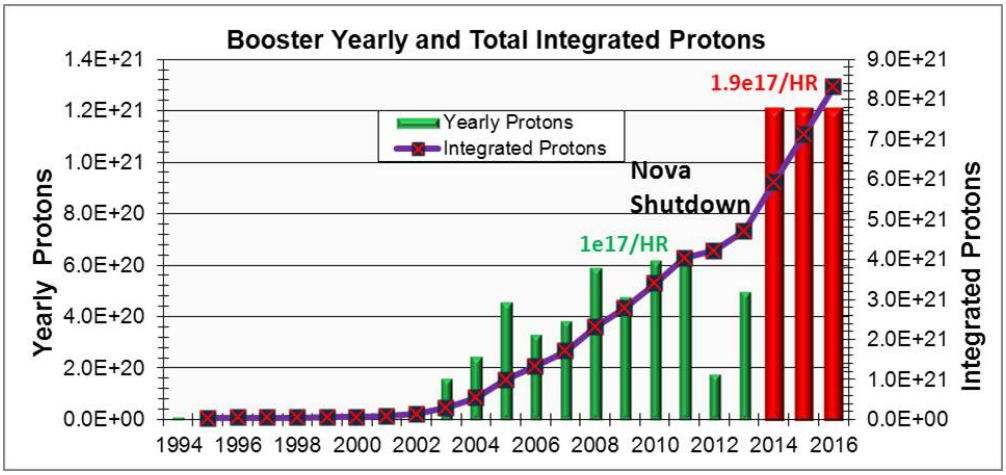

Figure 7.3: Yearly and integrated proton flux (including PIP planned flux increase).

7.3 Recycler

The $(g-2)$ experiment requires a low number of decay positrons in a given segment of the detector, and therefore requires that the full intensity of a Booster pulse (4×10^{12} protons) be redistributed into four bunches of 1×10^{12} protons each. These bunches should be spaced no closer than 10 ms to allow for muon decay and data acquisition in the detector. Because the revolution time of muons in the $(g-2)$ ring is 149 ns, the longitudinal extent of the bunches should be no more than 120 ns. The Recycler modifications needed to achieve these requirements will be made under the Recycler RF AIP, and are described below.

7.3.1 Recycler RF

The proposed scheme for $(g-2)$ bunch formation [3] uses one RF system, 80 kV of 2.5 MHz RF. The design of the RF cavities will be based on that of existing 2.5 MHz cavities which were used in collider running, but utilizing active ferrite cooling. The ferrites of the old cavities and the old power amplifiers will be reused in the new system.

In order to avoid bunch rotations in a mismatched bucket, the 2.5 MHz is ramped "adiabatically" from 3 to 80 kV in 90 ms. Initially the bunches are injected from the Booster into matched 53 MHz buckets (80 kV of 53 MHz RF), then the 53 MHz voltage is turned off and the 2.5 MHz is turned on at 3 kV and then ramped to 80 kV. The first 2.5 MHz bunch is then extracted and the remaining three bunches are extracted sequentially in 10 ms intervals. The formation and extraction of all four bunches takes three Booster cycles, or 2 Booster batches can be rebunched into eight bunches and extracted to $(g-2)$ in four Booster cycles. This limits the $(g-2)$ experiment to using three of the available eight Booster batches in every 1.33 s Main-Injector NOνA cycle, or four in a 1.4 s Main-Injector cycle..

Simulated 2.5 MHz bunch profiles are shown in Fig. 7.4. The 53 MHz voltage was ramped down from 80 to 0 kV in 10 ms and then turned off. The 2.5 MHz voltage was snapped to 3 kV and then adiabatically raised to 80 kV in 90 ms. The maximum momentum spread is $dp/p = \pm 0.28\%$. The overall efficiency is 95%, and 95% of the beam captured is contained within 120 ns. Roughly 75% of the beam is contained in the central 90 ns and 60% in 50 ns.

Although the Recycler is not yet configured to do such RF manipulations, by using the 2.5 MHz coalescing cavities in the Main Injector, the proposed bunch-formation scheme was tested with beam. In general, the agreement between simulations and data is very good. For illustration, the comparison between the beam measurements and the simulations for the case in which the 2.5 MHz voltage is ramped adiabatically from 3 to 70 kV in 90 ms is shown in Fig. 7.5.

Extraction from the Recycler and primary proton beam transport will be described in the beamline section, Sec. 7.5.

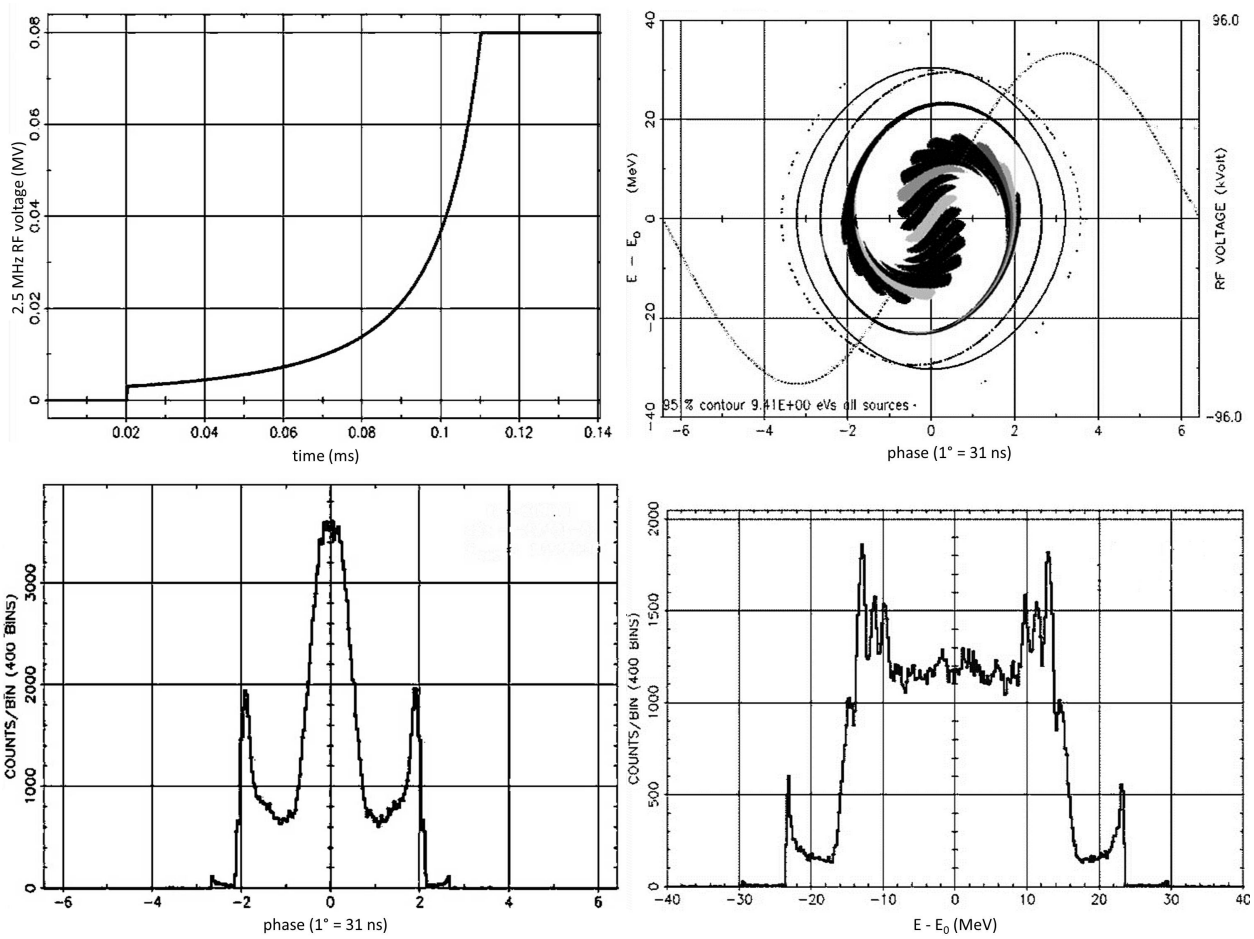

Figure 7.4: Results of RF simulations: 2.5 MHz voltage curve (upper left), phase space distribution (upper right), phase projection (lower left) and momentum projection (lower right).

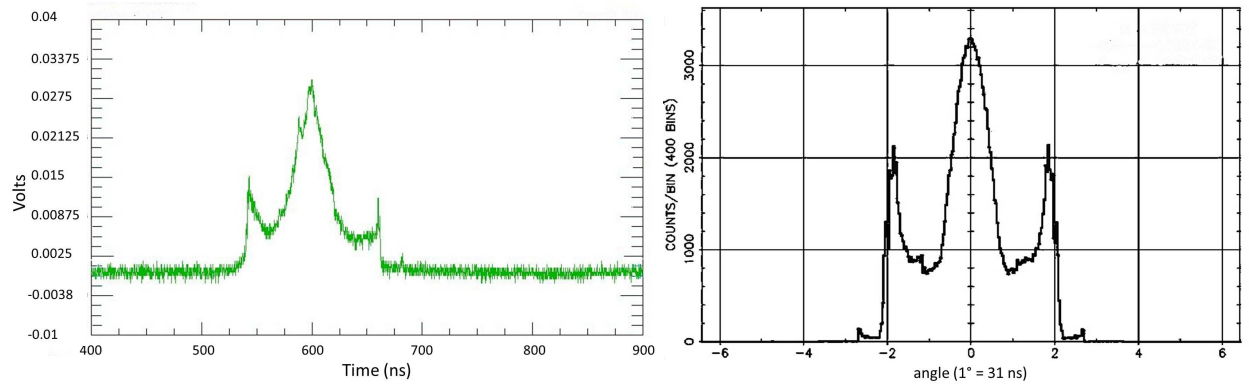

Figure 7.5: Comparison of beam profile (left) with simulation (right) for the case in which the 2.5 MHz voltage is ramped "adiabatically" from 3-70 kV in 90 ms. In both profiles, 95% of the particles captured are contained within 120 ns.

7.4 Target station

The $(g-2)$ production target station will reuse the existing target station that was operated for antiproton production for the Tevatron Collider since 1985, while incorporating certain modifications. The $(g-2)$ target station will be optimized for maximum π^+ production per proton on target (POT) since the experiment will utilize muons from pion decay. Repurposing the antiproton target station to a pion production target station takes full advantage of a preexisting tunnel enclosure and service building with no need for civil construction. Also included are target vault water cooling and air ventilation systems, target systems controls, remote handling features with sound working procedures and a module test area. Figure 7.6 shows the current target-station (vault) layout. The overall layout of the target-vault modules will be unchanged from that used for antiproton production. The major differences in design will include different primary and secondary beam energies, polarity of the selected particles, and pulse rate. Upgrades to pulsed power supplies are required.

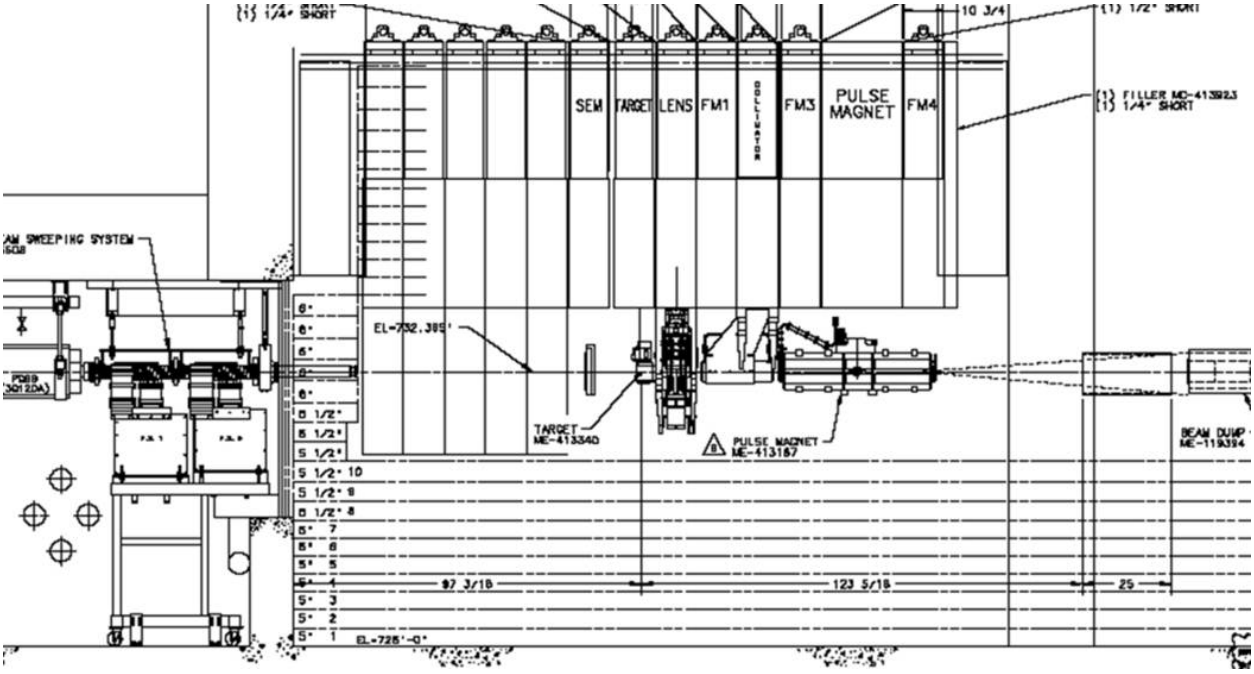

Figure 7.6: Layout of the $(g-2)$ target station.

The production target station consists of five main devices: the pion production target, the lithium lens, a collimator, a pulsed magnet, and a beam dump. Once the primary beam impinges on the target, secondaries from the proton-target interaction are focused by the lithium lens and then momentum-selected, centered around a momentum of 3.11 GeV/c, by a pulsed dipole magnet (PMAG). This momentum is slightly above the magic momentum needed to measure the muon anomalous magnetic moment in the downstream muon ring. The momentum-selected particles are bent 3° into a channel that begins the M2 beamline. Particles that are not momentum-selected will continue forward and are absorbed into the target-vault beam dump. An overview of some of the required beam design parameters for the $(g-2)$ target system can be found in Table 7.2.

Parameter	FNAL $(g-2)$ 12 Hz
Intensity per pulse	10^{12} p
Total POT per cycle	16×10^{12} p
Number of pulses per cycle	16
Cycle length	1.33 s
Primary energy	8.89 GeV
Secondary energy	3.1 GeV
Beam power at target	17.2 kW
Beam size σ at target	0.15-0.30 mm
Selected particle	π^+
$\lvert dp/p \rvert$ (PMAG selection)	10%

Table 7.2: Beam parameters for the target station.

One significant difference the $(g-2)$ production target station will have from the antiproton production target station is the pulse rate at which beam will be delivered to the target station. The $(g-2)$ production rate will need to accommodate 16 pulses in 1.33 s with a beam pulse-width of 120 ns. This is an average pulse rate of 12 Hz. The antiproton production pulse rate routinely operated at 1 pulse in 2.2 s or 0.45 Hz. This is a challenging factor that drives the cost of the design since the lithium lens and pulsed magnet will need to pulse at a significantly higher rate. Figure 7.2 shows a possible $(g-2)$ pulse scenario for pulsed devices and timing for proton beam impinging on the target.

7.4.1 The $(g-2)$ production target and optimization of production

The target to be used for the $(g-2)$ experiment is the antiproton production target used at the end of the Tevatron Collider Run II. This target is expected to produce a suitable yield of approximately 10^{-5} π^+/POT within $|dp/p| < 2\%$ based on simulations. This target design has a long history of improvements for optimization and performance during the collider run. The target is constructed of a solid Inconel 600 core and has a radius of 5.715 cm with a typical chord length of 8.37 cm. The center of the target is bored out to allow for pressurized air to pass from top to bottom of the target to provide internal cooling to the Inconel core. It also has a cylindrical beryllium outer cover to keep Inconel from being sputtered onto the lithium lens from the impinging protons. The target has a motion control system that provides three-dimensional positioning with rotational motion capable of 1 turn in 45 s. This target and the target motion system need no modifications or enhancements to run for the $(g-2)$ experiment. Figure 7.7 shows a drawing and a photo of the current target.

Beam tests were performed to measure the yield from this target in 2012 [2]. The instrumentation measured total number of charged particles and did not differentiate between particle species. Measurements were recently repeated using a Cerenkov counter to measure the particle composition of the beam; data analysis is still in progress. The yield of positive 3.1-GeV secondaries from 10^{12} 8-GeV protons on target measured in the beam tests was about 85% of the 9.3×10^8 particles predicted [4] using a G4beamline [5] simulation at the

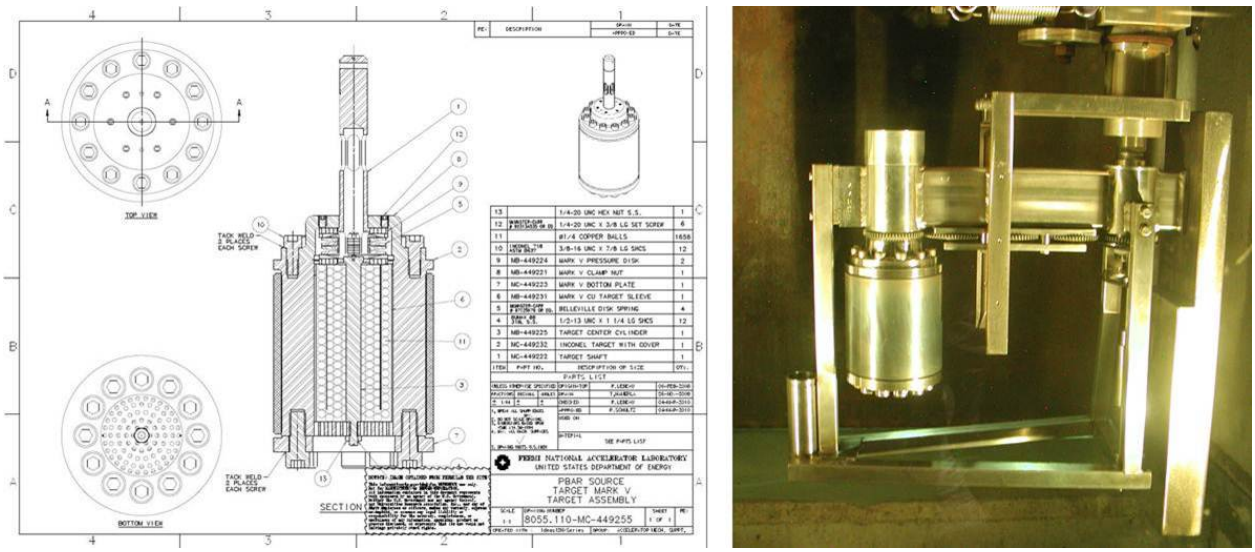

Figure 7.7: Current default target to be used for the $(g-2)$ target station.

704 location in the AP2 beamline shown in Fig. 7.8, and about 70% of the 4.3×10^7 particles at the 728 location [2]. The spot size of the beam on target was $\sigma_x \approx \sigma_y >\sim 0.5$ mm. As discussed in the beamlines section, we plan to reduce the spot size to 0.15 mm.

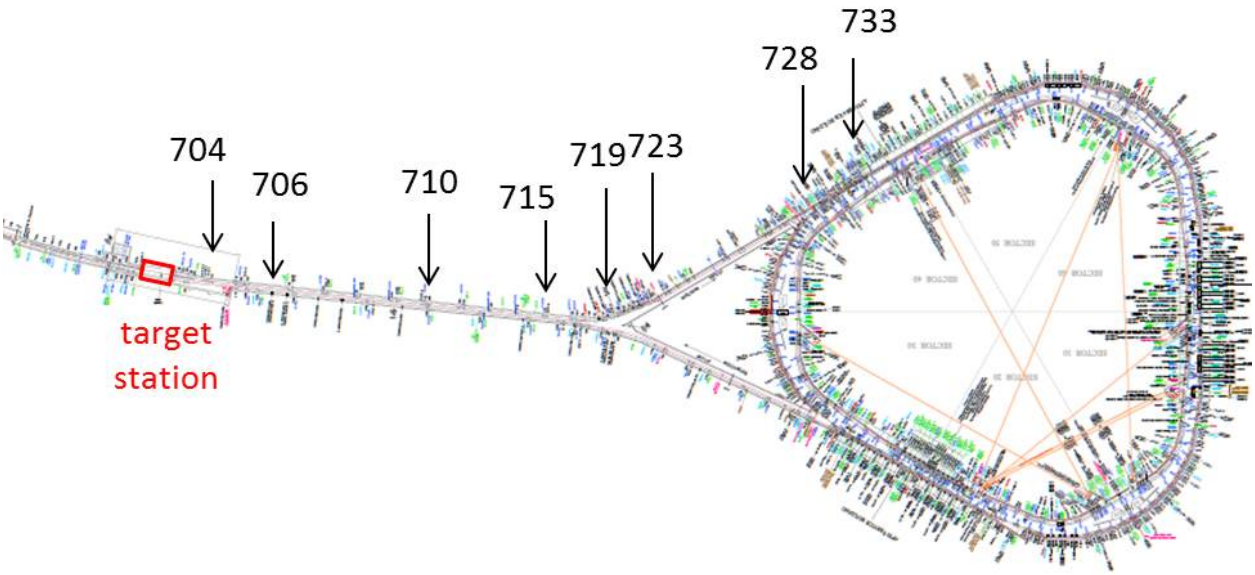

Figure 7.8: Locations in AP2 line.

The spot size of the beam on the target is an important parameter in determining the pion yield. Initial values for the spot size were simply scaled from the $\sigma_x = \sigma_y = 0.15$ mm size of the beam for 120-GeV antiproton production to $\sigma_x = \sigma_y = 0.55$ mm for 8.9 GeV. Optimized results from MARS [6] simulations (Fig. 7.9) for the impinging-proton spot size can be seen in Fig. 7.10. The simulation result demonstrates that if the spot size is reduced from the original 0.55 mm to 0.15 mm, a ∼15% increase in pion production can be achieved for the current target-to-lens distance of 28 cm. These modifications are not directly made to the target station or target components but to the beamline just upstream of the target. Details of the beamline optics incorporating this optimization for pion yield can be found in Sec 7.5.4. Combining the spot size with optimization of the target-to-lens distance discussed in Sec. 7.4.2 gives an improvement of ∼30%.

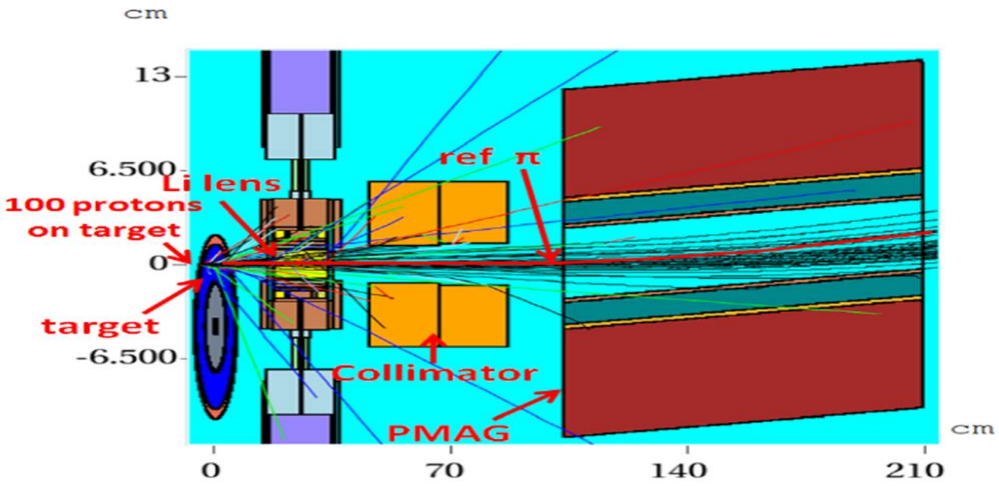

Figure 7.9: Graphical representation of target system used in MARS for simulated yield results.

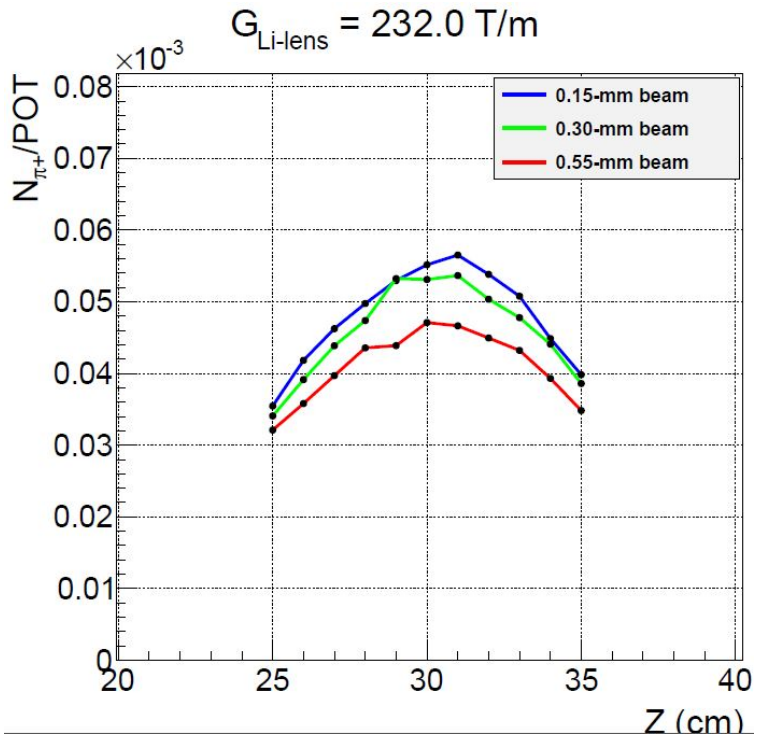

Figure 7.10: MARS simulation results for optimization of the distance between the target and the lithium lens for three beam spot sizes on target.

7.4.2 Focusing of secondaries from the target

The lithium collection lens is a 1 cm radius cylinder of lithium that is 15 cm long and carries a large current pulse that provides a strong isotropically focusing effect to divergent incoming secondaries after the initial interaction of impinging particles with the target [11]. The lithium lens cylinder is contained within a toroidal transformer, and both lens and transformer are water cooled. The peak current produced by the secondary of the transformer is a factor 8 larger that the primary peak current. Figure 7.11 is a drawing of the lithium lens depicting (a) the transformer and lens body, and (b) details of the lithium cylinder.

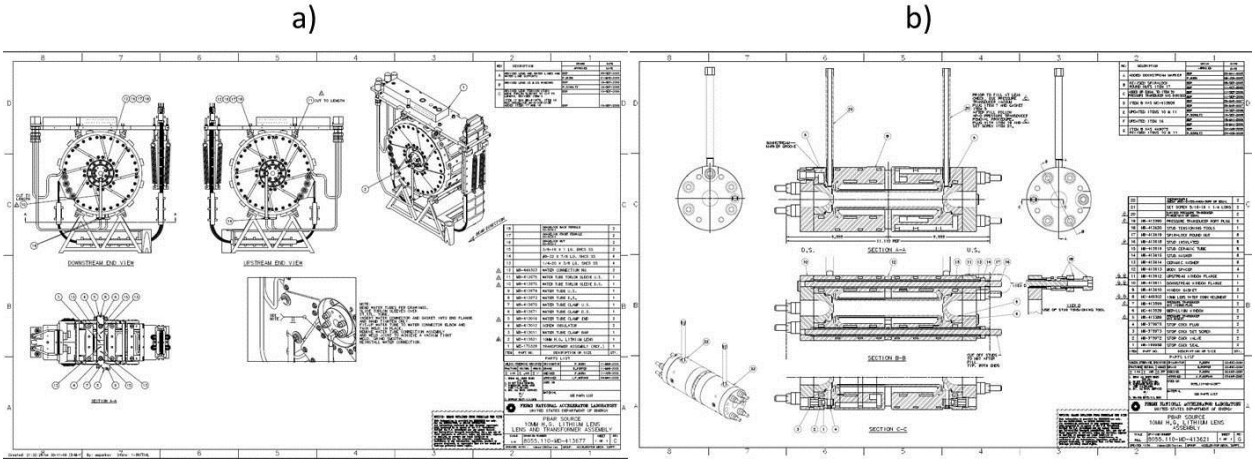

Figure 7.11: Drawing of the lithium lens and transformer (a) and the lithium cylinder body (b).

During antiproton production for the Collider Run II, the lens pulsed at a peak secondary current of 450 kA, which is equivalent to a gradient of 670 T/m at 8.9 GeV/c with a base pulse width of 400 μs. Scaling the lens gradient for use at 3.11 GeV/c for $(g-2)$, the gradient required will be 232 T/m at a pulsed secondary current of 155 kA with the same 400 μs pulse width. (The peak current produced by the secondary of the transformer is a factor of eight larger that the primary peak current.) The gradient for $(g-2)$ will still accommodate the same range of focal lengths from the target to the lens with the nominal distance taken to be 28 cm. The range of distances from the target to the lens is limited by the design of the target vault area for Colliding beam and is costly and difficult to change. Table 7.3 provides an overview of required operating parameters.

Accommodating the $(g-2)$ 12-Hz average pulse rate for the lithium lens is one of the biggest challenges and concerns for repurposing the antiproton target station for $(g-2)$. Even though the peak current and gradient will be reduced by a factor of about 3, the pulse rate will increase by a factor of 24 compared to the operation for antiproton production. Resistive and beam heating loads, cooling capacity, and mechanical fatigue are all concerns that are warranted for running the lithium lens at the $(g-2)$ repetition rate.

Therefore, in order to gain confidence that the lens will be able to run under these conditions, a preliminary ANSYS [7] analysis has been conducted. This analysis simulated thermal and mechanical fatigue for the lens based on the pulse timing scenario in Fig 7.2 and

Lens operation	Pulse width (μs)	Peak secondary current (kA)	Gradient (T/m)	Pulses per day
Antiproton production	400	450	670	38,880
$(g-2)$ pion production	400	155	232	1,036,800

Table 7.3: Comparison of lithium lens parameters for $(g-2)$ operations and antiproton production.

at a gradient of 230 T/m. These results were compared to results from a similar analysis for the lens operating under the antiproton-production mode of a gradient of 670 T/m at a pulse rate of 0.5 Hz [8]. Figure 7.12 (left) shows the ANSYS output thermal profile of a cutaway of the lens operating at 12 Hz. The lithium body corner is a temperature-sensitive location and should avoid lithium melting temperatures of 453.75 K. The corner temperature was found to reach a maximum temperature of 376 K. The plot on the right of Fig. 7.12 is the increase in maximum temperature of the lithium over the 16 pulses, depicting a change in temperature of 22 K when the operating temperature has come to equilibrium. We conclude from this analysis that the lithium lens is adequately cooled to operate at the nominal $(g-2)$ pulse rate.

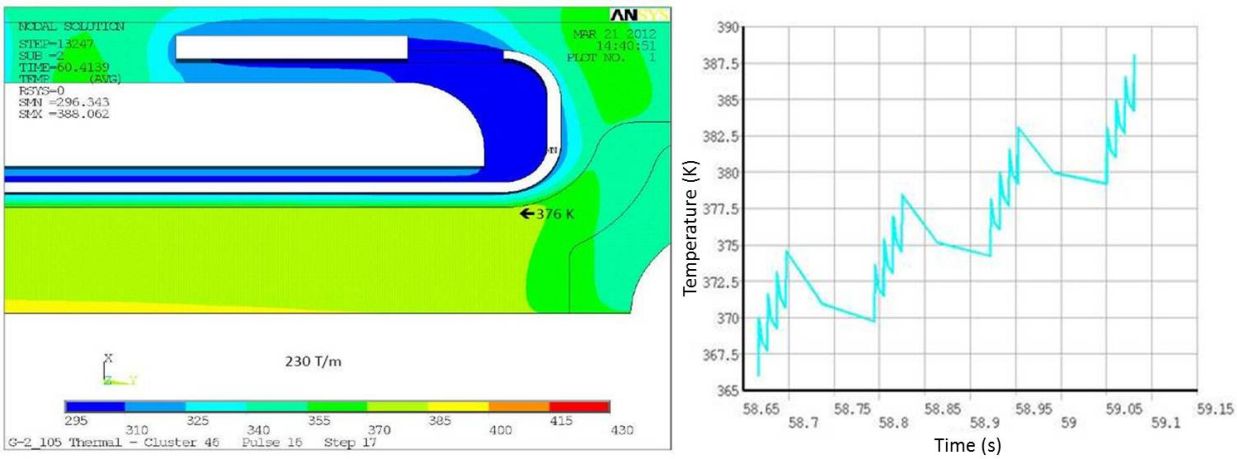

Figure 7.12: Simulated thermal profile from ANSYS for the lens operating at an average pulse rate of 12 Hz *(left)* depicting little beam heating and a corner temperature of 376 K. *(right)* Plots showing lens temperature increase over the 16 pulses.

Mechanical fatigue was also assessed for the lithium lens. Figure 7.13 depicts a constant life fatigue plot developed for the lens from the ANSYS analysis. The two red lines represent upper and lower estimates of fatigue limits for the lens material. The red data points represent fatigues for gradients of 1000 T/m, 670 T/m, and two points at 230 T/m for a lithium preload pressure of 3800 and 2200 psi, respectively. For the lens operating in the antiproton production conditions of 670 T/m, the mechanical fatigue was a large concern in the lens design. It appears that for the $(g-2)$ case, the mechanical fatigue will be a comparatively small concern.

This initial assessment of the lithium lens suggests that is should be able to operate at

the $(g-2)$ repetition rate. However, since the operation of the lithium lens at the average 12 Hz rate is crucial, testing of the lens at 12 Hz was needed. The lens has been pulsed in a test station at a 12 Hz rate in order to confirm that 1M pulses per day can be achieved and sustained over many months. The lens was pulsed 80 million times without problems, and data from these tests were used to confirm predictions of the ANSYS model.

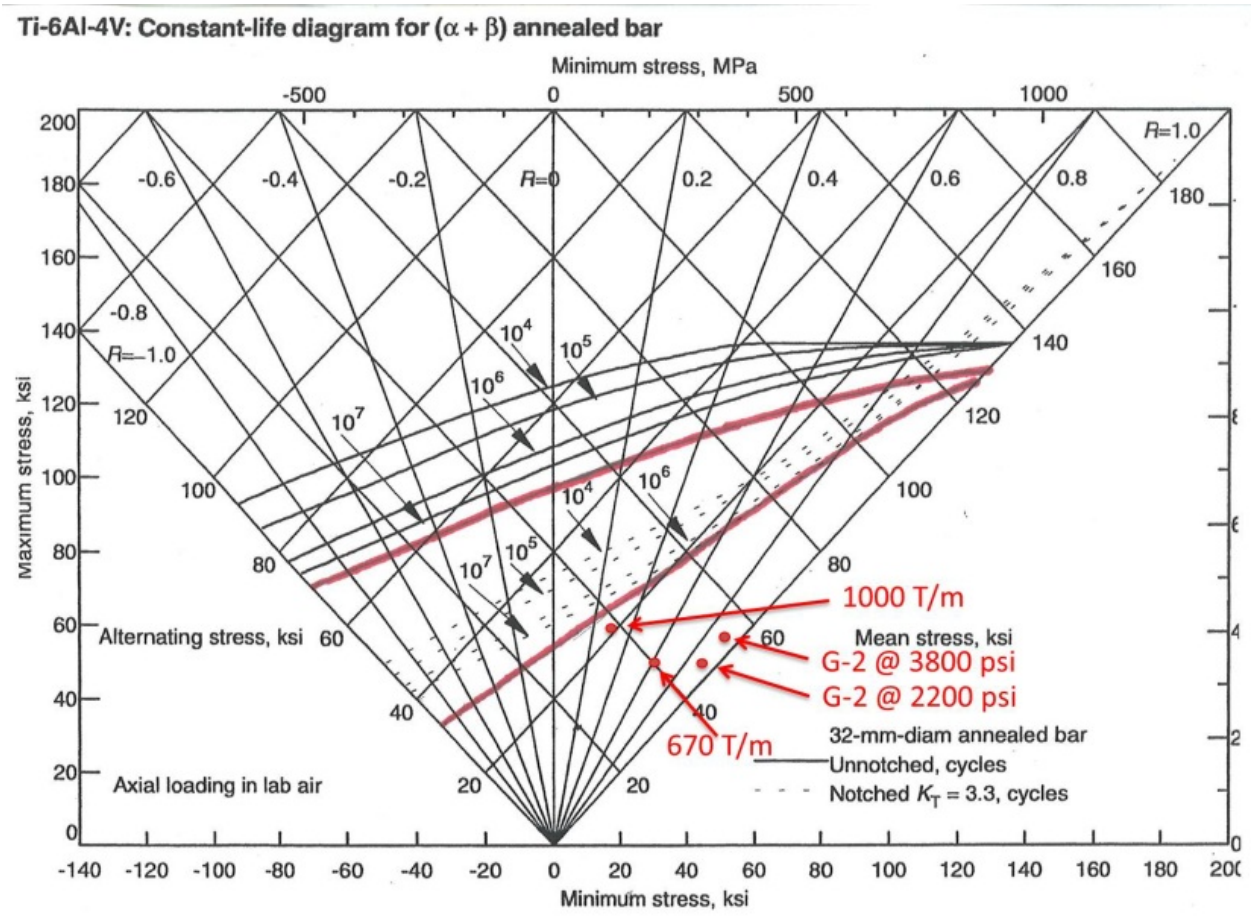

Figure 7.13: Constant-life fatigue plot of the lithium lens for antiproton and $(g-2)$ modes showing that mechanical fatigue for the $(g-2)$ pulse rate is a small concern.

The same ANSYS analysis was also used to determine if the repetition rate of the lens pulsing could be increased above 12 Hz (or 16 pulses in 1.33 s) for operational periods that may allow an increased repetition rate [9]. Lens thermal estimates for rates of 20, 24 and 28 pulses in the 1.33-s time period were conducted and analyzed. Figure 7.14 shows the results of this analysis. There are two concerns with increasing the repetition rate above 12 Hz. First, as the temperature rises and approaches the lithium melting temperature there is an increased risk of lithium leakage due to increased plasticity. The plasticity this close to the melting temperature is incredibly hard to model or predict. Pulsing at 15 Hz seems possible, but 18 Hz and above seems risky in this regard. The second concern is that as the temperature increases, so does the stress on the septum wall. In addition, the yield temperature of a material decreases as the temperature increases. While 20, 24 and 28 pulses

per cycle have been modeled thermally, a structural analysis has not been done as of this writing. Simple scaling suggests that 15 Hz again seems possible but 18 Hz seems risky. This needs to be modeled to say with more certainty.

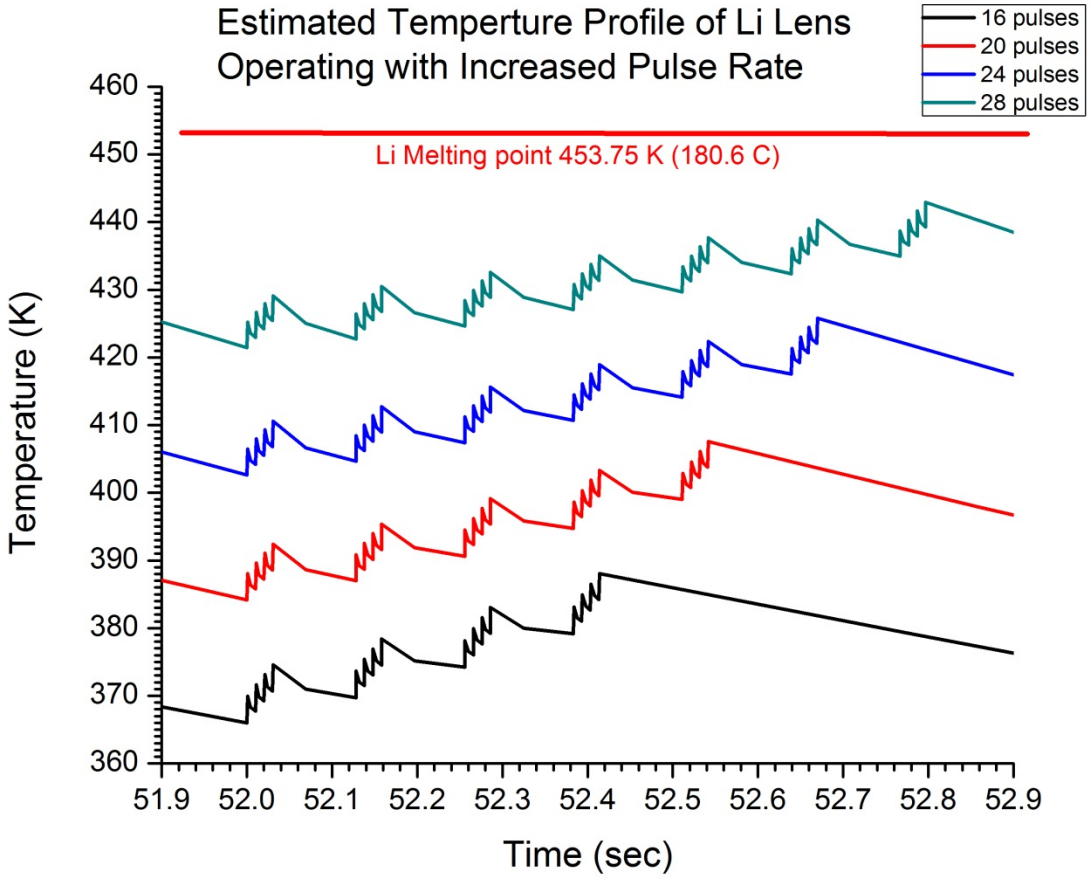

Figure 7.14: Temperature profile of the Li lens operating with increased pulse rate as modeled using ANSYS.

Temperature and stress effects with increased lens gradient were also considered. This has the same risks as increasing the pulse rate because the ultimate effect of increased thermal loading is the same. Due to the fact that the beam heating is so low compared to the joule heating, it is possible to ignore the beam heating and simply scale the joule heating for a first-order approximation. For example, a 25% increase in the repetition rate (from 12 to 15 Hz) corresponds to a 25% increase in thermal loading. Understanding that thermal power is I^2R, a 12% increase in current and gradient would correspond to a 25% increase in thermal loading. So 260 T/m would be equivalent to a repetition rate of 15 Hz.

In order to optimize the yield of pions from the target system as a function of lens gradient and target-to-lens distance, MARS simulations were conducted [10]. Figure 7.10 shows the results of the MARS simulation. For a nominal gradient of 232 T/m, pion production peaks at a target-to-lens distance of 30 cm to 31 cm. If we can increase the lens gradient, then a larger target-to-lens distance would be optimal, and a larger increase in yield could be possible as shown in Fig. 7.15.

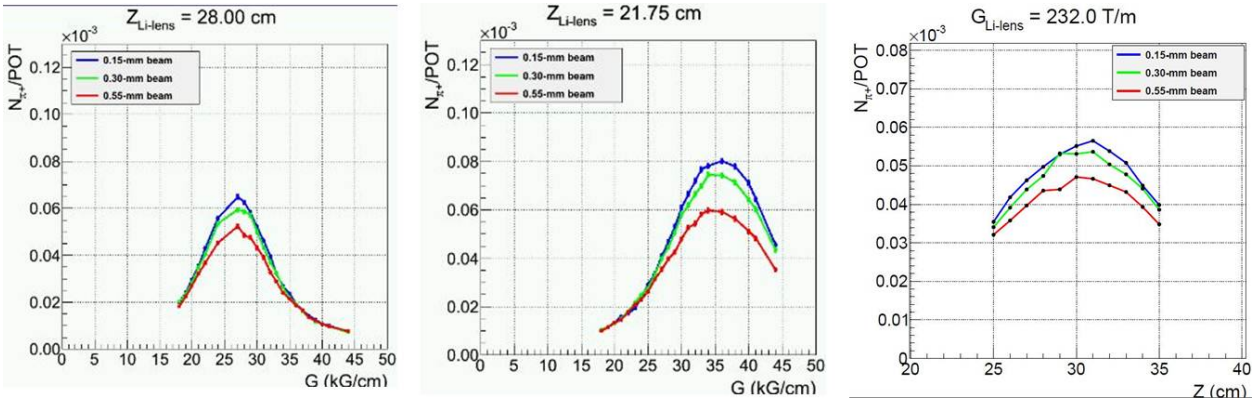

Figure 7.15: MARS simulation results for optimization of target-to-lens distance and lens gradient shown for three beam spot sizes on target.

Table 7.4 is an overview of the nominal operating parameters for the Li lens which will be the used for $(g-2)$ operation. Much attention has been given to the Li lens to confirm that it will be able to operate under the $(g-2)$ pulse rate scenario. There are three suitable lens spares that can be used during the $(g-2)$ data-taking period. The major upgrade to the Li lens system will be to modify the power supply to operate at the $(g-2)$ pulse rate. Details of the power supply design are presented in Sec 7.4.4.

Lens parameters	Value
Nominal gradient	232 T/m
Nominal peak lens current	155 kA
Nominal target to lens distance	30 cm
Min target to lens distance	21.75 cm
Max target to lens distance	33.4 cm
Max Power Supply Current	25 kA
Max gradient (for max PS output)	301 T/m

Table 7.4: Operating parameters for the lithium lens.

7.4.3 Pulsed magnet (PMAG) and collimator

The pulsed magnet, shown in Fig. 7.16, selects 3.115 GeV/c positive particles and bends them 3° into the channel that begins the M2 beamline. The magnet will operate with a field of 0.53 T and is 1.07 m long with an aperture of 5.1 cm horizontally and 3.5 cm vertically. It is a single-turn magnet that has incorporated radiation-hard hardware such as ceramic insulation between the magnet steel and the single-conductor bars, as well as Torlon-insulated bolts [11]. The pulsed magnet has a typical pulse width of 350 μs and similarly to the lithium lens, will need to accommodate the $(g-2)$ pulse rate shown in Fig. 7.2. The pulsed magnet is water cooled. In addition to the magnet currently in the target vault, there are three spares.

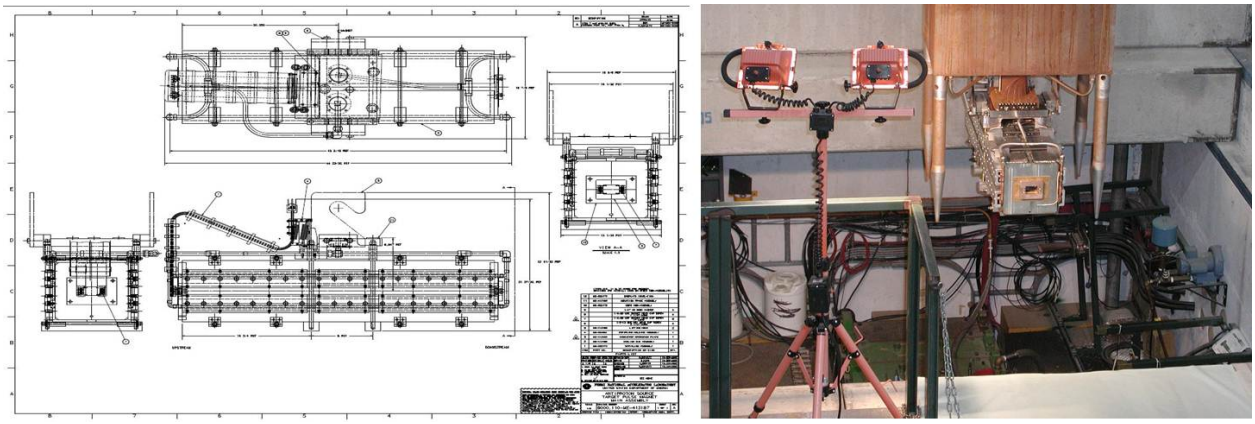

Figure 7.16: Pulsed magnet (PMAG) used for momentum-selection of pions.

One initial concern regarding the pulsed magnet was that while operating in the polarity needed to collect positive secondaries, the magnet would have an increase in energy deposited in the downstream end of the magnet compared to antiproton production where negative secondaries were collected. An increase in energy deposition could potentially lead to magnet failures, and therefore running with positive polarity might require a redesign of the magnet. A MARS simulation was conducted to look at the energy deposition across the entire pulsed magnet compared to the antiproton production case. The simulated magnet was segmented in order to highlight sensitive areas. The simulation concluded that although the map of energy deposition for the positive particle polarity with 8-GeV protons on target was different than for the antiproton production case (120-GeV protons on target), there were no locations where the deposited energy was higher, and the total was an order of magnitude lower [12]. The negative particle polarity case was more than two times lower for 8-GeV primary beam than for 120-GeV. Therefore a new pulsed magnet design was not needed and the plan is to use the device currently installed.

In order to accommodate the $(g-2)$ pulse rate, the pulsed magnet power supply will also need to be modified into one similar to the new supply for the lithium lens with improved charging capability. Details of the power supply design are presented in Sec. 7.4.4.

A collimator is located directly upstream of the pulsed magnet. The purpose of the collimator is to provide radiation shielding to the pulsed magnet to improve its longevity. It is a water-cooled copper cylinder 12.7 cm in diameter and 50.8 cm long. The hole through

the center of the cylinder is 2.54 cm diameter at the upstream end, widening to a diameter of 2.86 cm at the downstream end. The existing collimator is currently planned to be used without modification.

7.4.4 Lithium-lens and pulsed-magnet (PMAG) power supplies

The lithium-lens and pulsed-magnet power supplies will both need to be upgraded in order to meet the $(g-2)$ pulse rate scenario shown in Fig. 7.2. The requirements and specifications for the lens and pulsed-magnet power supply systems can be seen in Table 7.5. During the design process, it was found to be cost-beneficial to use the same power supply design for both supplies since their load characteristics and power supply output are similar. Both systems currently have existing power supplies that will be modified to produce the $(g-2)$ power supplies. Modifications to the existing supplies will include new larger charging supply systems, additional enclosures to house a large capacitor bank for bulk energy storage, and new power supply controls [13].

Power Supply Specification		
	Lens	**PMAG**
device		
type	transformer-lens	1-turn magnet
location	AP0	AP0
inductance	3.54 μH, from transformer primary	2.56 μH
resistance	12.31 $m\Omega$	2.61 $m\Omega$
current program		
pulsed	1/2 sinewave	1/2 sinewave
peak nominal current	20 kA	15.3 kA
peak maximum current	25 kA	18 kA
pulse base	400μs (same as existing)	355μs (same as existing)
maximum rep rate	100 Hz	100 Hz
average rep rate	12 Hz	12 Hz
maximum ave rep rate	18 Hz	18 Hz
regulation		
drift and stability	$\pm$0.1% of maximum	$\pm$0.1% of maximum
other		
AC input	480 VAC, 3-phase	480 VAC, 3-phase
cooling	air and/or LCW	air and/or LCW
controls	accelerator timing system	accelerator timing system
power supply location	AP0, must fit within present power-supply footprint	AP0, must fit within present power-supply footprint

Table 7.5: Lithium-lens and pulsed-magnet power supply requirements and specifications.

Fig. 7.17 shows a high-level schematic diagram that will be used for the design of the power supplies. The lens and PMAG power supplies both require similar half-sinewave pulsed currents. These high-power pulses are provided through a solid-state switch (pulsed SCRs) that connects a charged capacitor bank (Pulsed Cap Bank) to the load. After the pulse, the capacitor-bank voltage is brought back to the correct polarity through a "Charge Recovery" circuit. The design of the power supply includes a "Charge Transfer" mechanism to minimize the pulsed loading on the 480-VAC distribution systems. Without this feature, a costly dedicated 13.8 kV/480 VAC transformer would have been necessary to operate the power supplies. The Charge Transfer hardware consists of a 12-pulse rectified power supply, a large capacitor bank, and a high-voltage solid-switch (IGBT). Between load pulses, the IGBT switch closes and transfers energy from the capacitor bank to the pulsed capacitor bank to make up for the energy lost during the pulse. Since the capacitor bank is much larger (by a factor >30) than the pulsed capacitor bank, this helps reduce the effect on the AC line of the 10 ms burst of pulses. The "Filter Choke" in series with the capacitor bank further evens out the pulsing. Given the age of the existing power supply controls and the added Charge Transfer feature required, a completely new control system will be designed and built. The re-designed pulsed power supply will also incorporate a "deQ-ing" system to maintain the required 0.1% regulation of the Pulsed Cap Bank energy.

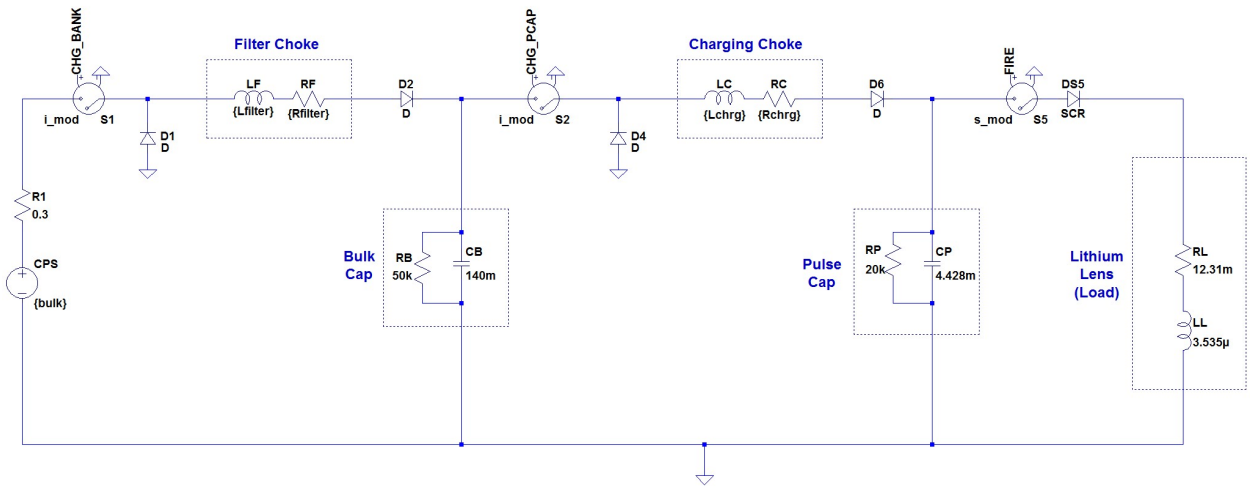

Figure 7.17: Lithium-lens and pulsed-magnet power supply high-level schematic.

In order to accommodate all of the modifications to the existing power supplies, the size of their enclosures must increase and the layout of the components will be changed. Figure 7.18 shows the existing power supplies that are located at the AP0 target hall.

Figure 7.19 shows the layout of the power supplies including the changes to incorporate the new components. An additional enclosure will be added to hold the charging inductors and the new power supply controls. The energy storage section, made up of a parallel array of dry-film capacitors, will be housed in the middle enclosure above the large pulse capacitors

Figure 7.18: Existing lens and PMAG power supplies at AP0.

which will be reused. Two new phase-controlled DC charging supplies, one each for the lens and PMAG will replace the existing 480-VAC line transformers as shown in Fig. 7.20.

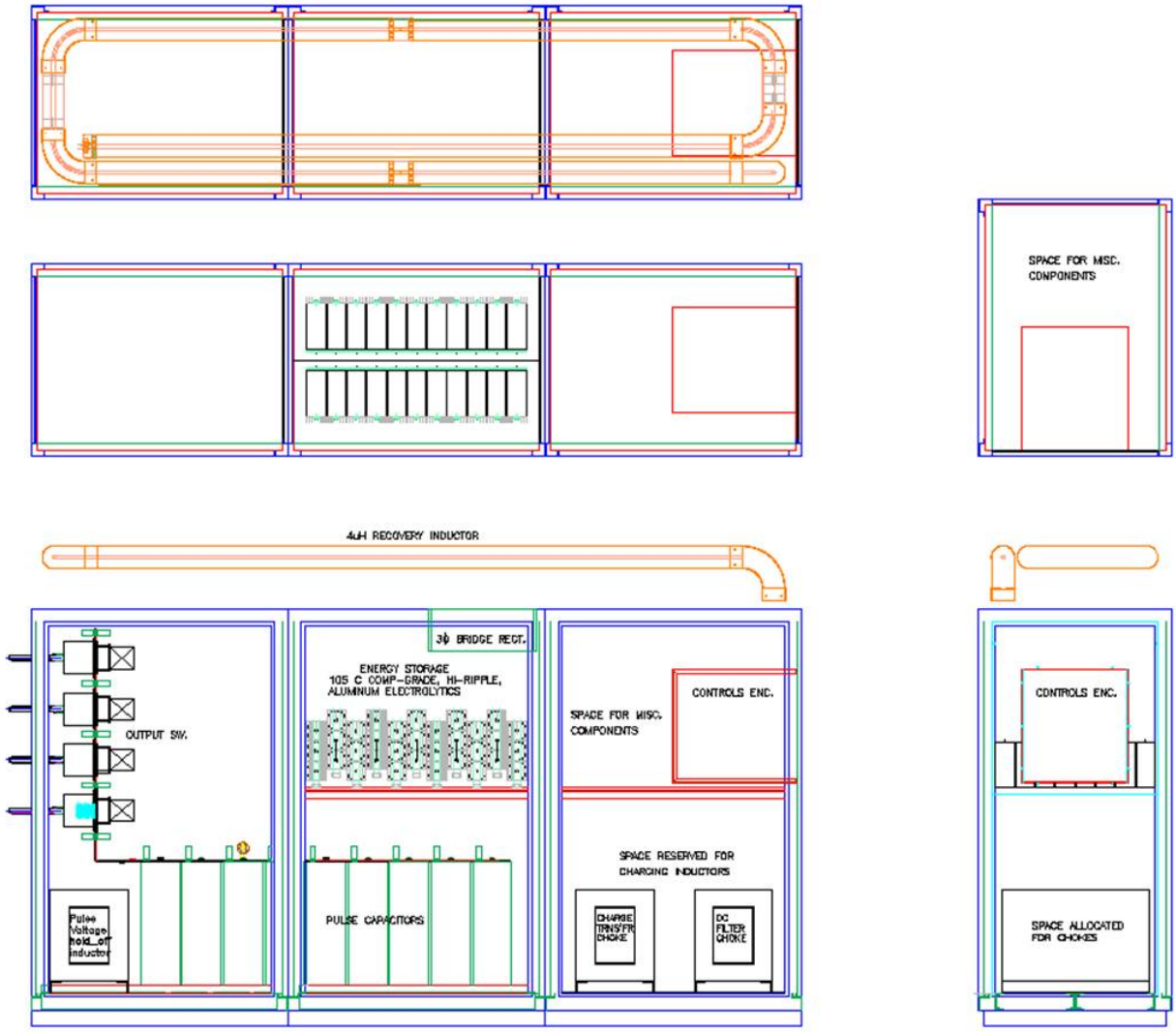

Figure 7.19: Power supply layout including new components. Note that the proposed bulk cap bank will utilize dry film types rather than the electrolytics shown, due to cost and reliability issues.

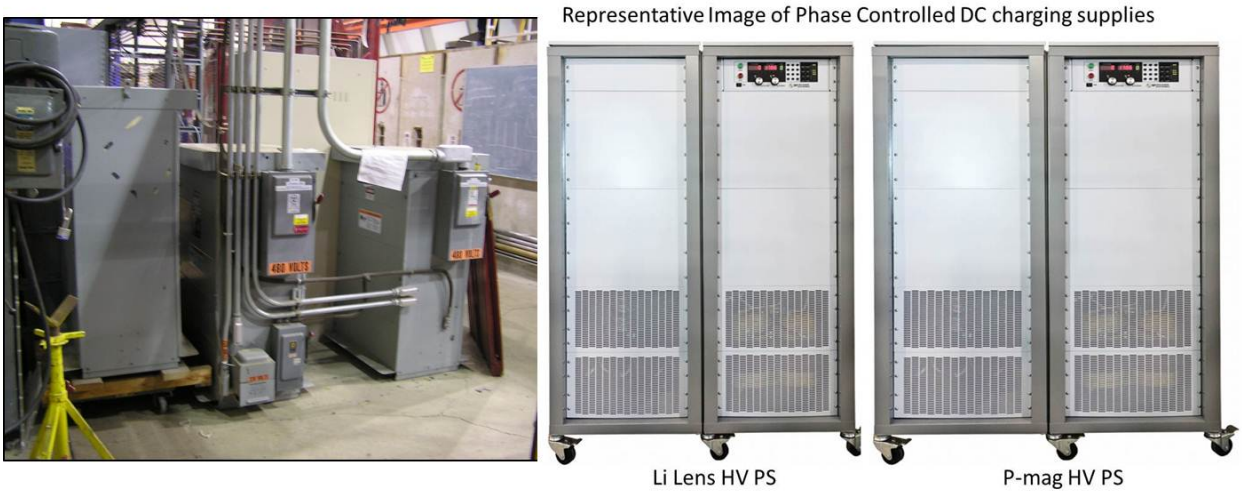

Figure 7.20: Existing 480 VAC transformers *(left)* that will be replaced by new phase controlled DC charging supplies *(right)*.

7.4.5 Target station beam dump

The target-station beam dump absorbs particles which are not momentum-selected by the pulsed dipole magnet and continue straight ahead. The location of the beam dump can be seen in Fig. 7.21. The current beam dump has a graphite and aluminum core which is water cooled, surrounded by an outer steel box. The graphite core is 16 cm in diameter and 2 m in length, and is designed to handle a beam power of 80 kW [14]. The existing dump has a known water leak that developed at the end of the collider run, and will be replaced with an updated copy of the 80 kW beam dump, shown in Fig. 7.22. The maximum beam energy load for $(g-2)$ would occur if $(g-2)$ takes advantage of extra cycles, for example if the NOνA experiment were not able to run. At a rate of 18 Hz, the beam energy load would be 25 kW, which is easily accommodated with the current dump design.

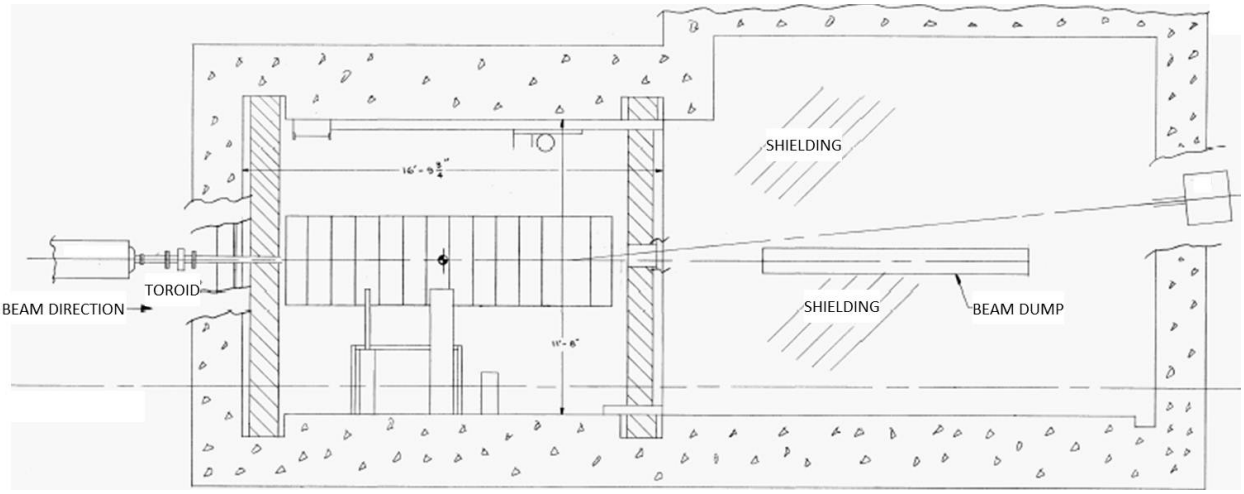

Figure 7.21: Layout of the target-station beam dump.

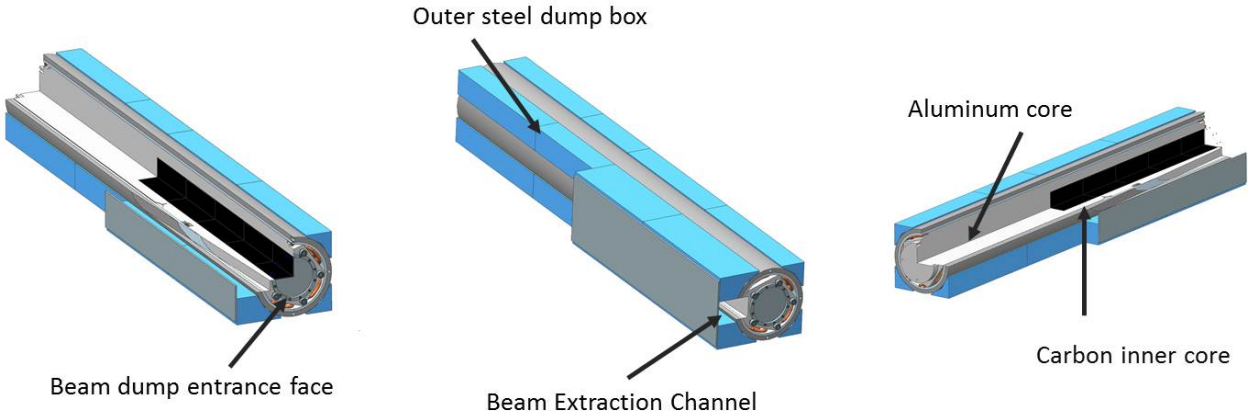

Figure 7.22: Design of the AP0 beam dump core.

Target station beam dump removal and installation

The AP0 beam dump has been in operation for 27 years and upon removal of the beam dump core from the dump shield it will be found to be highly activated. Therefore, MARS simulations have been conducted on the existing beam dump in order to estimate the residual radioactive dose [15]. An estimate of the residual dose is needed in order to develop a detailed plan for the removal of the existing beam dump and the installation of the new beam dump. A detailed plan for removing the dump will be essential for controlling worker radiation exposure levels and preventing the spread of radioactive contamination. Table 7.6 shows the results of the MARS simulation which estimates the radiation dose rates for different parts of the beam dump core. The sum column represents the upper limit of peak dose rate. Rates at the upstream core on contact are estimated to be 427 rem/h.

Location	2001	2004	2007	2011	2014	sum
beam-right dump core	0.03	0.23	1.30	23.00	0.02	24.6
beam-left dump core	0.03	0.18	1.10	18.00	0.02	19.3
bottom of dump core	0.03	0.20	1.20	20.00	0.02	21.4
top locator plate	0.01	0.07	0.54	12.00	0.01	12.6
upstream core	1.30	15.00	61.00	350.00	0.06	427.4
downstream core	1.10	12.00	52.00	290.00	0.04	355.1
right side plug	0.01	0.03	0.20	4.70	0.01	4.9
left side plug	0.00	0.02	0.18	4.10	0.01	4.3
upstream lower plug face	0.00	0.00	0.03	0.56	0.00	0.6
downstream lower plug face	0.01	0.03	0.24	5.20	0.01	5.5

Table 7.6: Summary of partial peak radiation dose rates in rem/h at contact with various surfaces of the beam dump and beam dump plug. The peak dose rates are taken from the MARS histogram results for each irradiation/cooling period. The upper limit of peak dose rate is indicated in the sum column.

Based on the MARS radiation dose rate results, the plan for removing the beam dump will include constructing a steel coffin that the beam dump will be placed in once removed. The coffin design is shown in Fig. 7.23. The approximate weight of the coffin is 10,200 lb, and the approximate weight of the coffin, dump assembly, and dump locator plate assembly at 13,100 lbs. The coffin is made of 4-in plates of 1018 Steel, cold drawn, UNS G10180 with top or side lift points and a detachable lid.

The beam dump will be removed and placed inside the coffin and then lowered and stored in the bottom of the hot rack storage located at AP0. It is possible that the coffin and beam dump will be transported to the on-site Neutrino Target Service Building (NTSB) in the future for long term storage. Figure 7.24 shows a photo of the front face of the beam dump as taken in 2003 and also of the top of the dump plug below the surface of the shielding blocks.

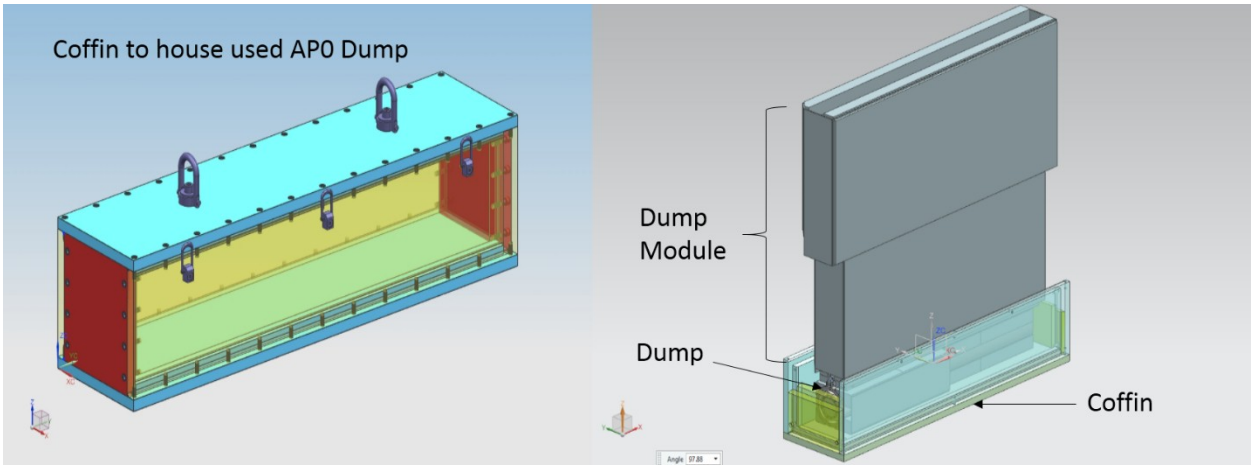

Figure 7.23: Steel coffin that will be used to house the removed beam dump to shield and mitigate radiation concerns of the beam dump.

Figure 7.24: *(left)* Photo of the front face of the beam dump as taken in 2003. *(right)* Looking down on the top of the dump plug below the surface of the shielding blocks .

7.5 Beam Transport Lines

7.5.1 Overview of $(g-2)$ beamlines

The existing tunnel enclosures and beamlines connecting the Recycler Ring to the Delivery Ring will be largely reused for $(g-2)$ operation. However, there are fundamental differences between the way the Rings and beamlines were operated for Collider Operation and how they will be used to support the Muon Campus. A high-intensity, 8 GeV kinetic energy proton beam will be transported to the AP0 Target Station in $(g-2)$ operation and to the Delivery Ring for the Mu2e experiment. The increase in intensity from Collider Operation in conjunction with the beam size of the 8 GeV beam will present challenges for efficient beam transfer. The beamlines downstream of the AP0 Target Station will need to be reconfigured to connect to the D30 straight section of the Delivery Ring. New extraction lines will be constructed to transport beam from the D30 straight section to the $(g-2)$ and Mu2e experiments. Careful planning is required for the D30 straight section of the Delivery Ring due to the presence of both the injection and extraction points. The extraction line will also need to support both single-turn extraction for $(g-2)$ and resonant extraction for Mu2e.

7.5.2 Beamline Changes from Collider Operation

During antiproton ("Pbar") operation in Collider Run II, the P1 line connected to the Main Injector at the MI 52 location. The P1 line supported operation with three different beam energies, 150 GeV for protons to the Tevatron, 120 GeV for Pbar production and SY120 operation, and 8 GeV for protons and antiprotons to and from the Antiproton Source. (SY120 refers to the "Switchyard" of beamlines used for the 120-GeV fixed-target program.) The junction between the P1 and P2 lines occurs at F0 in the Tevatron enclosure. The P2 line ran at two different beam energies, 120 GeV for antiproton production and SY120 operation and 8 GeV for protons and antiprotons to and from the Antiproton Source. The P2, P3 (for SY120 operation), and AP1 lines join at the F17 location in the Tevatron enclosure. The AP1 line also operated at 120 GeV and 8 GeV, but is not used for SY120 operation. The AP3 line only runs at a kinetic energy of 8 GeV. The AP3 line connects with the AP1 line in the Pre-Vault beam enclosure near the Target Vault and terminates at the Accumulator.

After the conversion from collider to NOνA and $(g-2)$ operation, the Recycler will become part of the proton transport chain and will connect directly with the Booster. There will be a new beamline connection between the Recycler Ring and the P1 line. The P1 line will become a dual energy line, with no further need to deliver 150 GeV protons with the decommissioning of the Tevatron. The P2 line will continue to operate at both 8 GeV for the Muon experiments and 120 GeV for SY120 operation. The AP2 and AP3 lines will need to be completely dismantled and reconfigured to support both the transport of muon secondaries via the Target Station for $(g-2)$ and protons via the target bypass for Mu2e. The $(g-2)$ 3.1 GeV secondary beamline emanating from the Target Station and the Mu2e 8 GeV primary beamline bypassing the Target Station will merge and follow a single line to the Delivery Ring. The new injection line will connect to the Delivery Ring in the D30 straight section. The extraction line also originates in the D30 straight section and has to be capable of supporting both resonant and single-turn extraction.

The beamlines that made up the Antiproton Source, those that have an "AP" prefix, will be modified, reconfigured and renamed prior to $(g-2)$ operation. The AP1 line will only operate at an energy of 8 GeV and will be renamed M1. The AP1 line will be largely unchanged, with the exception of the replacement of some magnets to improve aperture and the addition of a Final Focus quadrupole triplet at the end of the line. The AP2 line will become two separate beamlines and no longer be continuous. The upstream end of the line will be part of the pion decay channel for the $(g-2)$ experiment and will be renamed M2. It will provide a connection from the Pbar AP0 Target Station to the M3 line, which will continue the pion decay channel to the Delivery Ring. The downstream section of AP2 will become the abort and proton removal line from the Delivery Ring. The reconfigured AP3 line will be required to transport both 8 GeV beam for the Mu2e experiment and also a 3.1 GeV secondary beam for the $(g-2)$ experiment and will be renamed M3. The 18.5° right bend will be changed from a three to a two dipole configuration in order to avoid higher beta functions in this region. The M3 line will also be modified to connect to the Delivery Ring (formerly Debuncher) instead of the Accumulator. The extraction line connecting the Delivery Ring to the experiments will be called M4. The M5 line will vertically branch from the M4 line shortly after leaving the Delivery Ring and continue to the $(g-2)$ storage ring in the MC-1 building. Figure 7.25 compares the Pbar beamline configuration with that to be used for $(g-2)$ and Mu2e operation. In general, the AP1, AP2 and AP3 lines will refer to the old Pbar beamline configuration and M1, M2, M3, M4 and M5 will refer to the beamline configuration for $(g-2)$ operation.

Figure 7.26 shows another view of the Muon Campus beamlines, including the experimental halls.

Most of the common improvements to the beamlines and Delivery Ring that benefit Mu2e, $(g-2)$, and future experiments will be incorporated into several Accelerator Improvement Projects (AIPs). They are the Recycler RF AIP, Cryo AIP, Beam Transport AIP, and Delivery Ring AIP. The Recycler RF AIP, as the name implies, will provide an RF system in the Recycler that is capable of forming the short 2.5 MHz bunches required by the experiments. The Cryo AIP provides cryogenics for the $(g-2)$ storage ring and to the Mu2e solenoids. The Beam Transport AIP will complete a connecting beamline between the Recycler and P1 Line and will be responsible for replacing magnets at key locations to improve aperture. The Delivery Ring AIP has numerous improvements that are of common benefit to both $(g-2)$ and Mu2e, such as the injection and abort/proton removal systems. Table 7.7 summarizes which improvements are contained in the various AIPs, as well as those that will be managed as part of the Mu2e and $(g-2)$ projects. Project Managers for the various projects will work closely together to ensure they interface properly. Virtually all of the work that is incorporated into the AIPs must be completed prior to beam operation to $(g-2)$.

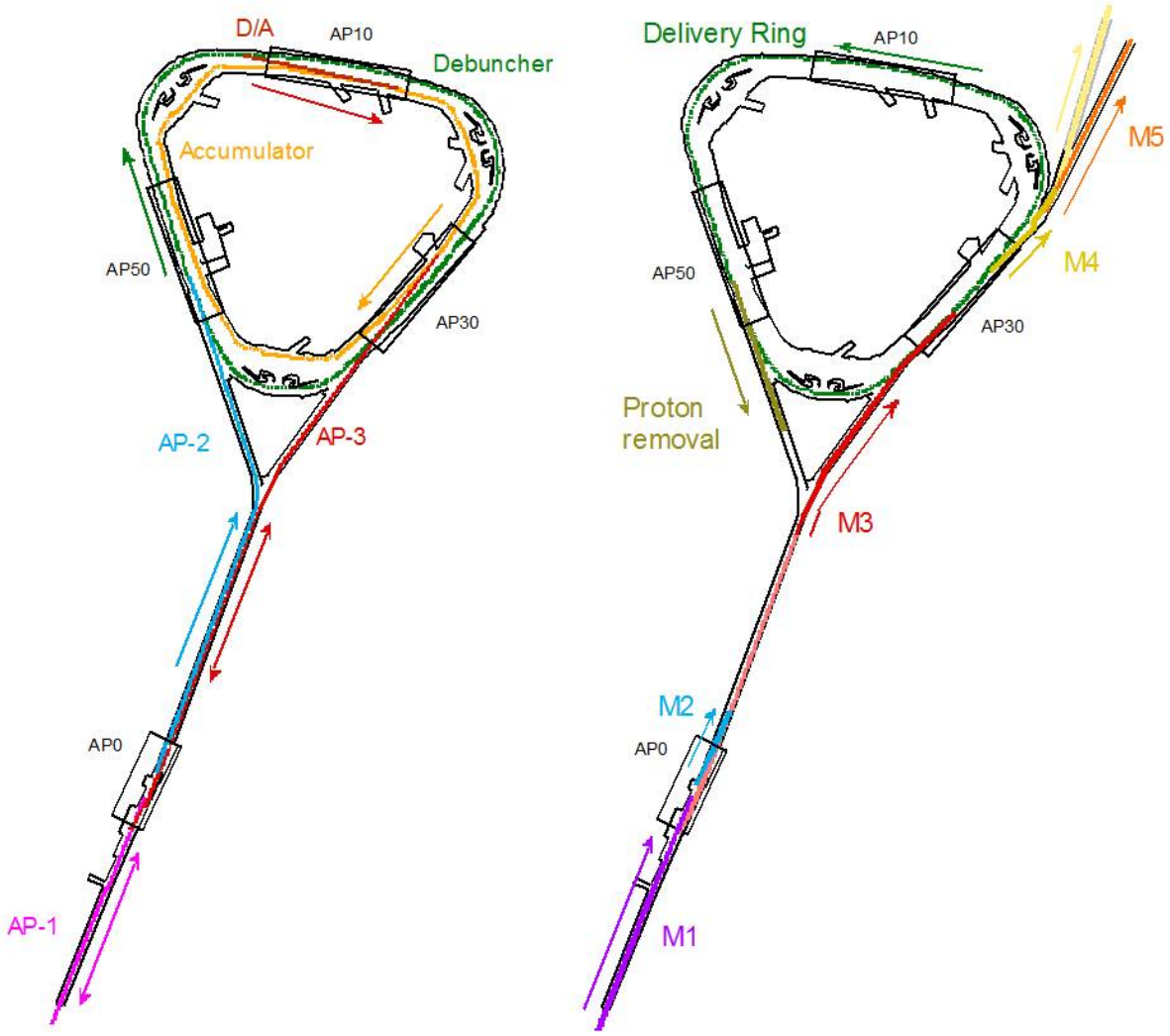

Figure 7.25: Layout of the Antiproton Source beamlines (left) and the reconfigured beamlines for $(g-2)$ operation (right).

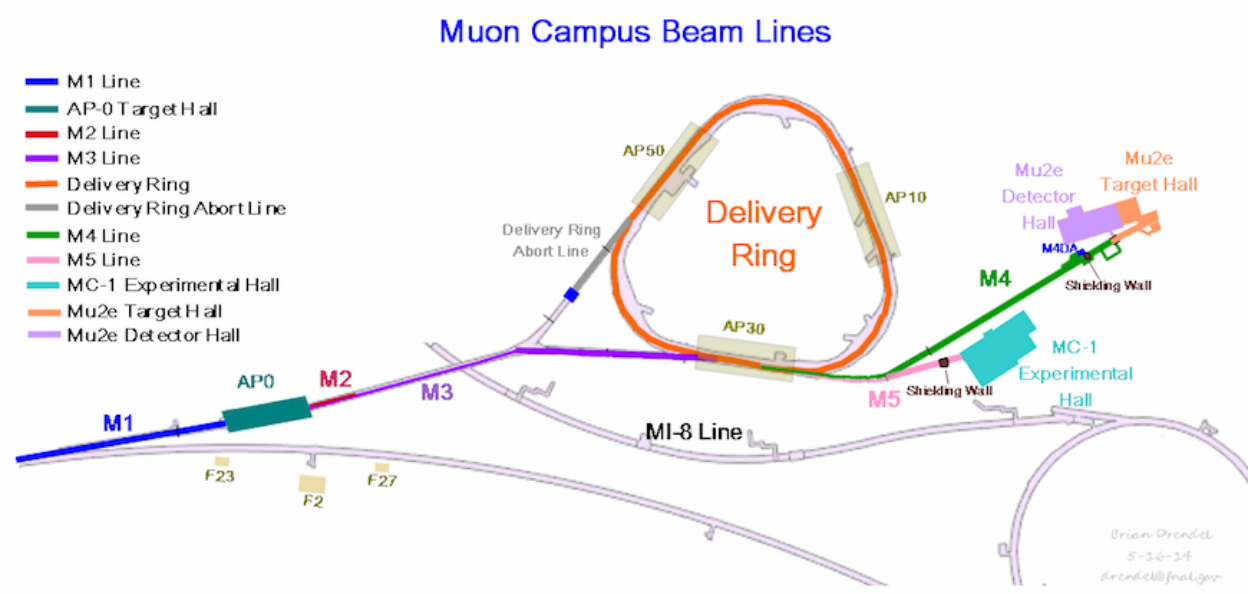

Figure 7.26: The Muon Campus beamlines and experimental halls.

Description	Project	Comment
Cryogenics	CR AIP	
Recycler RF upgrade	RR AIP	
Recycler extraction/P1 stub line	BT AIP	
P1,P2 and M1 aperture upgrade	BT AIP	**M1 final focus quadrupoles on ($g-2$)**
Reconfigure AP2 and AP3	**($g-2$)**	**New lines are called M2 and M3**
Final focus to AP0 Target Station	**($g-2$)**	
AP0 Target Station upgrades	**($g-2$)**	
Beam transport instrumentation	BT AIP	
Beam transport infrastructure	BT AIP	
Delivery Ring injection	DR AIP	
D30 straight section preparation	**($g-2$)**	
Delivery Ring modification	DR AIP	
DR abort/proton removal	DR AIP	
Delivery Ring RF system	*Mu2e*	
Delivery Ring controls	DR AIP	
Delivery Ring instrumentation	DR AIP	*DCCT and Tune measure are Mu2e*
Resonant extraction from DR	*Mu2e*	
Fast extraction from DR	**($g-2$)**	
Delivery Ring infrastructure	DR AIP	
Extraction line to split	**($g-2$)**	**Upstream M4 line**
Extraction line from split to Mu2e	*Mu2e*	*Downstream M4, including extinction*
Extraction line from split to ($g-2$)	**($g-2$)**	**Beamline to MC-1 building**

Table 7.7: Beamline, Delivery-Ring, and other upgrades and associated project: ($g-2$) project, Mu2e project, Delivery Ring Accelerator Improvement Project (DR AIP), Beam Transport (BT) AIP, Recycler RF (RR) AIP, and Cryo (CR) AIP.

7.5.3 Proton Beam Transport to the Target Station

Beam transport of the 8 GeV primary beam from the Recycler Ring (RR) to the Target Station closely resembles the scheme used to transport 120 GeV protons for antiproton production in Collider operation. The most notable differences are the change in beam energy and the switch from the Main Injector to the RR as the point of origin for the P1 line. The beamlines will be modified to 1) provide a connection between the RR and P1 line, 2) improve aperture to accommodate the larger beam size and intensity, and 3) reconfigure the final focus region in order to reach the desired spot size on the production target. Table 7.8 lists the beamlines connecting the RR with the Target Station and their respective lengths.

Beam Line	Length (m)
RR to P1	43
P1	182
P2	212
AP1 (M1)	144
RR to Target Total	581

Table 7.8: Recycler Ring to Target beamline lengths.

Recycler Ring to P1 line stub

Operation of $(g-2)$ and Mu2e requires the transport of protons from the RR rather than the Main Injector. A new transfer line from the RR to the P1 beamline will be constructed to facilitate proton beam transport from the RR to the Delivery Ring. This new beamline provides a way to deliver 8 GeV kinetic energy protons to the Delivery Ring, via the RR, using existing beam transport lines and without the need for new civil construction.

Beamline Design The P1 line is lower in elevation than the RR, thus the beam will be extracted downward. This will be accomplished with a horizontal kicker that will displace beam into the field region of a Lambertson magnet that will bend beam down. The kickers are located immediately downstream of the RR 520 location and the Lambertson will be just downstream of the RR 522 location. Due to space limitations, only two vertical bend centers made up of the Lambertson and a dipole are used in the new line. An integer multiple of 360° in betatron phase advance between the two bending centers is required to cancel the vertical dispersion from the bends. The new beamline needs to intercept the existing P1 line in a location that doesn't disturb the extraction trajectory from the Main Injector, which will be retained for SY120 operation. That junction point will be located near quadrupole Q703.The angles of both the Lambertson and the vertical bending magnet (V903, VBEND in Fig. 7.27) were obtained by matching the site coordinates from the RR to P1 line using TRANSPORT [16] code. Figure 7.27 shows the layout of the new line, with the existing P1 line drawn in red.

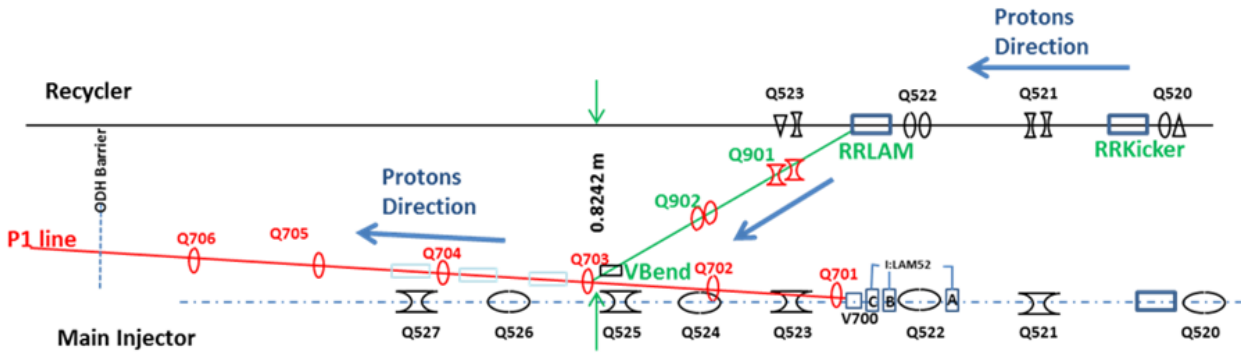

Figure 7.27: The new Recycler Ring to P1 connecting beamline.

Kickers The $(g-2)$/Mu2e extraction kicker will be of the same design as the kickers used during collider operation, but will be potted instead of using Fluorinert for electrical insulation. The physical dimensions and properties of the kickers are listed in Table 7.9. The plan is to reuse the ceramic vacuum chamber from old RR kicker magnets, which are slightly smaller than the standard RR vacuum chamber. The kicker system will be made up of two magnets producing 0.79 mr bend each for a total kick of 1.58 mr. The new kicker power supplies will be located in the MI-52 service building. Power supplies for the new beamline magnets will also be located at MI-52. This service building will be expanded to accommodate the new power supplies.

Recycler Extraction Kicker RKB-25	
Parameter	Value
Ferrite length	46.6 in
Case length	64.0 in
Insert length	67.78 in
Print number	ME-481284
Maximum strength (each)	0.279 kG m
Maximum kick (each)	0.94 mr @ 8 GeV/c^2
Required kick (each)	0.79 mr @ 8 GeV/c^2
Rise time, 3% - 97%	140 ns

Table 7.9: RR extraction kicker parameters.

Lambertson The Lambertson magnet will be rolled 2.7° from the vertical and V903 rolled -4.0° to provide a small horizontal translation in order to create the proper horizontal trajectory required to match to the P1 line. The V903 dipole magnet is a 1.5-m long "ADCW"-type that will provide a 21 mr bend, matching the bend of the Lambertson. There will be two permanent quadrupoles and two electromagnetic trim quadrupoles located between the Lambertson and vertical dipole magnets that make up the dogleg between the RR and P1 line. Due to space constraints, the permanent quadrupoles are shifted downstream from their

ideal locations by 0.25 m. A more detailed technical description of the design features of the new beam line stub can be found in Ref. [17]. Figure 7.28 shows the lattice functions from the Recycler to the AP0 Target Station.

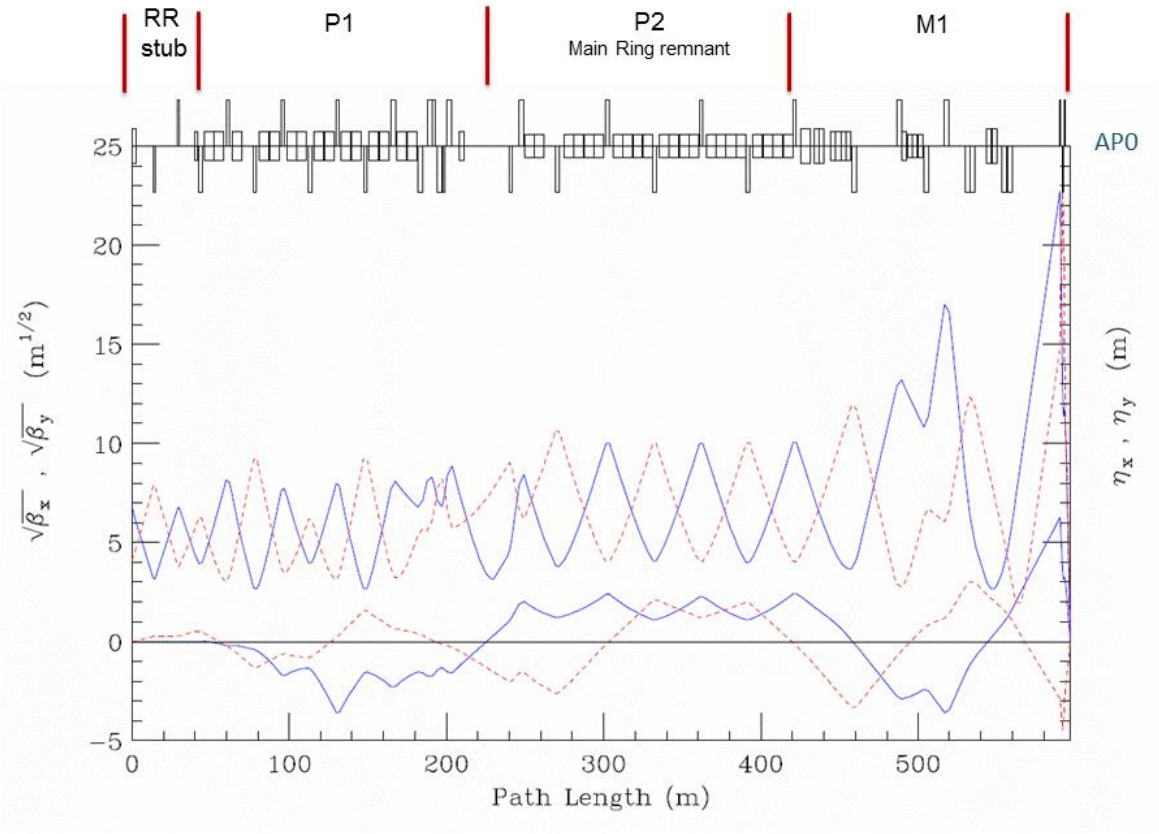

Figure 7.28: Lattice functions for primary beamlines from the Recycler to the Target Station.

Recycler orbit The RR extraction scheme incorporates a permanent horizontal 3-bump in the RR to improve aperture. The bump displaces the circulating beam outward 25 mm at the upstream end of the Lambertson (RLAM). Figure 7.29 shows the trajectories of the circulating and extracted beams, including the horizontal bump at the Lambertson. The bump is created by horizontal trim dipoles at the 524, 522 and 520 locations. The extraction kickers displace the extracted beam inward 25 mm at the same location. This creates a separation of the RR circulating beam and extracted beam at the front face of the Lambertson of 50 mm.

Apertures The Recycler extraction Lambertson has an adequate aperture for both the circulating and extracted beams. Figure 7.30 shows the footprint of both beams at the Lambertson for both a 10σ and 6σ beam size. The vertical bend magnet has a relatively

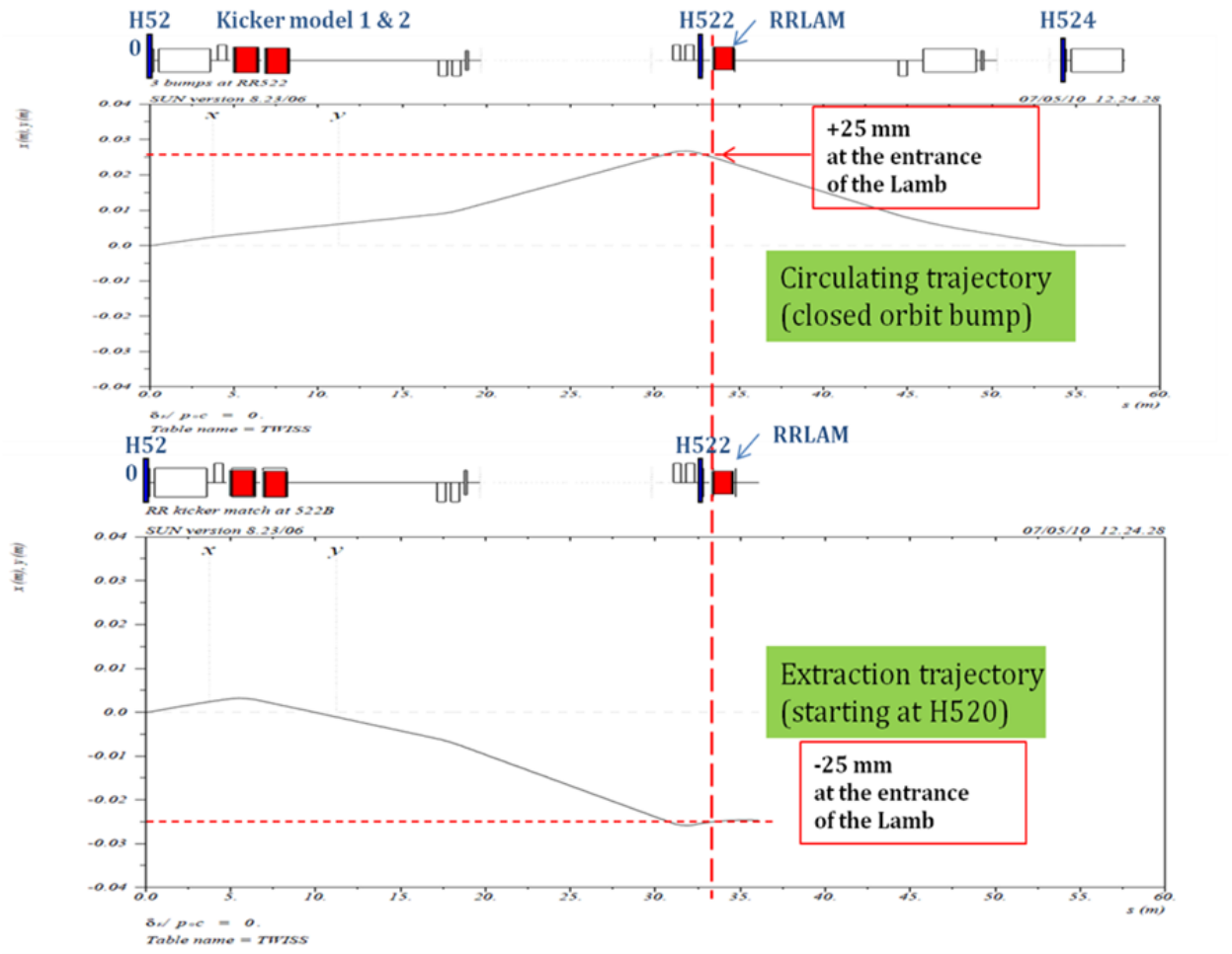

Figure 7.29: Horizontal trajectories for circulating and extracted beam from the Recycler.

small physical horizontal aperture, but is located where the horizontal beta functions are also small. The horizontal acceptance of the vertical dipole is actually larger than that of the Lambertson, despite the smaller physical aperture. The quadrupole and trim magnets are modeled after those in the Recycler and have good apertures.

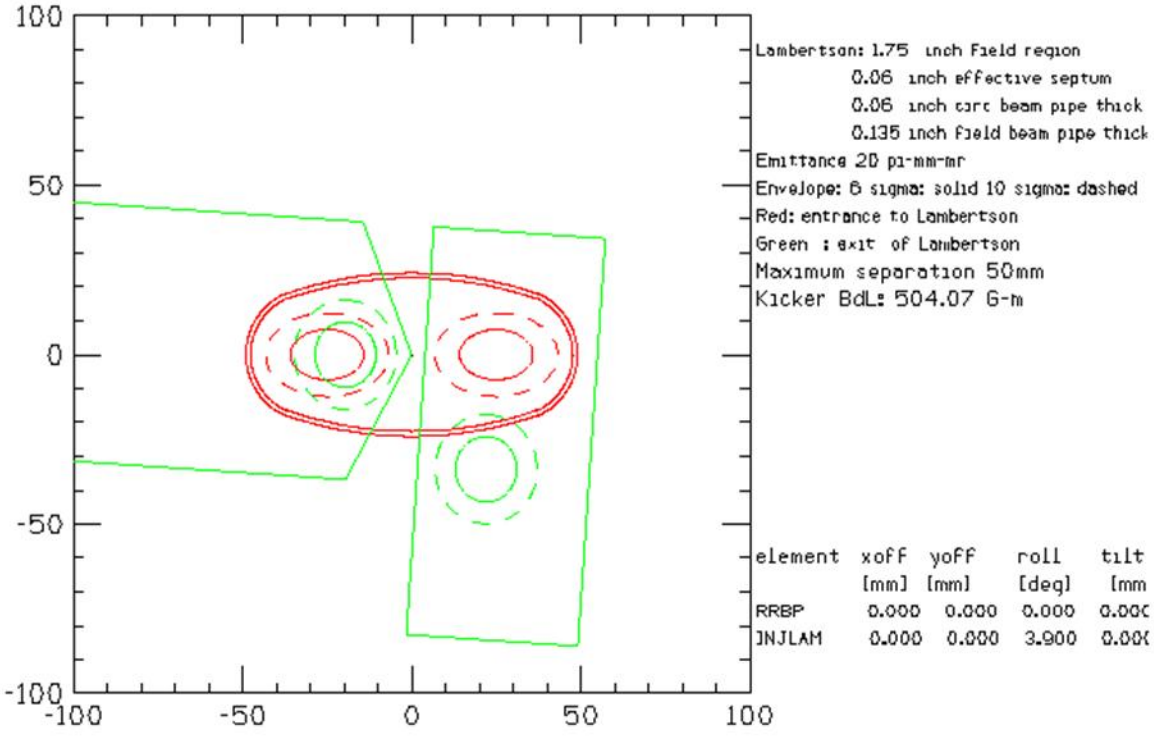

Figure 7.30: Beam sizes at the entrance (red) and exit (green) of the extraction Lambertson. The dashed outline represents 10σ and the solid outline 6σ beam for a normalized emittance of 18π mm-mr.

7.5.4 P1, P2 and M1 Aperture Improvements

The increased intensity and beam size planned for muon operation will lead to unacceptably high beam loss unless apertures are improved in the P1, P2 and M1 lines. Limiting apertures in these beamlines were identified during Collider Run II which simplified the process of identifying locations to improve for Muon operation. The elimination of M1 120 GeV operation for antiproton stacking provides an opportunity to improve the aperture utilizing weaker magnets that previously were not practical for use as replacements.

The introduction of the P1-line stub has eliminated several aperture restrictions that were associated with Main Injector extraction. In particular, the vertical C-magnets that follow the MI-52 Lambertson will be avoided with the new stub line. Most of the P1 line after the P1-line stub has good aperture, until the former junction area with the now decommissioned Tevatron. The vertical dipole at the 714 location was installed as a C-magnet because of its proximity with the Tevatron and has a small horizontal aperture. The decommissioning of the Tevatron allows the replacement of this magnet with a conventional dipole that will increase the horizontal acceptance by more than 50%. The new magnet must also be capable of producing enough field strength to operate at 120 GeV and support SY120 operation. The four Tevatron F0 Lambertsons will no longer be needed to inject protons into the Tevatron and can be removed to improve the aperture, also in the horizontal plane.

The P2 line will remain a dual-energy line supporting $(g-2)$ and SY120 operation, so the junction between the P2, M1, and P3 beamlines at F17 will remain. The aperture for both $(g-2)$ and SY120 operation will substantially improve with the proposed replacement of the F17 C-magnets with a large aperture CDA dipole magnet that both beams will pass through. The B3 dipole at the F-17 location has good aperture and will remain; the B3 and CDA will be bused together and run from one power supply. The B3 and CDA are powered to bend beam into the M1 line and not powered for SY120 beam that will continue from the P2 line into the P3 line. Figure 7.31 shows a comparison of the existing and planned magnet layouts at F17.

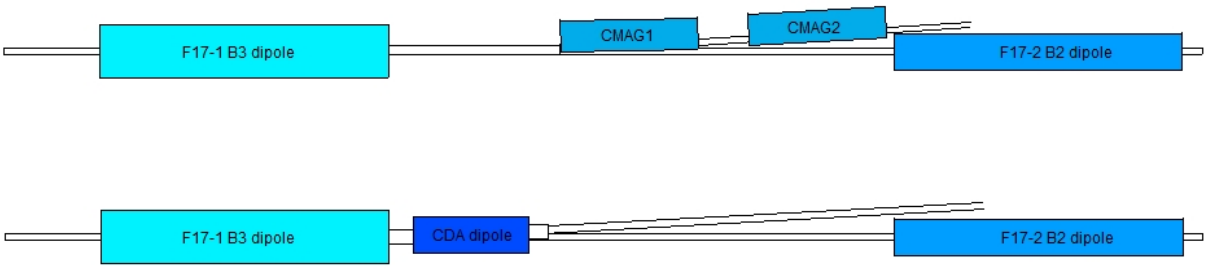

Figure 7.31: Existing *(upper)* magnet layout with two small aperture C-magnets and the planned *(lower)* layout with a single large aperture CDA dipole.

M1 will only operate at 8 GeV for $(g-2)$ operation, so the eight small-aperture EPB dipole magnets that make up the HV100 and HV102 strings can be replaced with larger-aperture, weaker dipoles. The number of dipoles can be reduced from four to two in each string. The 1.5 m MDC dipole magnets have a pole gap that is 2.25 in instead of 1.5 in and

provides more than a factor of two increase in acceptance. Several trims will also be replaced or relocated to complete the aperture upgrade. Replacement trims will be repurposed from the Accumulator. The final-focus region at the end of M1 is described separately in the next section. Table 7.10 is a listing of M1 Line magnets and highlights the magnets that have been changed to improve the physical apertures in the RR to Target Station lines. Reference [17] has a more detailed explanation of the devices used to improve the aperture and how the improvements will be implemented.

Magnet	Type	Current (A)	Power Supply
F17B3	B3	280.0	I:F17B3
F17CDA	**CDA**	**280.0**	**I:F17B3**
HT100	SY Bump	25.0	M:HT100
HV100A	**MDC**	**92.3**	**M:HV100**
HV100B	**MDC**	**92.3**	**M:HV100**
Q101	3Q120	4.8	M:Q101
VT11A	SY Bump	25.0	M:VT101A
VT101	**NDA**	**25.0**	**M:VT101**
Q102	3Q120	3.2	M:Q102
HV102A	**MDC**	**87.3**	**M:HV102**
HV102B	**MDC**	**87.3**	**M:HV102**
Q103	3Q120	7.2	M:Q103
Q104	3Q120	10.3	M:Q104
Q105A	3Q120	2.6	M:Q105
Q105B	3Q120	2.6	M:Q105
M:HT105	**NDA**	**25.0**	**M:HT105**
V105A	EPB	56.1	M:V105
V105B	EPB	56.1	M:V105
Q106A	3Q120	0.9	M:Q106
Q106B	3Q120	0.9	M:Q106
Q107A	3Q120	0.0	M:Q107
Q107B	3Q120	0.0	M:Q107
VT108A	**NDA**	**25.0**	**M:VT108**
HT108A	**NDA**	**25.0**	**M:HT107**
VT108B	**NDB**	**25.0**	**M:VT108**
HT108B	**NDB**	**25.0**	**M:HT107**
Q108A	**SQD**	**369.2**	**M:Q108A**
Q108B	**SQE**	**421.9**	**M:Q108B**
Q108C	**SQD**	**372.7**	**M:Q108C**

Table 7.10: M1-line dipoles, quadrupoles, and trims (HT and VT prefix). Magnets that were changed to improve aperture are shown in bold (the old Q108A&B and Q109A&B 3Q120 quadrupoles were also removed).

Final Focus Region

The desired spot size on the production target, a proton beam σ in both planes of 0.15 mm, is the same as what was used in antiproton production during collider operation. Because the beam momentum is 8.89 GeV/c for $(g-2)$ operation instead of the 120 GeV/c that was used for antiproton production, much smaller beta functions are required to achieve this spot size (0.068 m vs. 0.878 m, respectively). The existing quadrupole configuration in AP1 cannot produce the desired spot size and will need to be changed in order to achieve the desired spot size with good beam transmission. Figure 7.32 shows a modified version of the scheme proposed in Ref. [18], where a quadrupole triplet replaces the last quadrupole, PQ9B, in the AP1 line. Figure 7.32 shows the optics of the entire M1 line, with the final focus occurring on the far right. The quadrupoles making up the triplet need to be as short as possible while concurrently producing a very strong integrated gradient. The PQ8A&B and PQ9A magnets are not powered and can be removed to improve aperture. Larger aperture NDA and MDB trim magnets from surplus Pbar inventory will replace HT107 and VT108 to provide adequate aperture.

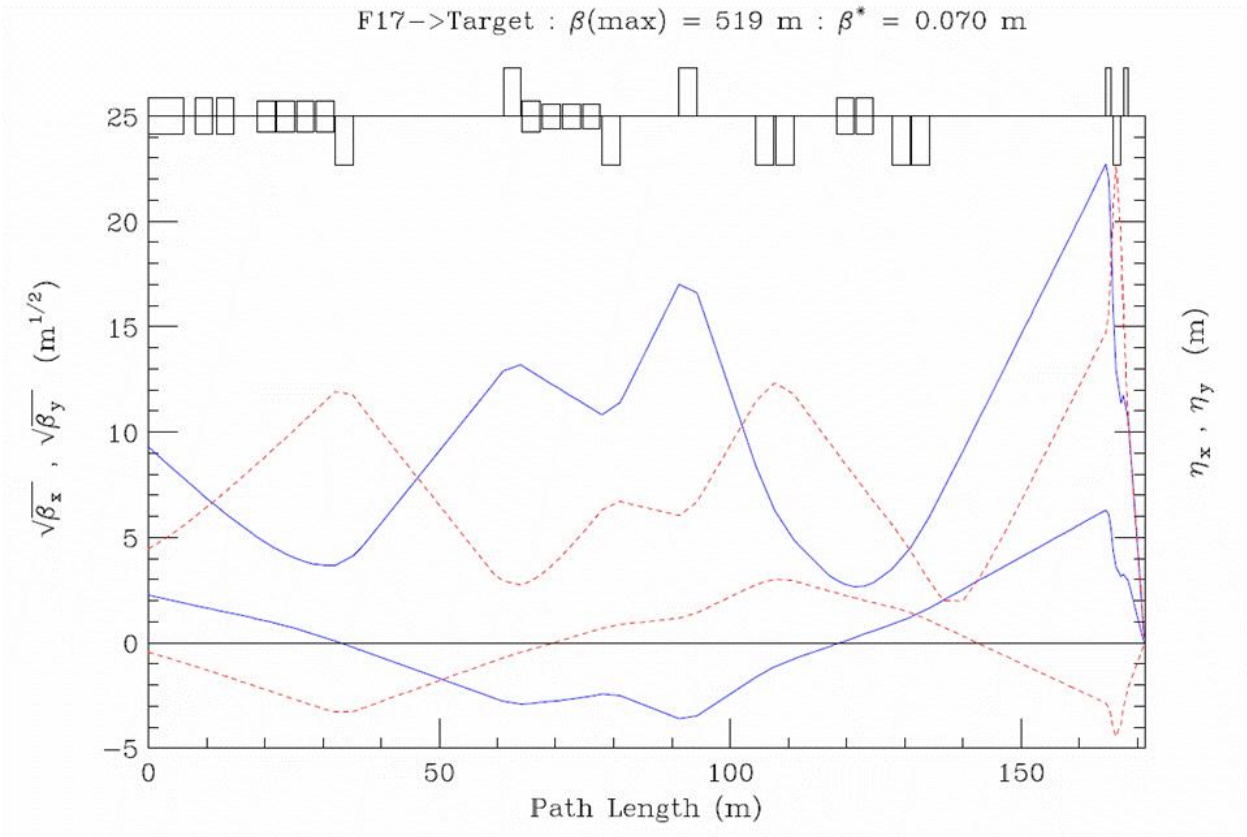

Figure 7.32: Beta functions (horizontal is blue, vertical is red in upper traces) and dispersion functions (horizontal is blue, vertical is red in lower traces) for the M1 line. The Final Focus quadrupole triplet is on the far right side of the plot.

The best compromise between maximizing integrated field, minimizing quadrupole length and providing adequate aperture, from available magnets, is to use a triplet made of an SQD – SQE – SQD combination. The three magnets will all be repurposed from the decommissioned Pbar AP2 and AP3 lines. The quadrupoles are required to run up to 425 A in order to achieve the desired 0.15-mm spot size, which is close to the highest currents these types of magnets have ever operated at. The SQE magnet in the middle of the triplet is the strongest Pbar quadrupole available and operates at the highest current of the triplet quadrupoles.

7.5.5 M2 and M3: Pion to muon decay beamlines

The M2 and M3 lines are designed to capture as many magic-momentum muons from pion decay as possible. The M2 line will be rebuilt from parts of the former AP2 line, which transports secondary beam from the Target Station. The M3 line, primarily rebuilt from the former AP2 and AP3 lines, begins as a target-bypass which will be used by the Mu2e experiment to transport primary 8-GeV protons. For $(g-2)$, the M2 line crosses the tunnel into the M3 line at the upstream end of the Transport Enclosure. Focusing of the secondary beam within the Target Station is limited by available space in the target vault. Immediately following the Target Station, the M2 line starts with an existing series of four quadrupoles, followed by eight more quadrupoles and a dipole, which then match into the lattice of the M3 line. Figure 7.33 shows the existing Pbar beamlines versus the new configuration with the M2 line merging into the M3 line.

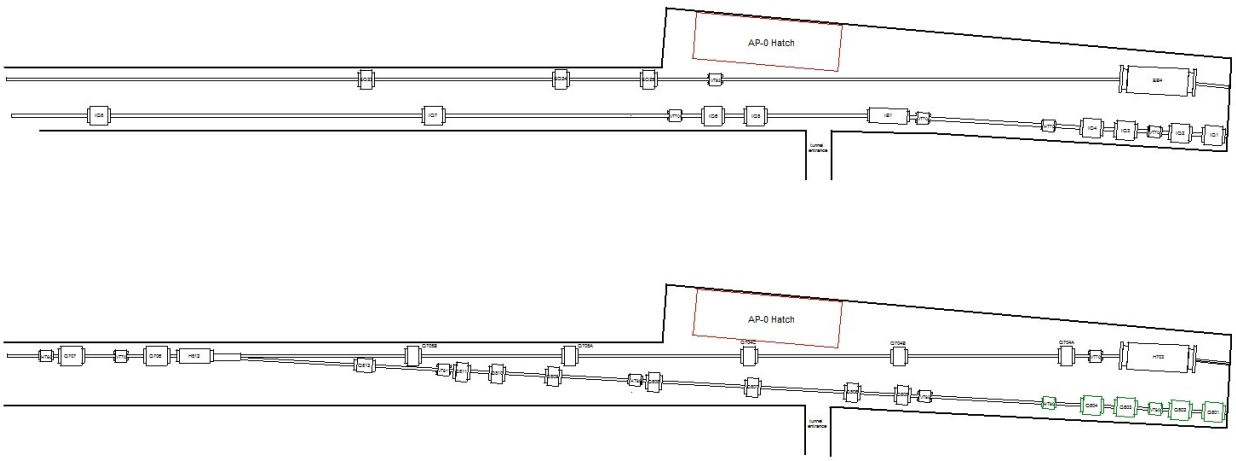

Figure 7.33: Present AP2 and AP3 configuration downstream of Target Vault *(top)* and M2 line merging into M3 line *(bottom)*.

Design layout

With the exception of a few specialized insertions, the upstream M2 and M3 lines largely track the trajectories of the former AP2 and AP3 lines. The first 22 m of M2, including the Target Station, remains unchanged from the AP2 configuration. Pions collected from the lithium lens are transported into the M2 line via the existing PMAG dipole, which bends the beam through 3° (52 mr). A second dipole from AP2, which had bent the beam another 3° to align it with the left side of the tunnel, has been removed. The M2 line continues across the tunnel, intersecting the M3 line 28 m further downstream (50 m total M2-line length from the lithium lens to the M3 line). At the intersection point, a large aperture 5D32 dipole provides the second 3° bend required for beam to match the M3-line trajectory. The magnet layout in the vicinity of the M2/M3 merge is constrained by the physical dimensions of the magnets, summarized in Fig. 7.34.

To cancel the horizontal dispersion created by PMAG, there is 540° of horizontal phase advance between the PMAG dipole in the Target Station and the 5D32 switch dipole at the M2/M3 merge. The 5D32 dipole has an unusually large pole width that can accommodate both the beams from the M2 line and the upstream M3 line. The magnet is simply switched on and off to change between the $(g-2)$ and Mu2e modes of operation. The 5D32 dipole also has a 4.125-in pole gap that can provide more than 40π-mm-mr acceptance with the 24-m vertical beta function at the downstream end of the magnet. The optics of the M2 line and the M3 line immediately after the merge is shown in Fig. 7.35.

The M3 line between the M2/M3 merge and Right Bend insertion has short matching sections on each end with a long transport FODO section making up most of that part of the line. The FODO cells are characterized by a 90° phase advance and 5.50-m half-cell length. The M3 line upstream of the Right Bend follows the path of the old AP3 line and can be built with existing AP2 and AP3 devices. This part of M3 must maintain small beta functions to serve as a continuation of the muon decay channel. Since the M3 line must also operate with 8-GeV protons for Mu2e operation, scaled magnet currents must be within power-supply and magnet operating limits. Figure 7.36 shows the beta and dispersion functions of M2 and M3 upstream of the Right Bend.

A specialized insertion created by two SDB dipoles bends the beam horizontally 18.5° (323 mr) to the right, aligning with the existing AP3 line. The 18.5° horizontal bend has the two bend centers separated by a quadrupole triplet of SQEs to generate the 180° of betatron phase advance needed to locally cancel the horizontal dispersion. There are short matching sections on either side of this insertion to transition in and out of FODO lattices. The beam continues for 63.0 m to the beginning of the geometric and optical matching section between the M3 line and the Delivery Ring (DR) injection point in the D30 straight section. The FODO cells in this region are characterized by 72° of phase advance and a half-cell length of 5.613 m.

This final injection section satisfies multiple, interleaved design constraints:

- Providing the optical match between the lattice functions of the M3 line and those of the DR;
- A 86 mr horizontal right bend to align with the D30 straight section, and;
- An overall 4-ft elevation drop from M3 to the DR, performed in two steps.

The first step of the drop in elevation uses two MDC dipoles bending through 67.8 mr. The second down-bend is provided by a SDD dipole bending downward at 102.3 mr.

Embedded in the level beamline section between the first and second elevation step changes, two MDC dipoles bend horizontally, each through 43.1 mr to align the trajectory with the D30 straight section. The dipoles form an achromatic bend embedded in the achromatic vertical descent to the Delivery Ring. The final nine quadrupoles in the line perform the optical match between the 72° FODO cells and the Delivery Ring. Figure 7.37 shows the path of the M2 and M3 lines from the Target Station to the Delivery Ring.

The final stages of injection occur entirely in the vertical plane, with the final up-bend produced by a combination of a C-magnet (also called a septum dipole) in the beamline, followed by a large-aperture focusing quadrupole Q303 and a pulsed magnetic septum dipole

in the Delivery Ring. The C-magnet bends upward 35 mr, and steers the beam 11.6-cm high off-axis through Q303, generating another 30 mr of upward vertical kick. The septum adds 35 mr of bend up. Three kicker modules upstream of quad Q202 close the trajectory onto the orbit of the Delivery Ring. Figure 7.38 shows the optics for this part of the M3 line.

The total beamline length from the face of the target-station lithium lens to mid-quad Q202 in the Delivery Ring is 296 m. Parameters of the main magnets are listed in Table 7.11. Figure 7.39 shows the complete path of the $(g-2)$ beam through M2 and M3 from the Target Station to the Delivery Ring.

Magnet	Type	Current (A)	Power Supply
Q801	SQC	95.2	D:Q801
Q802	SQC	107.0	D:Q802
VT802	NDB	25.0	D:VT802
Q803	SQC	107.0	D:Q802
Q804	SQC	132.3	D:Q804
HT804	NDB	25.0	D:HT804
VT804	NDB	25.0	D:VT804
Q805	SQA	45.7	D:Q805
Q806	SQA	260.9	D:Q806
Q807	SQA	260.9	D:Q806
Q808	SQA	260.9	D:Q806
HT808	NDB	25.0	D:HT808
Q809	SQA	260.9	D:Q806
Q810	SQA	77.7	D:Q810
Q811	SQA	279.9	D:Q811
VT811	NDB	25.0	D:VT811
Q812	4Q24	143.3	D:Q812
H812	5D32	903.6	D:H812
		M2/M3 merge	
Q706	SQD	82.7	D:Q706
VT706	NDB	25.0	D:VT706
Q707	SQD	104.4	Q707
HT707	NDB	25.0	D:HT707
Q708	SQB	83.8	D:Q708
Q709	SQC	94.7	D:Q709
HT709	NDB	25.0	D:HT709
Q710	SQC	94.7	D:Q709
Q711	SQC	94.7	D:Q709
Q712	SQC	94.7	D:Q709
Q713	SQC	94.7	D:Q709
Q714	SQC	94.7	D:Q709
Q715	SQC	94.7	D:Q709
Q716	SQC	94.7	D:Q709
Q717	SQC	94.7	D:Q709
Q718	SQC	94.7	D:Q709
HT718	NDB	25.0	D:HT718
Q719	SQC	94.7	D:Q709
Q720	SQC	94.7	D:Q709
Q721	SQC	94.7	D:Q709
Q722	SQC	94.7	D:Q709
VT722	NDB	25.0	D:VT722
Q723	SQC	94.7	D:Q709
Q724	SQC	87.3	D:Q724
VT724	NDB	25.0	D:VT724
HT724	NDB	25.0	D:HT724

Magnet	Type	Current (A)	Power Supply
Q725	SQD	74.8	D:Q725
Q726	SQB	88.5	D:Q726
H726	SDB	364.1	D:H726
Q727	SQE	84.7	D:Q727
Q728	SQE	81.4	D:Q728
VT728	NDB	25.0	D:VT728
D:Q728	SQE	84.7	D:Q727
H729	SDB	364.1	D:H726
Q730	SQC	77.0	D:Q730
Q731	SQC	77.0	D:Q730
HT732	NDA	25.0	D:HT732
Q732	SQC	77.0	D:Q730
Q733	SQC	77.0	D:Q730
Q734	SQC	77.0	D:Q730
Q735	SQC	77.0	D:Q730
Q736	SQC	77.0	D:Q730
VT736	NDA	25.0	D:VT736
Q737	SQC	77.0	D:Q730
Q738	SQC	77.0	D:Q730
Q739	SQC	77.0	D:Q730
HT739	NDA	25.0	D:HT739
Q740	SQC	77.0	D:Q730
Q741	SQC	77.0	D:Q730
Q742	SQC	90.0	D:Q742
V742	MDC	307.7	D:V742
HT742	NDA	25.0	D:HT742
Q743	SQB	73.3	D:Q743
VT743	NDB	25.0	D:VT743
V743	MDC	307.7	D:V742
Q744	SQB	72.7	D:Q744
HT744	NDA	25.0	D:HT744
H744	MDC	192.4	D:H744
Q745	SQE	100.7	D:Q745
Q746	SQD	90.0	D:Q746
Q747	SQD	90.0	D:Q746
Q748	SQE	100.7	D:Q745
H748	MDC	192.4	D:H744
Q749	SQC	89.6	D:Q749
Q750	SQD	219.8	D:Q750
V750	SDD	428.1	D:V750
Q751	4Q16	57.5	D:Q751
Q752	4Q16	57.5	D:Q751
ICMAG	MSDA	248.9	D:ICMAG
Q303 (DR)	LQE	456.5	D:QT303
ISEP	SEPT	8,750.0	D:ISEP

Table 7.11: M2- and M3-line dipoles, quadrupoles and trims (HT and VT prefix) from the Target Station to the Delivery Ring.

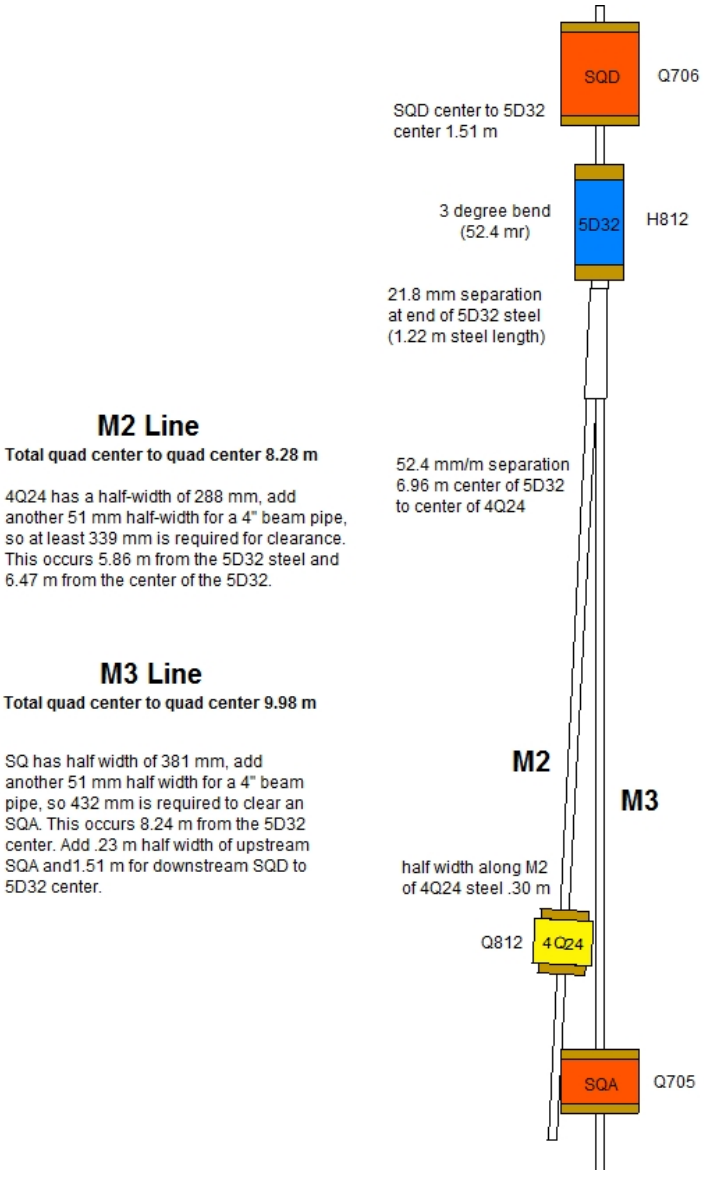

Figure 7.34: M2/M3 merge geometry.

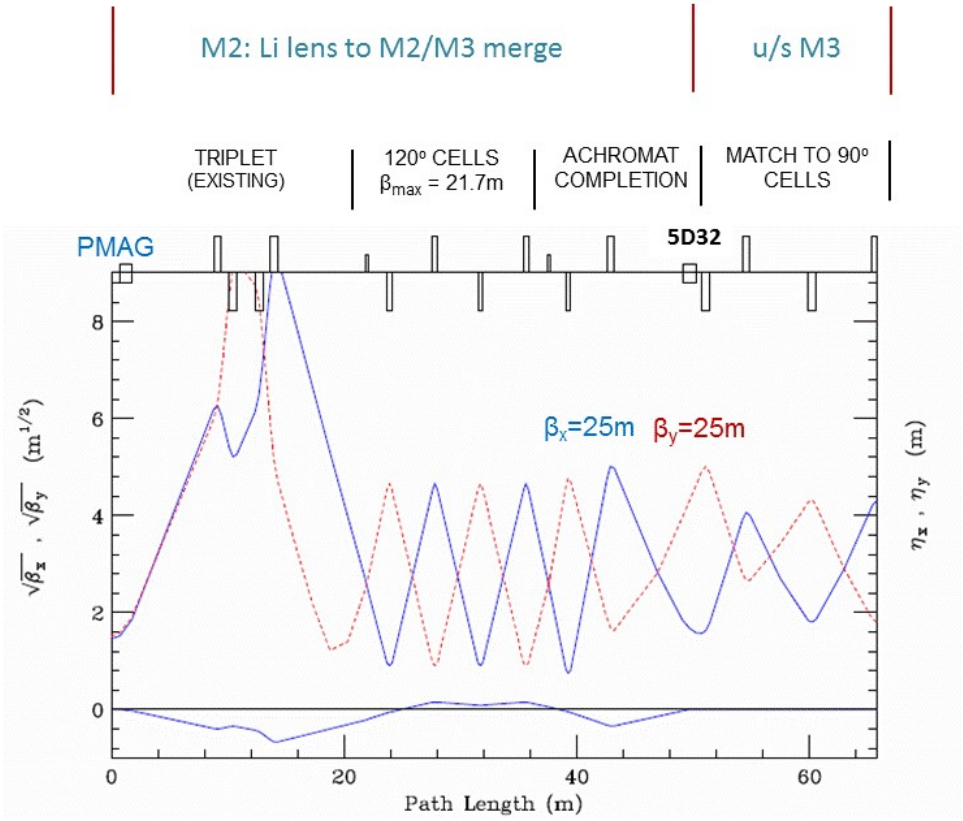

Figure 7.35: M2-line beta functions above and dispersion functions below (horizontal blue and vertical red), including the 5D32 dipole at the M2/M3 merge, and match into M3.

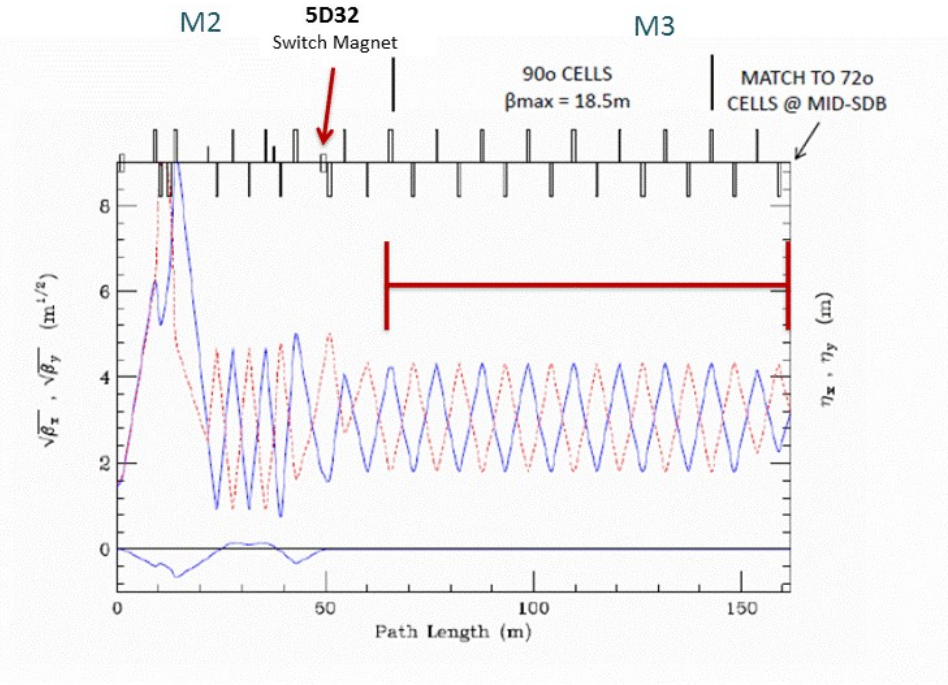

Figure 7.36: M2- and M3-line beta functions above and dispersion functions below (horizontal blue and vertical red), ending at the first "Right Bend" dipole.

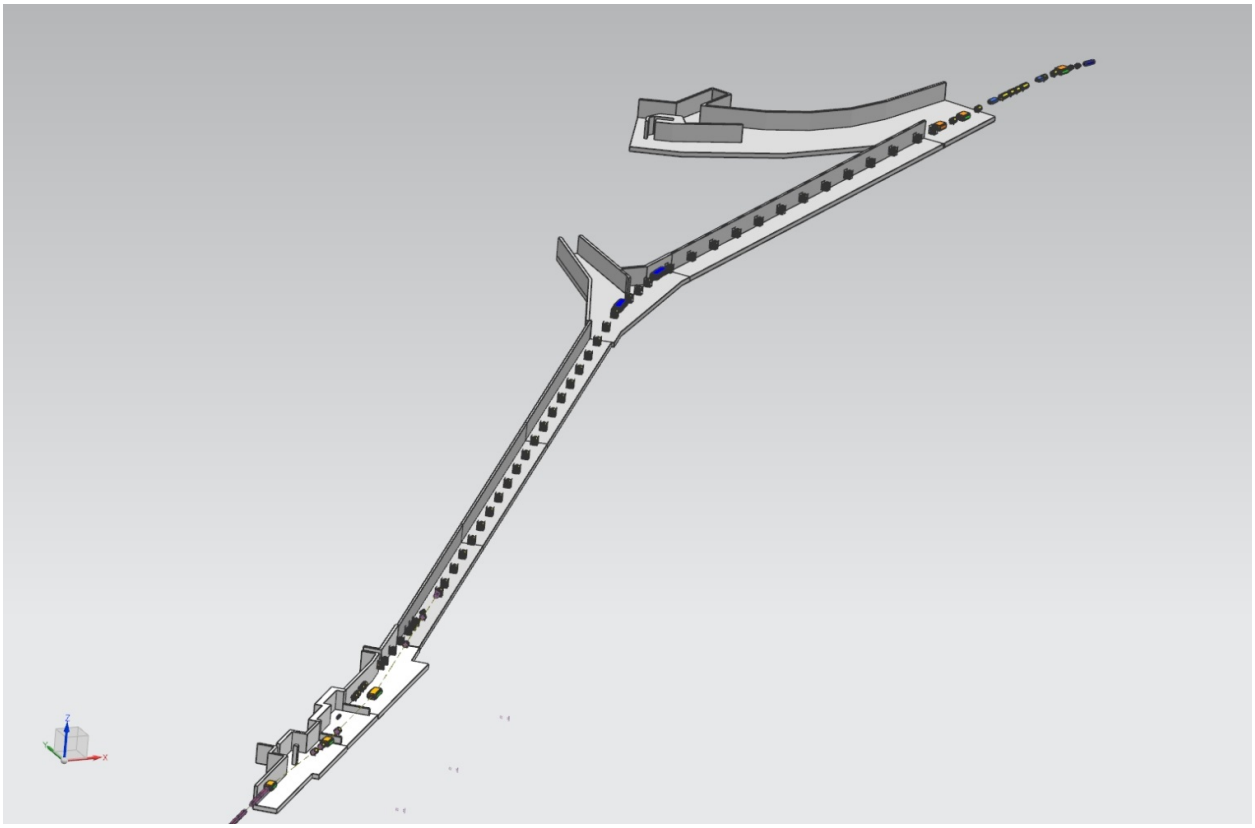

Figure 7.37: M2 and M3 lines from Target Station to Delivery Ring.

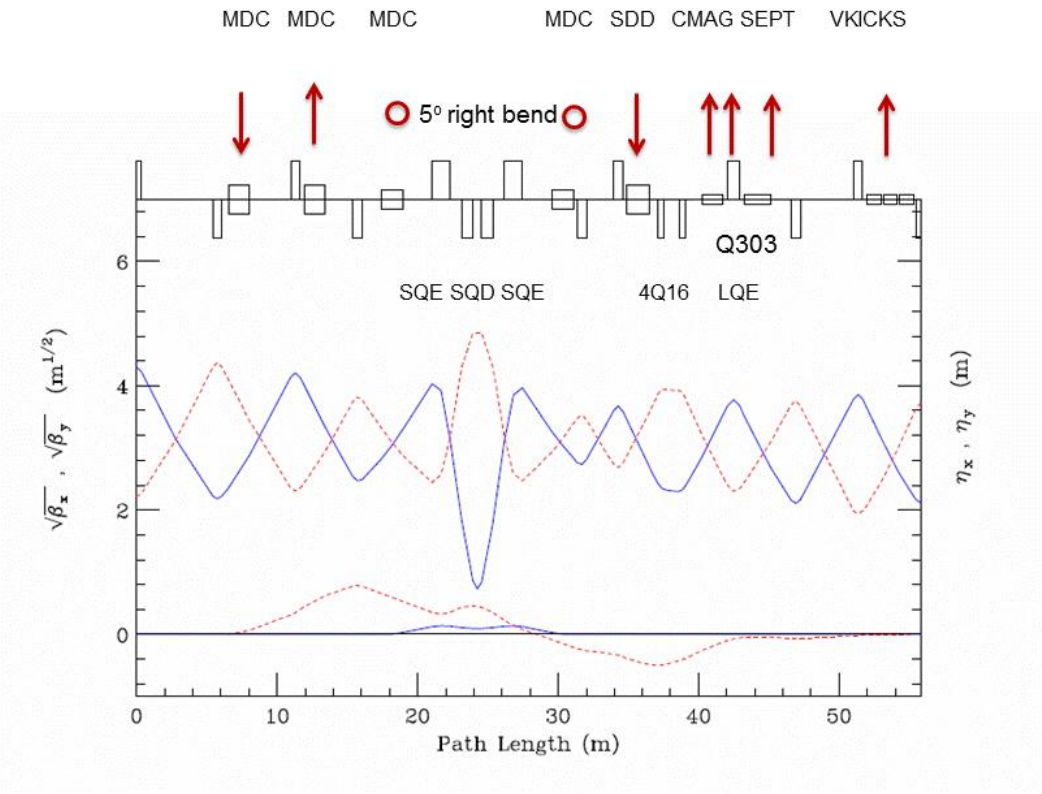

Figure 7.38: Downstream section of the M3 line, through the vertical and horizontal translations to match into the Delivery Ring, beta functions above and dispersion functions below (horizontal blue and vertical red).

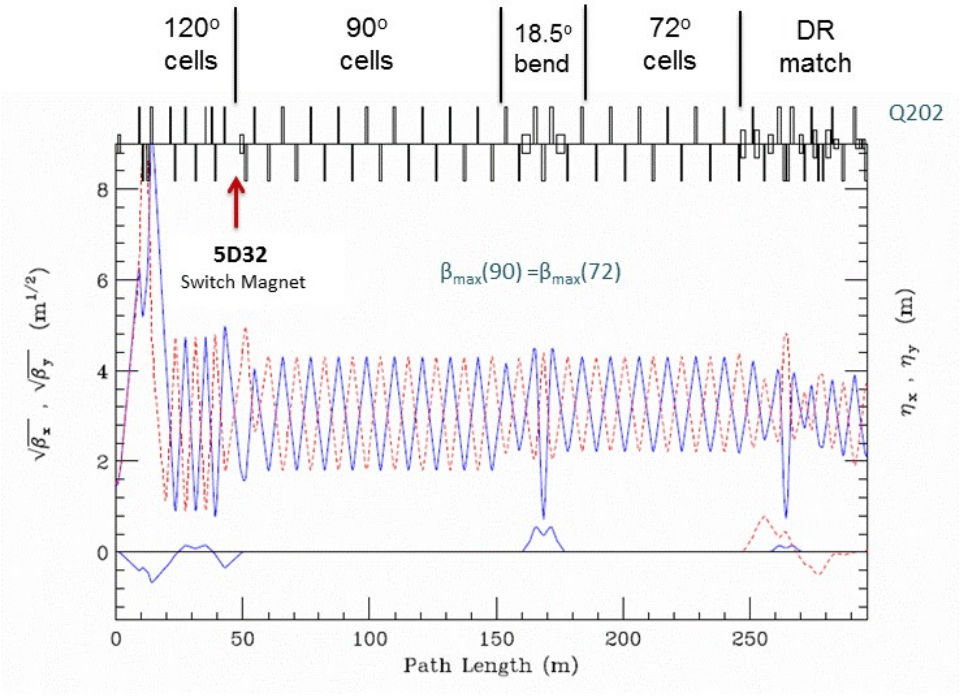

Figure 7.39: M2 and M3 lines from the Target Station to the Delivery Ring.

7.5.6 Delivery Ring

The Pbar Debuncher ring will largely remain intact for $(g-2)$ operation and will be renamed the Delivery Ring for its new role in providing muons to the experiment. A considerable amount of equipment left over from Pbar operation will need to be removed from the Debuncher. Most of the equipment targeted for removal was used for stochastically cooling the antiproton beam during collider operation and is not needed for $(g-2)$. Some of these devices also have small apertures, so the ring acceptance will be improved with their removal. The cooling tanks in the D30 straight section also need to be removed to provide room for the new injection and extraction devices.

The Pbar Accumulator ring will not be needed for $(g-2)$ and Mu2e operation and will become a source of magnets, power supplies and other components for use in the reconfigured beamlines. In particular, the downstream section of M3 and the M4 (extraction) line will be largely made up of former Accumulator components. Some larger-aperture magnets will also be needed in the injection and extraction regions and will come from the Accumulator or other surplus sources.

Rings Lattice and Acceptance

The original design lattice for the Debuncher will be used for the Delivery Ring with few modifications. The lattice has a 3-fold symmetry with additional mirror symmetry in each of the three periods, with three zero-dispersion straight sections: D10, D30 and D50. The original lattice parameters were largely dictated by the requirements for Pbar stochastic cooling and the RF systems. The Debuncher was designed with a large transverse and longitudinal momentum acceptance in order to efficiently RF-debunch and stochastically cool antiprotons from the production target. This lattice design is also well suited for $(g-2)$ operation. During Collider Run II, the original lattice was distorted somewhat in order to reduce the beam size in the stochastic cooling tanks that had limiting apertures. Since these tanks will be removed, the lattice that will be used for $(g-2)$ will revert back to an earlier Debuncher optics that incorporated improvements over the original design lattice. Figure 7.40 shows the lattice functions for one period of the Debuncher.

It should be noted that the design acceptance of the Debuncher was 20π mm-mr, while the (g-2) acceptance requirement is 40π mm-mr. During the 25 years of Pbar operation, numerous aperture improvements were undertaken to boost the acceptance of the Debuncher. After the final Collider Run II aperture improvements were put in place in 2007, the measured acceptance of the Debuncher was as high as 33π mm-mr in both transverse planes. The $(g-2)$ design goal of a 40π mm-mr acceptance for the Delivery Ring, while reusing as much of the original equipment as possible, presents a difficult challenge.

The transverse acceptances of the Debuncher dipole, quadrupole, sextupole, and trim magnets are quite large. The smallest magnet acceptance is in the vertical plane of the dipoles and is approximately 54π mm-mr on one end, growing to 79π mm-mr on the other end. The dipoles have a 90π-mm-mr or larger horizontal acceptance (90π-mm-mr for the $\pm 2\%$ momentum spread and locations with the largest dispersion) and the other magnets have a 100 π-mm-mr or larger acceptance in both planes. Since the original Debuncher lattice will not be significantly changed for $(g-2)$ operation, the main Delivery-Ring magnets will

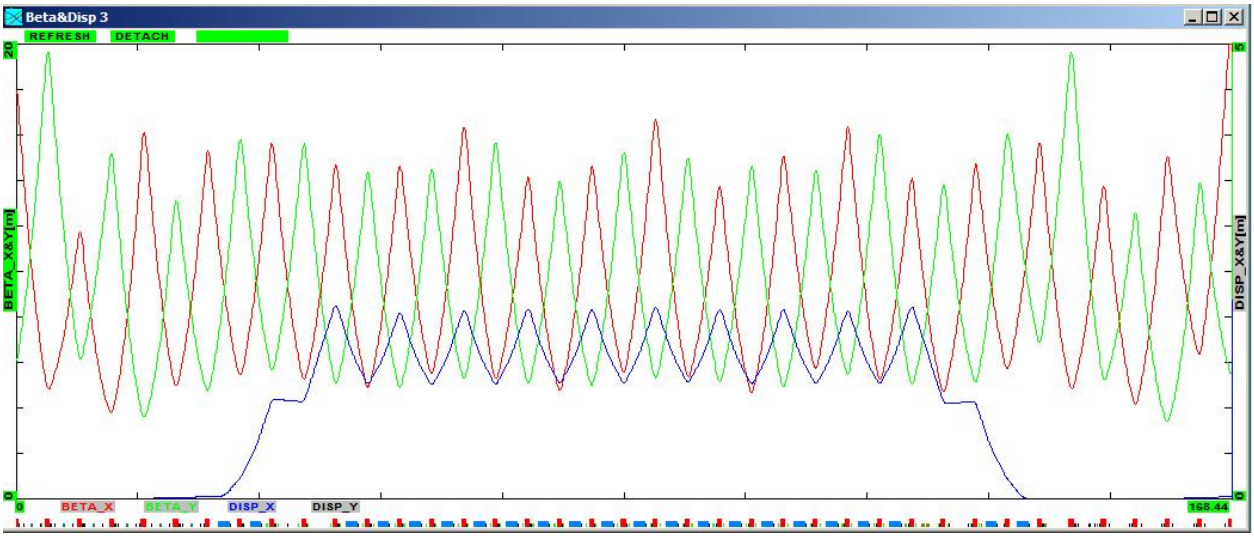

Figure 7.40: Debuncher/Delivery Ring lattice functions through 1/3 of the ring. β_x is in red, β_y in green, and horizontal dispersion in blue.

not be limiting apertures. In general, devices with a physical aperture of 50 mm or greater provide an acceptance of over 40π mm-mr in the Debuncher, and select locations can provide that acceptance for devices that have an aperture of 40 mm, as long as they are relatively short in length.

During Collider operation, the smallest physical apertures in the Debuncher came from stochastic cooling tanks, RF cavities, instrumentation, and devices used for injecting and extracting beam. Many of these devices will be removed as part of the repurposing of the Debuncher for the muon experiments. Some of these devices, most notably the kickers, will be retained in the interest of economy and/or complexity and lead-time of manufacture. Other devices, such as the injection septum, will be new devices with necessarily small physical apertures in order to provide enough bend strength.

There is only one RF cavity planned for the Delivery Ring, which is needed to support Mu2e operation and will have an aperture similar to the Debuncher rotator cavities (approximately 80 mm). Since the rotator cavities had an acceptance that was greater than 100π mm-mr, the new cavity will have ample aperture for use in both Mu2e and $(g-2)$ operations. RF cavities used for antiproton production will be removed prior to $(g-2)$ operation. A diagnostic RF system, DRF-3, will remain to facilitate closed orbit measurements in the Delivery Ring.

Many of the beam detectors used during Pbar operation had small physical apertures in order to improve sensitivity. Since the beam intensities when running $(g-2)$ are expected to be even smaller than those seen during Pbar operation, designers will need to be mindful of the aperture needs of the $(g-2)$ experiment. Similarly, when instrumentation is being considered for reuse in the Delivery Ring, the physical aperture and proposed tunnel location will be analyzed for adequate acceptance.

Both injection from the M3 line and extraction to the M4 line take place in the D30 straight section. Injection will be located in the upstream half of the straight section, and the pulsed magnetic septum and kicker magnets will have small apertures in order to provide

adequate bending strength. The septum has a small aperture in both planes, while the kicker is primarily limited in the horizontal plane. The septum is a modified Booster-style (BSE) magnetic septum magnet. The septum modifications involve increasing the pole gap from 28 mm to 47 mm in order to greatly improve the horizontal acceptance, and reducing the septum thickness from 14 mm to 9 mm to increase the vertical acceptance. The injection kicker system will be made up of two surplus Pbar AP4 injection kicker magnets. The horizontal aperture is only 41 mm and will likely be one of the limiting apertures of the Delivery Ring. The extraction kicker system will be made up of two Pbar extraction kicker magnets. They have a vertical aperture of 41 mm and will also be one of the limiting apertures of the Delivery Ring.

Kickers and Septa

The kickers and septa required for $(g-2)$ operation will need to operate at a much higher frequency than that used for antiproton production, with peak rates increasing as much as a factor of 30. In an effort to make the new kicker systems more economical and eliminate a long lead-time device, existing Pbar kicker magnets will be reused. Kickers will be required for injection and extraction from the Delivery Ring as well as for proton removal. Table 7.12 compares kicker parameters for existing Pbar systems to the specifications for the $(g-2)$ injection and proton-removal kickers. The rise and fall time specifications for $(g-2)$ are generally less strict than what was needed for antiproton production, due to the short bunch length of the muons (and protons). Decreasing the rise time of the proton removal kicker, however, will reduce the number of turns required in the Delivery Ring to adequately separate the protons from the muons. Although the Pbar kicker magnets are suitable for reuse, new power supplies will be needed to operate at the increased rate. Resistive loads for the kickers will need to be cooled with Fluorinert. A single Fluorinert distribution system is planned, with piping bridging the distance between the load resistors from kickers in the D30 and D50 straight sections.

Kicker (modules)	Integrated Field (kG-m)	Kick Angle (mr)	Rise Time 95%/5% (ns)	Fall Time 95%/5% (ns)	Flat Top Time (ns)
Debuncher Extraction (3)	1.34	4.6	150	150	1500
Debuncher Injection (3)	1.81	6.1	185	185	1500
Delivery-Ring Injection (2)	0.64	6.2	n/a	800	300
Delivery-Ring Extraction (2)	0.77	5.8	450	n/a	200
Delivery-Ring Proton Removal (1)	0.52	6.2	180	n/a	270

Table 7.12: Existing Pbar (top) and future $(g-2)$ (bottom) kicker strength and waveform specifications.

The septa and pulsed power supplies used during Pbar operation are not suitable for rapid cycling and cannot be used for $(g-2)$. The septa have no internal cooling to handle the increased heat load from the planned high duty cycle, and the power supplies are not able to charge quickly enough. The Booster-style septum magnet design will be modified to have the necessary size and field strength required for use in the injection and proton

removal systems. The power supplies used in the Booster to power the septum magnets also appear to be a good fit. Although they are designed to operate at a lower frequency (15 Hz) than the peak needed for $(g-2)$, the lower operating current (for 3.1 GeV/c versus 8.89 GeV/c momentum) should more than compensate for changes to the heat load and mechanical stresses due to the increased pulse rate. The new septa can be the same length as their Pbar counterparts so they can comfortably fit between quadrupoles in the injection and proton removal regions.

Delivery Ring D30 straight section

The Delivery-Ring injection and extraction regions will both be located in the D30 straight section. Due to the physical constraints of the tunnel, the M3 line will trace a path above the Delivery Ring before descending. Similarly, the M4 line will be located above the Delivery Ring until the ring bends away at the edge of the straight section. In both cases, the tight quadrupole spacing in the Delivery Ring leaves little room for the descending and ascending beamlines. The extraction line will closely follow the trajectory of the decommissioned AP4 (Booster to Debuncher) line. The tunnel in this region has an existing stub region that the extraction line will pass through, eliminating the need for civil construction to widen and strengthen the tunnel. Figure 7.41 shows the layout of injection and extraction devices in the D30 straight section.

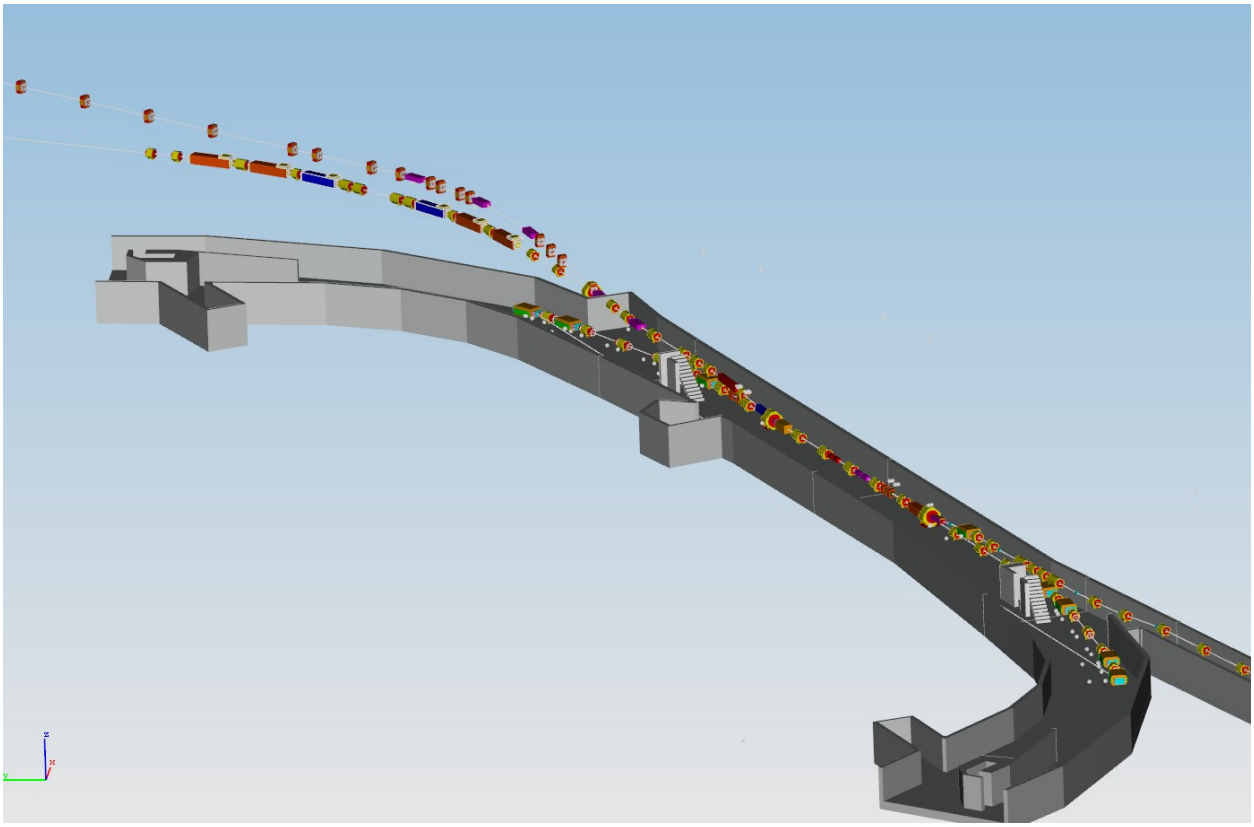

Figure 7.41: D30 straight section, injection on right, extraction on left.

The work required to prepare the D30 straight section for the new beamlines is considerable. Without modification, both the M3 and M4 lines would have physical conflicts with existing utilities and ring devices in the areas of elevation change to and from ring level. The existing cable trays on the Debuncher side of the ring are also where magnet hangers will be required for the new beamlines. The cable trays are full of cables, many of which need to be retained or replaced in order to operate the beamlines. The Debuncher, cable trays, utilities, lighting, cable routing, and numerous other subsystems will need to be relocated as part of the D30 straight section reconfiguration. Although not required for $(g-2)$ operation, extensive radiation shielding will be installed in the tunnel for Mu2e, so the reconfiguration must accommodate the future shielding.

The main features of the reconfiguration are as follows

- The AP3 beamline must be removed and devices temporarily stored for future use in the new beamlines. Accumulator magnets must be removed to allow room for tunnel activities.
- Debuncher magnets in and adjacent to the D30 straight section must be temporarily removed to allow access to the equipment that needs to be relocated or replaced. Stochastic cooling tanks that are no longer needed will be removed.
- Removal of existing Debuncher cable trays, relocated to the center of the tunnel, addition of cross-over trays from the Accumulator side to augment central trays.
- Removal of existing cabling to make way for new cabling to support the reconfigured beamlines and Delivery Ring. In addition to magnet cables, there are also safety system, instrumentation, network, abort link, shunt and motion control cables to be maintained or replaced.
- Relocation of tunnel utilities, primarily cooling water, electrical power infrastructure and tunnel lights.
- Reconfiguration of the main power supply buses that bypass all or part of the straight section (Main Bend bus, QF bus, QD bus, QSS bus, SF bus, SD bus).
- Installation of M3 and M4 lines, including injection and extraction devices.
- Reinstallation of Delivery Ring, including relocation of magnets to accommodate the reconfigured ring elements (motion controlled quad stands, large aperture quadrupoles at D3Q3 and D2Q5)

Figures 7.42 and 7.43 provide an overview of the D30 straight section reconfiguration, showing blocks of devices for removal and installation.

Injection

The M3 line runs above the Delivery Ring in the upstream end of the D30 straight section and ends with a vertical translation into the ring. M3 injection will be achieved with a combination of a C-magnet, D3Q3 quadrupole, magnetic septum, and kicker magnets, which

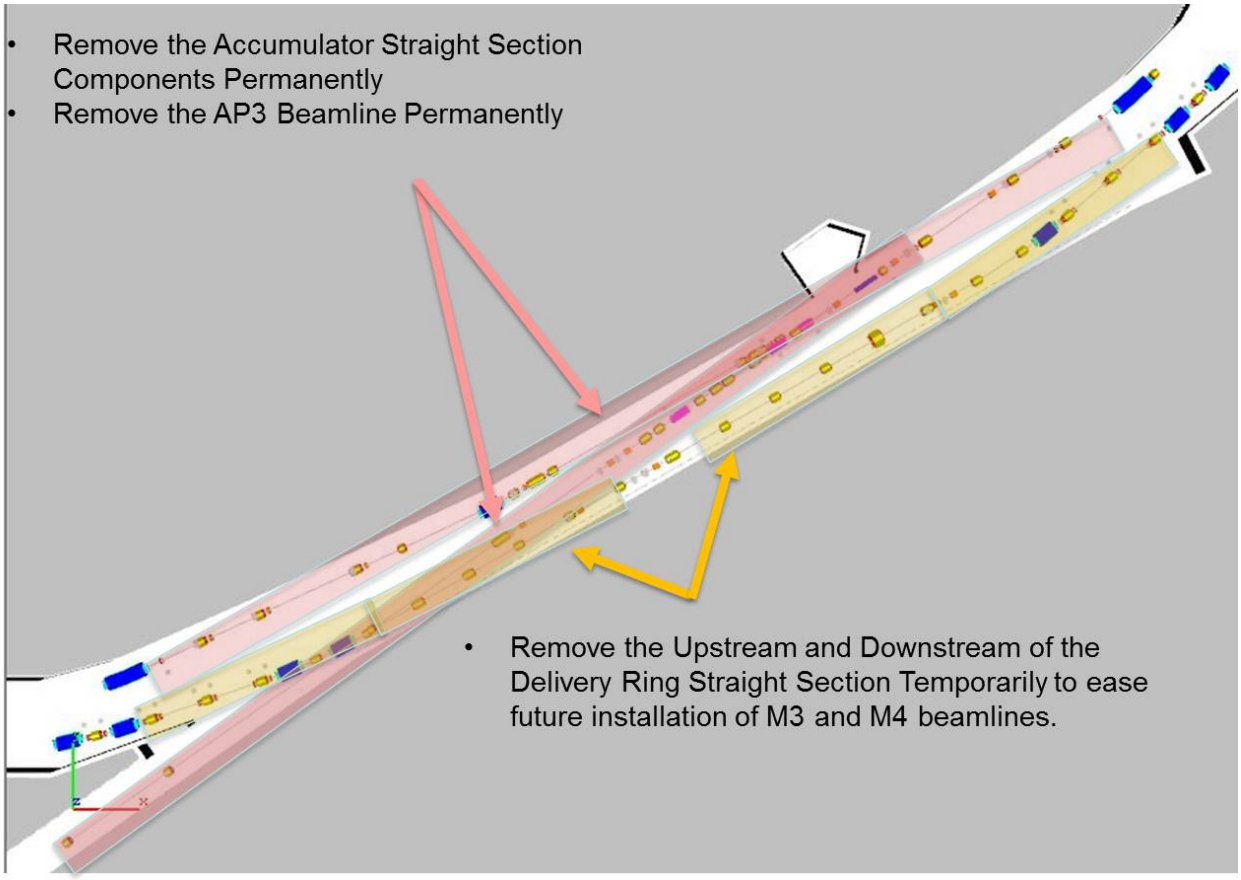

Figure 7.42: Devices in the D30 straight section to be removed.

will all provide vertical bends. The septum and C-magnet are both based on existing designs, which reduces overall costs, but modified to improve the aperture. Both magnet designs required modifications in order to attain the $(g-2)$ acceptance goal of 40π mm-mr.

The magnetic septum is a modified Booster-style (BSE) magnet, with an increased pole gap and a thinner septum to improve aperture. The BSE magnet has a 1.1-in pole gap, which will be increased to 1.85 in for the new septum. Similarly, the C-magnet is a larger aperture (2.1 in instead of 1.6 in) and shorter (2.2 m instead of 3.0 m) version of C-magnet designs already in use and has been designated an MSDA magnet. An identical C-magnet is used in the extraction region, but with different vacuum pipe geometry. The descending beam in M3 will pass through the C-magnet first and will be bent upward by 35 mr. The beam will continue well above the center of the D3Q3 quadrupole and receive a 30-mr upward kick. Since the beam is up to 140 mm above the centerline of the quadrupole, a large-bore quadrupole magnet is required in order to provide adequate aperture. The large quadrupole at D3Q3 will be the LQE magnet from the D2Q5 location, which will be replaced by an 8-in quadrupole, as described below. The LQx magnets were designed to have a substantial good-field region that extends between the poles. Similar arrangements with LQ magnets can be found in Pbar at D4Q5 (former AP2 injection, planned proton removal) and D6Q6 (former Debuncher extraction). The injected beam then passes through the field region of the

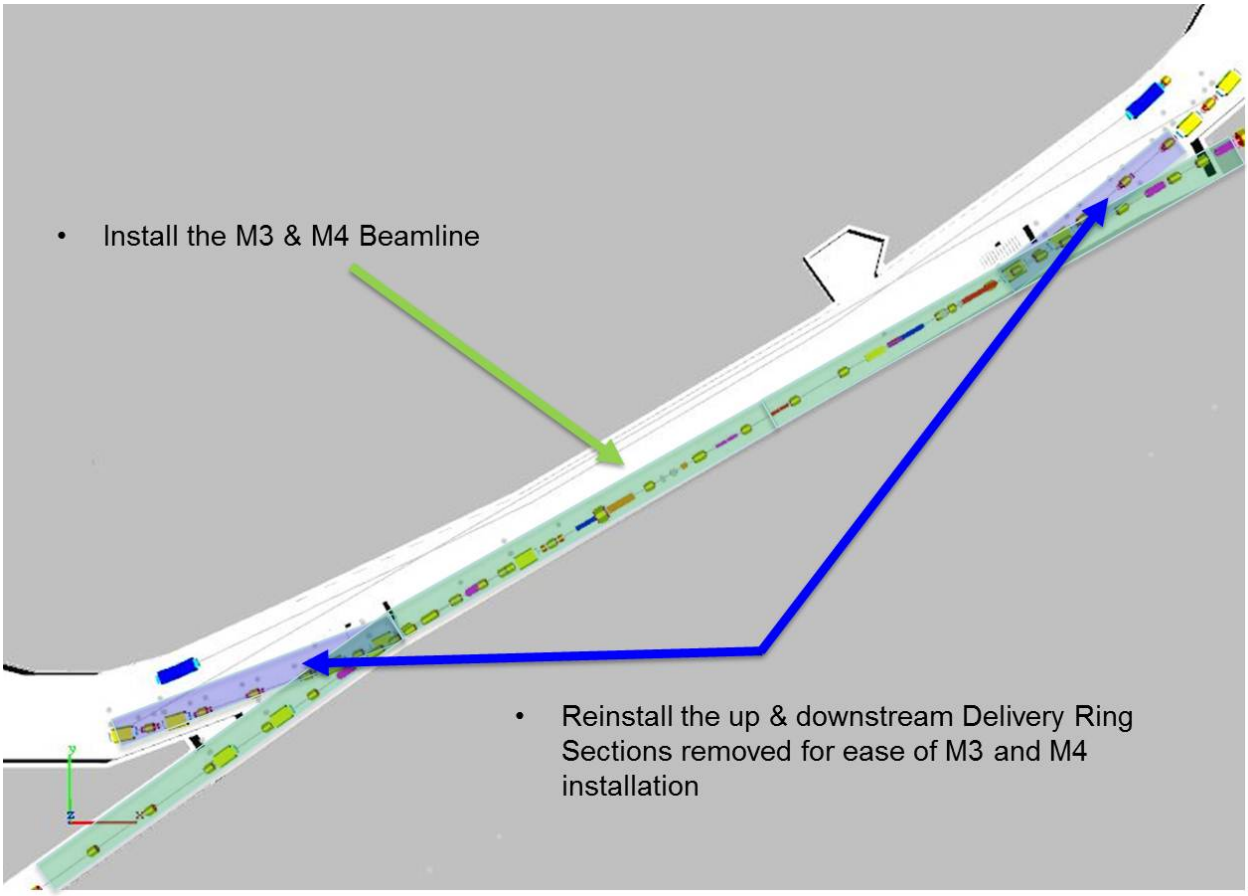

Figure 7.43: Devices in the D30 straight section to be installed.

septum magnet and receives a 39-mr upward bend as required for the necessary trajectory entering the injection kicker magnets. The beam leaves the septum with a 4-mr residual angle, because the septum and kicker are not 90° apart. The kicker magnets provide a final 6.1-mr vertical bend to place the injected beam on the closed orbit of the Delivery Ring.

The two-module injection kicker system is located between the D30Q and D2Q2 magnets. To minimize the horizontal β function and maximize acceptance, the kickers will be located as close to the D2Q2 quadrupole as possible. Spare Pbar injection kicker magnets will be refurbished and reused for injection. The magnets are already designed to be oriented vertically, so little additional effort will be required to convert them to their new application. They will require a new motion-controlled stand, based on the existing Debuncher injection kicker stand. Kicker rise and fall time specifications and power supply information was provided in Table 7.12 and the accompanying text. Figure 7.44 shows the injection devices and their location in the Delivery Ring, along with their bend angles. Due to the large vertical excursion through the top of the D3Q2 magnet, a vertical bump across the injection region will be incorporated to lower the beam and improve the aperture. The quadrupole magnets at D2Q2, D30Q and D3Q4 will be displaced to create the bump by generating steering due to the beam passing off-center through the magnets. To create a 15-mm downward displacement at D3Q2, the magnets will be lowered by 8.1, 11.0, and 4.2 mm respectively.

It would be beneficial, but not necessary for 40π-mm-mr acceptance, to install an existing "extended star chamber" quadrupole at the D3Q2 location. SQC-312, in magnet storage, was previously located at D4Q4 in the Pbar AP2 injection area and has an extended top lobe in its star chamber. This magnet is slated for installation at D3Q2.

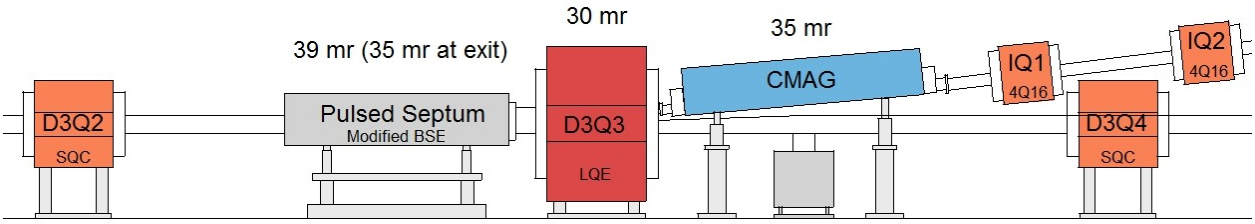

Figure 7.44: Delivery-Ring injection devices.

Extraction

Extraction from the Delivery Ring takes place in the downstream half of the D30 straight section. The extraction channel and the first 30 m of the M4 line will be used for both Mu2e resonant extraction and $(g-2)$ single-turn extraction. This arrangement avoids the complexity and additional expense of dual extraction lines in the limited available space. It also eliminates the need to remove potentially highly radioactive objects from the ring when switching between experiments. The ideal extraction configuration will provide enough aperture for both the Mu2e resonantly-extracted proton beam and the $(g-2)$ muon beam to be transported efficiently through the M4 line.

A Lambertson and C-magnet pair will be used, in conjunction with the intervening D2Q5 quadrupole, to bend the beam upward out of the Delivery Ring. In the interest of compatibility between $(g-2)$, Mu2e, and future muon experiments, a Lambertson magnet is required for extraction. The resonant-extraction process used for Mu2e is very restrictive on the size, strength, and location of the electrostatic septa that are required to split the extracted beam. The electrostatic septa will be located on either side of the D2Q3 quadrupole, and are expected to be about 1.5 m long for the upstream and 2.0 m long for the downstream septum. However, they will not be in place until after the $(g-2)$ run is completed. In order to achieve the goal of a combined extraction channel and beamline, the $(g-2)$ extraction kickers must be located in a lattice location that is $\sim n\pi/4$ radians from the Lambertson, where n is an odd integer, and in an area not already occupied by injection or extraction devices.

The $(g-2)$ extraction kickers will be located between the D2Q2 and D2Q3 quadrupoles. There will be two kicker modules of approximately 0.85 m length each. During the dedicated period of $(g-2)$ operation, the kickers will be located as close to the D2Q3 quadrupole as possible in order to minimize the vertical β function and maximize acceptance. The kicker magnets will be repurposed Pbar extraction kicker magnets that have a vertical aperture of

41 mm. The kicker magnets will be powered in series from a single power supply. There is also an alternative layout concept that would allow $(g-2)$ to operate after the Mu2e electrostatic septa are installed. The septum would need to be short enough to leave room for a single kicker near the D2Q2 quadrupole in this arrangement. Also, the kicker magnet would need to be modified in order to provide enough bending strength. The relocation of the kicker would also reduce aperture unless the β functions in this region could be suppressed by about 20%.

The Lambertson is a newly designed magnet, based on the NOνA MLAW Lambertson, but is shorter and has a larger aperture. This Lambertson design was based on an insertion length of 2 m or less and a larger pole gap of 2.2 in and has been designated as an MLG magnet. Figure 7.45 shows the solid model of the Delivery-Ring Extraction Lambertson. The Lambertson magnetic fields, including the fields in the "field free" region, have been extensively modeled [19].

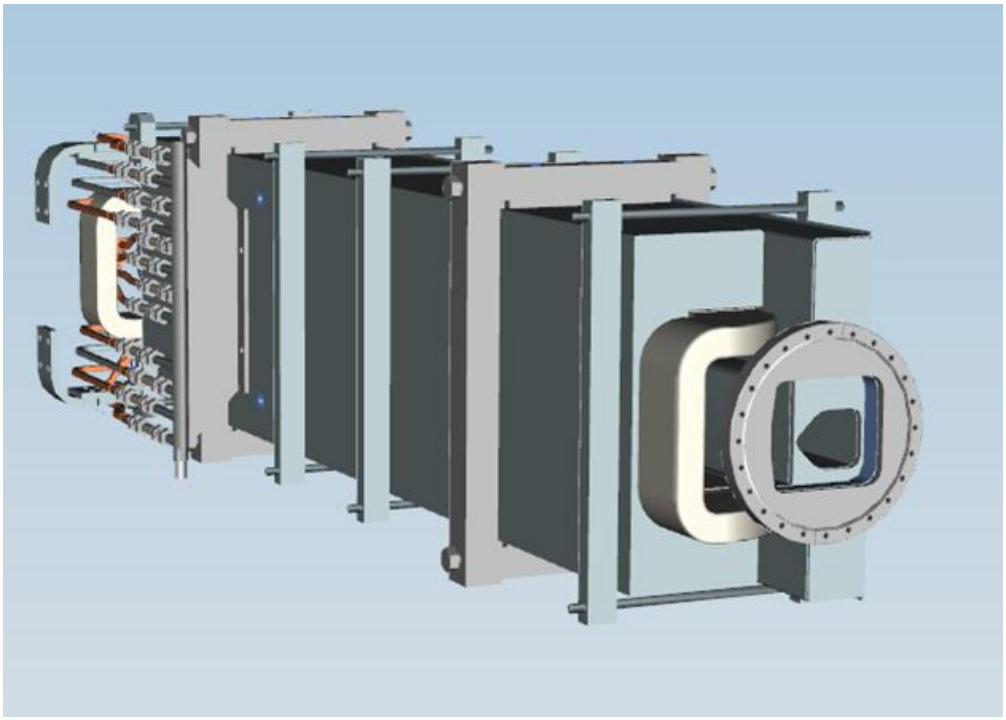

Figure 7.45: Delivery-Ring Extraction Lambertson, looking downstream.

The beam passing through the D2Q5 quadrupole has large offsets in both planes, due to the use of a Lambertson in the extraction process. The beam is kicked horizontally into the field region of the Lambertson, then bent upwards. There are two significant implications to the extraction design in order to achieve a 40π-mm-mr acceptance. The first is that a larger-aperture quadrupole is needed than the available Pbar LQ series. A surplus BNL 8-in quadrupole (8Q24) will be used to provide the additional aperture. Even with the increased aperture, a large horizontal 4-bump across the extraction region is required for $(g-2)$ beam to fit within the available physical aperture (the bump is not required for Mu2e operation). The quadrupole magnets at D2Q3, D2Q4, D2Q6 and D2Q7 will be displaced horizontally to create the bump by generating steering due to the beam passing off-center through the

magnets. To create a 40 mm outward displacement at D2Q5, the quadrupoles will be offset by 15.6, 11.3, 14.8 and 20.1 mm, respectively. They will all be displaced towards the right (wall) side so that beam will be bumped further to the right side through the Lambertson. Figure 7.46 shows the layout of the extraction devices for $(g-2)$ operation and 40π-mm-mr acceptance.

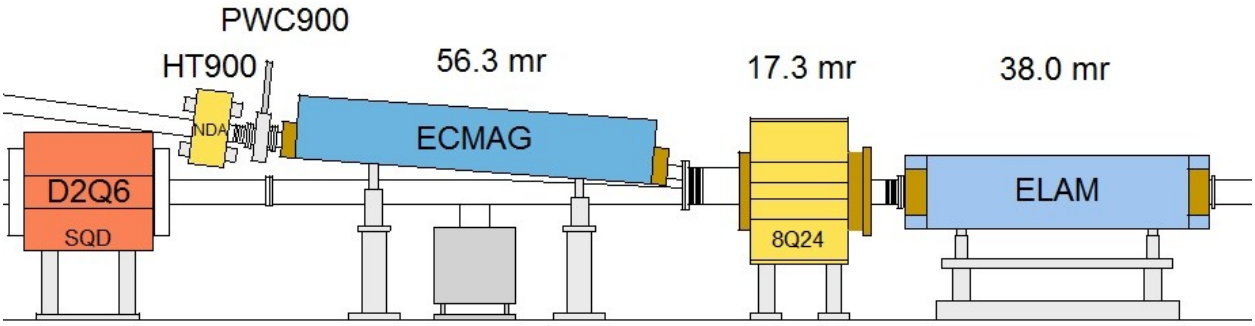

Figure 7.46: Delivery-Ring extraction devices.

Proton Removal (Abort) System

The proton removal system is an example of both repurposing an otherwise unneeded part of the Antiproton Source and implementing a dual function system that can be used by both the $(g-2)$ and Mu2e experiments. During Mu2e operation, an abort is needed to minimize uncontrolled proton beam loss and to "clean up" beam left at the end of resonant extraction. The proton beam must be removed quickly, by means of kicker magnets, in order to minimize losses in the ring. The $(g-2)$ experiment can benefit from the removal of protons before they reach the storage ring. The abort system can serve this purpose, as long as the protons sufficiently slip in time to create a gap for the kickers to rise through.

The old Debuncher injection point from the AP2 line in the D50 straight section will be used for the abort and proton removal systems. Recall that most of the AP2 line will be removed and replaced with the new M2 line that will merge with the M3 line upstream of the right bend. The downstream end of AP2, where antiprotons were formerly injected into the Debuncher, can now be used to extract protons from the Delivery Ring. This is made possible by the change in beam direction (as viewed from above) from clockwise to counterclockwise. The existing Pbar injection kicker magnets can be reused, although a new power supply will be needed to operate at the frequency needed to support Mu2e and $(g-2)$. The septum magnet and power supply will also need to be upgraded for the same reason. The new larger-aperture septum magnet will be identical to what was previously described for injection into the Delivery Ring. The section of the AP2 beamline being repurposed will require the addition of a vertical bending magnet to steer beam into the abort dump located in the middle of the Transport tunnel. Figure 7.47 shows the layout of the abort line.

The most economical plan to minimize the number of turns necessary to separate protons from muons is to only power the first kicker magnet, which provides the shortest rise time,

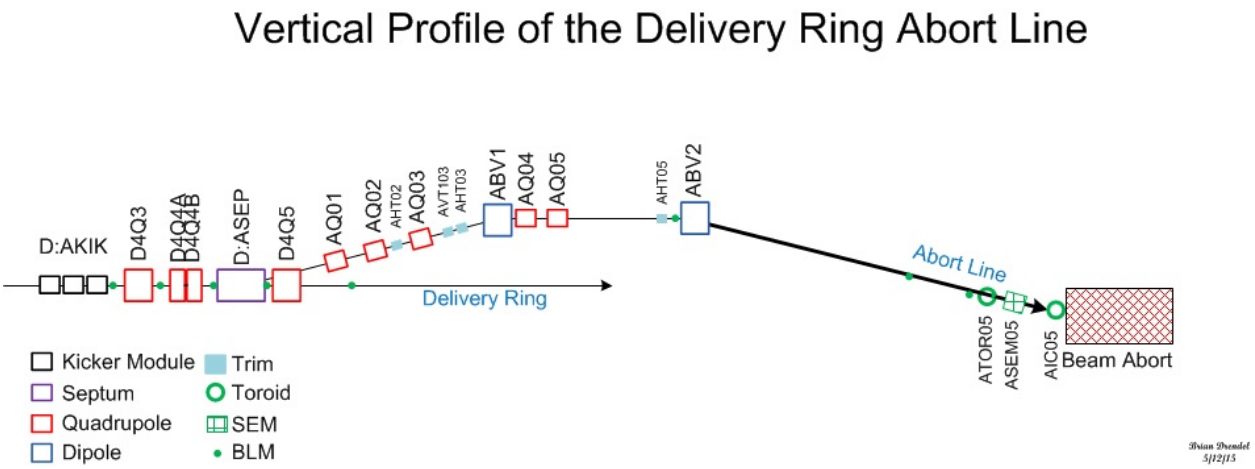

Figure 7.47: Side view of the Delivery Ring Abort/Proton Removal line.

a strong enough kick and requires only a single power supply. The rise time of the kickers with this configuration is about 180 ns. The kickers will be reconfigured for Mu2e operation, because all three kicker magnets are required to provide enough strength due to the higher beam momentum for Mu2e. For $(g-2)$ proton removal, the 180-ns rise time requires several revolutions around the Delivery Ring to provide enough gap between the muons and protons for the kicker to rise through. Table 7.13 lists the separation between the beams and the gap size for different numbers of turns. Four turns around the Delivery Ring would be required to cleanly remove all of the protons without disturbing the muons. All of the protons could be removed in three turns, but some of the muons would also be deflected. The table is based on the assumptions already stated: that the kicker rise time is 180 ns, the proton and muon bunch lengths are 120 ns and that the kicker should not disturb any of the muons.

	Muon vs. Proton		
	Centroid time difference (ns)	Gap size (ns)	Impact of proton removal kickers
Injection	40	None	Unable to kick protons only
1^{st} turn at Abort	91	None	Unable to kick protons only
2^{nd} turn at Abort	161	41	25% of protons removed
3^{rd} turn at Abort	231	111	85% of protons removed
4^{th} turn at Abort	301	181	Protons cleanly removed
5^{th} turn at Abort	371	251	Protons cleanly removed

Table 7.13: Efficiency of proton-removal system for different number of turns in the Delivery Ring, based on a 120-ns bunch length and 180-ns kicker rise time.

As the kicker magnets "fill" during the rising current waveform, the kicker magnetic field and bending strength increase proportionally. Protons are completely removed from the Delivery Ring when the kicker strength is about 85% of what is needed to center beam in the abort channel. Between 85% and 100% of the nominal kicker strength, some of the protons will be lost on the Abort Septum instead of traveling to the abort. When the kicker

strength is rising and below 85%, some of the protons remain in the Delivery Ring. In addition to separating the beams to improve removal efficiency, the percentage of protons removed can also be increased by firing the kicker earlier and disturbing part of the muons.

A side benefit of the muons taking multiple turns around the Delivery Ring is that virtually all of the pions will have decayed before the muons reach the storage ring. The primary potential problem with this proton removal concept is due to differential decay systematic errors caused by the different muon path lengths as they travel through the Delivery Ring. An analysis has been done that indicates that this will not be a significant problem [20].

7.5.7 Muon transport to storage ring: M4 and M5 lines

There are a number of physical constraints that dictate the design and geometry of the M4 and M5 beamlines.

- Beginning with the vertical extraction trajectory from the Delivery Ring, transition to the M4 line elevation of 48 in above the Delivery Ring.
- Vertically separate the M5 line from the M4 line and set the final elevation of M5 to that of the $(g-2)$ ring, 49 in above the MC-1 service building floor.
- The tunnel enclosures housing the downstream M4 line to Mu2e and M5 line to MC-1 are separated through two independent horizontal bend strings of 40.2° and 27.1°, respectively
- The horizontal bearing and final location of the M5 line from the horizontal bend center to the $(g-2)$ ring is set by the ring center and azimuthal orientation (injection point into the ring) which has now been fixed in site coordinates.

After extraction from the Delivery Ring is complete, beam passes through a series of vertical steering magnets through part of the M4 line, then bends upward into the M5 line and continues to the $(g-2)$ Storage Ring. The 30-m long upstream section of the M4 line, between the Delivery Ring and the beginning of the M5 line, must be capable of operating at 8 GeV/c momentum for operation to the Mu2e experiment. The large differences in beam size and energy place difficult, sometimes conflicting, demands on the optics and magnet selection for this part of the M4 line. The downstream part of M4, making up the bulk of the line, continues another 215 m to the Mu2e production target.. The M5 line is 100 m long and includes a horizontal bend string to provide the proper entry position and angle into the $(g-2)$ Storage Ring. The civil constraints of the local geography and proximity of the two beamlines and respective enclosures further complicate and restrict the layout of both external beamlines.

Civil Layout The local geography for much of the Muon Campus is shown in Fig. 7.48. Civil and geographical constraints (avoidance of wetlands, for example) dictate a $\sim$40° bend after extraction from the D30-straight-section to optimize the location of the Mu2e experimental hall. Another civil engineering constraint is the location of the MC-1 building and

$(g-2)$ storage ring. The $(g-2)$ experiment was positioned to avoid even low-level stray magnetic fields from Mu2e components on the one side (maximal distance from the strong Mu2e experimental solenoids) and Booster fields on the other. There are also utility corridors on the Booster side that further constrained the location of MC-1. Extending the M5 line would cause a conflict with the existing South Booster Road and reduce maneuvering room for delivering equipment. These factors set the minimum amount of left bend required for the M5 line at $\sim$27.1°.

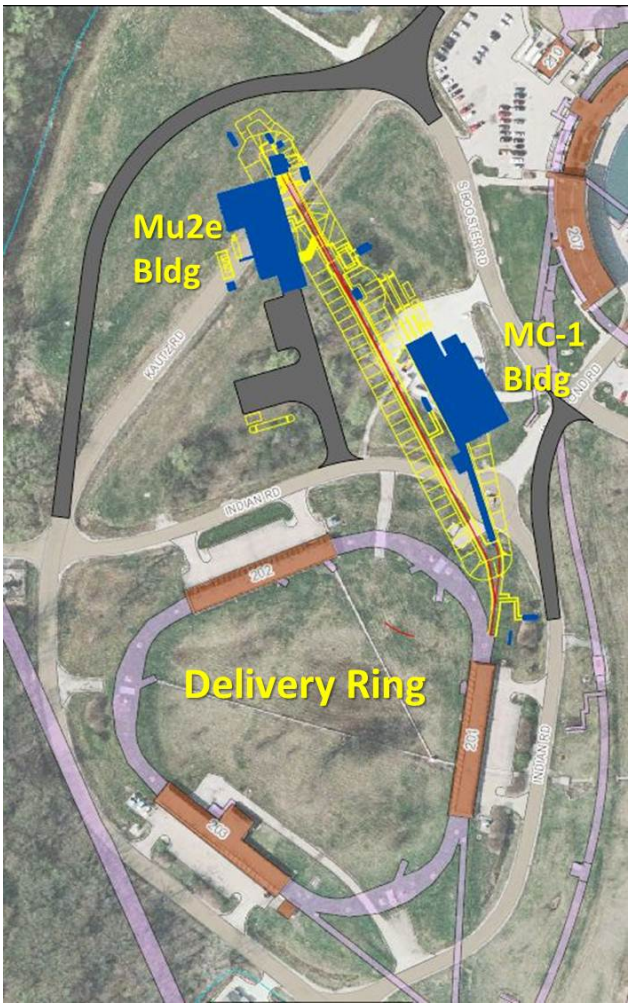

Figure 7.48: Tunnel enclosures and service buildings for the Delivery Ring, M4 and M5 lines, and experiments

The very short distance ($\sim$120 m) from the common extraction Lambertson to the $(g-2)$ storage ring mandates efficient, space-conserving separation of the M4 and M5 lines. Since physical separation from the Delivery Ring must occur vertically, the most efficient separation of the two lines is also vertical. This is accomplished by reversing a vertical-bend dipole in this section. Strong, independent horizontal left-bend dipole strings then direct beam to either the Mu2e or $(g-2)$ experiment. Final separation into independent civil enclosures is achieved by utilizing a large difference in the strengths of the left bends between the M4

and M5 lines. These strong horizontal left-bend strings must immediately follow the vertical separation stage in both lines. Rapid separation is particularly important for the M5 line given the short distance to the experiment and the need for bending and matching sections.

In summary, the M4 and M5 Lines must be designed with the following physical features:

- Horizontal kick into a Lambertson for vertical extraction from the D30 straight
- Vertical separation from the Delivery Ring magnetic components [section common to Mu2e/$(g-2)$ that takes advantage of existing tunnel civil construction]
- Vertical separation from Mu2e through a reversed vertical dipole. This section cleanly derives a separate beamline for $(g-2)$ by changing the bend strength and polarity of a single dipole between $(g-2)$ and Mu2e operation. Another dipole is added to the M5 line to level the beamline off at the storage ring elevation
- The final elevation of the M5 line (@225.1223 m above sea level) is 49 in above the projected civil elevation of the MC-1 experimental hall floor
- The final elevation of the M5 line is also 6.2 ft above the M4 line elevation (@223.2245 m) and 10.2 ft above the Delivery Ring elevation (@222.005097 m)
- A 27.09° horizontal bend string fixes the direction of the beamline from the D30 straight towards the geographic location chosen for the $(g-2)$ storage ring. (Mu2e has a 40.2° bend). The difference in bend eventually separates the two experimental beamline enclosures.

Beam Properties and Capability

- A horizontal kick into the field region of a Lambertson from the D30 straight section of the Delivery Ring towards the inside of the ring
- Horizontal Delivery Ring "bump" to move $(g-2)$ extracted beam away from the edge of the D2Q5 quadrupole aperture
- Beamline must transport a 40π mm-mrad acceptance and a momentum spread up to $\pm 0.5\%$ with small changes in beta functions for off-momentum particles (5% or less)
- Variable matching conditions at injection to the $(g-2)$ ring to accommodate the aperture restrictions of the current inflector and a possible new inflector.
- Beam position and angle scan capability in the final focus region of ± 1 cm, with no angle change, and ± 3 mr, with no position offset, both vertical and horizontal, to optimally tune injection into the storage ring
- 0.3 m reserved from last beamline element to the entrance of the $(g-2)$ ring backleg to avoid interference with fringe fields and to provide room for instrumentation for the experiment

Optics Insertions

- **M4/M5 ($g-2$) vertical achromat:** The ($g-2$) vertical achromat is a complex 7-bend achromat. The vertical bends include the extraction Lambertson, quadrupole steering from D2Q5, the C magnet, the first leveling bend (EDWA), two upward-bending MDC dipoles (one is reversed polarity from the Mu2e configuration) and a final reverse-bend CDC dipole. Achromatic optics are required in the M4/M5 lines to suppress vertical dispersion from the D30 vertical extraction system. Dispersion must be suppressed upstream of the horizontal left-bend string to avoid coupling between the two planes. Independent vertical dispersion cancellation must be implemented in the M4 and M5 lines to $(g-2)$ and in the M4 line to Mu2e.

- **M4/M5 separation of Mu2e and $(g-2)$:** To separate the two lines physically and optically, the separation must occur vertically due to space constraints. Although combined, the M4 line between the Delivery Ring and M5 line must be independently tunable in the vertical-bend section in order for both $(g-2)$ and Mu2e. The beamline tune of both lines must satisfy conditions for a vertical achromat.

- **M5 horizontal dispersion module:** An achromatic module of 3 equal-strength dipoles producing a 27.1° horizontal bend to the left. The dipole string is located after the final vertical bend.

- **M5 FODO cell transport section:** A FODO section between the horizontal bend string and the final focus section is designed to transport beam with minimal losses.

- **M5 final focus section:** A strong-focusing and tunable final focus telescope is designed to adjust and optimize optical parameters of injection into the ring. The design of the final focus must accommodate both the aperture restrictions in the inflector and overcome the strong-focusing fringe fields along the injection beam trajectory. The section must have the flexibility to accommodate a larger aperture Inflector, that requires larger beta functions in the Final Focus quadrupoles.

- **M5 matching:** The beamline also requires the necessary matching sections between the custom insertions and achromatic modules.

Only ∼85 m is available for the M5 beamline insertions after accomplishing the vertical elevation change. Space restrictions do not permit momentum collimation to be incorporated into the external beamline.

Beamline Sections

As stated above, the M5 beamline is best described in terms of its modular functionality. Correspondingly, the following descriptions detail the important sections, and discuss the design approach for each section, including a review of the extraction process. The location of each section in the overall external beamline layout is shown in Fig. 7.49.

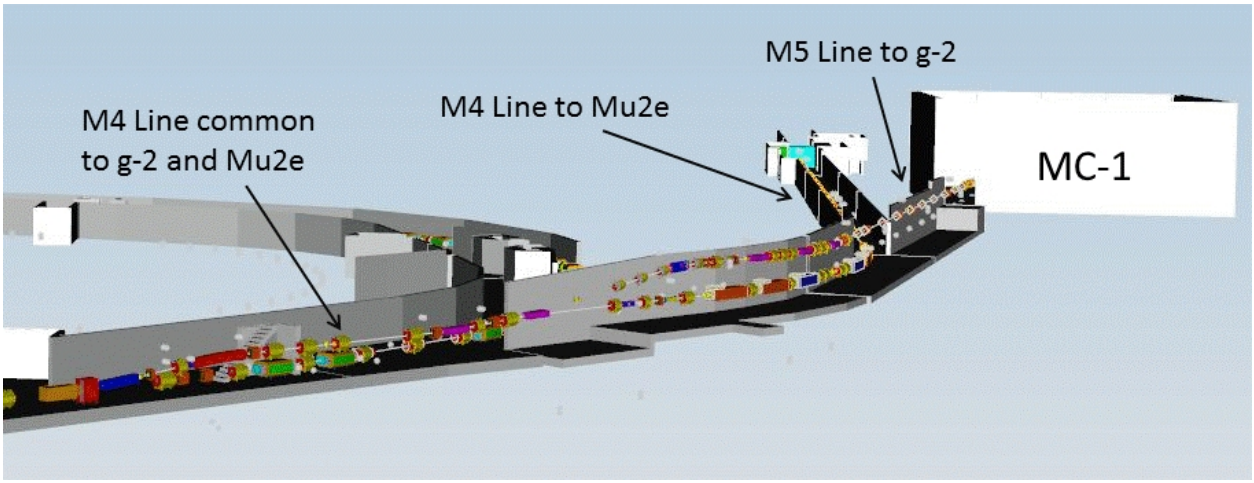

Figure 7.49: An overview of the Delivery-Ring extraction region, the shared upstream M4 line, and the downstream M4 and M5 lines.

The Vertical M4/M5 Section Once the beam clears the Delivery-Ring components, it can be steered onto a centered mid-plane trajectory. Steering trim magnets have been strategically placed to correct for any differences between the $(g-2)$/Mu2e and kicker/septa forms of extraction. The exact extraction orbit depends sensitively on the D30 quadrupole strengths, and these depend on the Delivery-Ring tunes established for resonant extraction or muon beam delivery for Mu2e and $(g-2)$, respectively. It is unlikely the quad strengths will be identical, but they are expected to be similar to each other. For the optics design described here,the 2004 Run II Debuncher operational strengths were used (a symmetric lattice ideally suited for $(g-2)$ operation).

The initial bend upwards is so strong (to clear the Delivery-Ring components), that the beamline must be leveled before the final M4-line elevation. This is necessary to allow sufficient space to implement a vertical achromat, which requires significant phase advance generated by quadrupoles. Leveling the beamline reference trajectory at an intermediate elevation allows a straight section to be inserted with sufficient space for a sequence of quadrupoles that generate the needed phase advance to cancel vertical dispersion after the final set of vertical bends. Given the still-limited vertical clearance and the need to have a large bend angle, an EDWA type dipole, which has small core dimensions, can be installed after D2Q6 with a bend equal and opposite to the combined bends of the Lambertson, C magnet, and D2Q5 focusing quadrupole. Leveling the line at 0.8128 m, or ∼32 in, above the Delivery-Ring centerline provides for a long elevated "straight" that allows SQ series quadrupoles to be installed without conflicts with the Delivery Ring below. The only conflicts are with the extended saddle coils of the DR dipoles, and these must be avoided.

Downstream of the vertical leveling bend, an achromat is implemented using four quadrupoles. This straight section is followed by two MDC dipoles for Mu2e with reverse bends (up/down) that elevate the Mu2e extracted beam to a final elevation of 1.22 m (4 ft) above the Delivery Ring. For $(g-2)$ operation, the last vertical dipole in the M4/M5 section reverses polarity and increases in strength to switch beam delivery from the M4 to the M5 line. For $(g-2)$, therefore, three dipoles are required (the last Mu2e vertical dipole is reversed), sending the

beam steeply upward to achieve rapid separation of the M5 line from the M4 line. This rapid separation proves critical in order to position the strong horizontal bend section; otherwise the ring location would have moved eastward into a utility corridor. The common M4/M5 part of the beamline thus extends from the C magnet to the vertical dipole, V907, (the last vertical dipole in the Mu2e configuration) after which the two beamlines are completely separate.

Figure 7.50 displays the achromatic optics of Delivery-Ring extraction from the center of the first quadrupole upstream of the Lambertsons to the end of the achromat. These optical functions are predicated on an assumed matched beam distribution extracted from the Delivery Ring. This may not be the case, and extracted beam properties may differ significantly between $(g-2)$ and Mu2e. Therefore it is important that the two vertical achromats have been separated between the M5 line and the M4 line and can be independently tuned. The physical layout of this section is shown in Fig. 7.51.

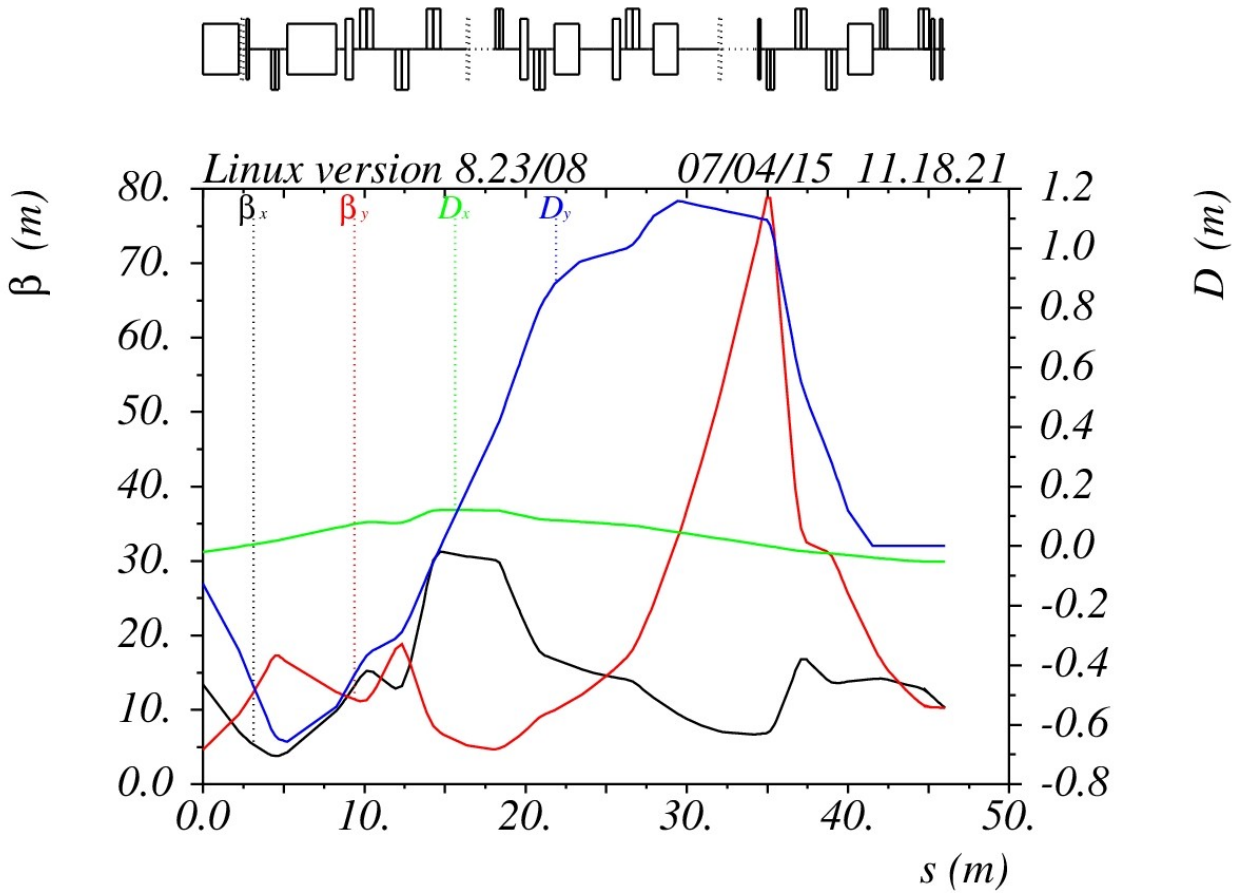

Figure 7.50: The extraction optics showing the Lambertson and C magnet (at left) followed by an opposite-sign vertical bend and quadrupoles to form the achromat. This is followed by a final bend up and then level again to the elevation of the beamline.

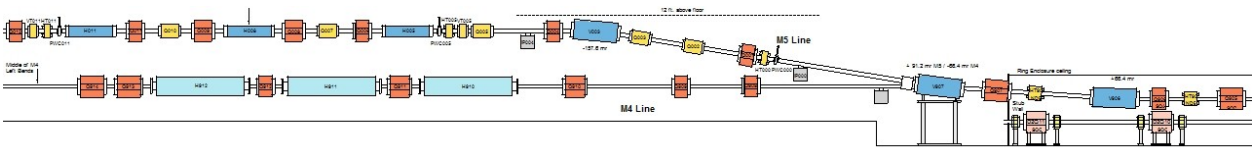

Figure 7.51: Layout of the extraction section showing the vertical bends and the separation of the beamlines to Mu2e and $(g-2)$.

Horizontal Bend String Immediately downstream of the vertical section, a strong westerly bend is required in order to meet the constraints of the location of the $(g-2)$ ring, particularly the critical bore coordinates through the yoke and inflector position. The horizontal separation of the M4 and M5 lines after the extended vertical separation requires the horizontal bend module to be located as close to the end of the vertical section and as compact as possible. The bend increases significantly with any further downstream translation of the bend center or rotation of the $(g-2)$ storage ring. The M5 horizontal bend string, as designed, is already close to the maximum bend that can be achieved in the limited space available. Thus, maintaining a feasible bend center location is central to an efficient beam transport design.

The location of the storage ring and MC-1 building predicates a westerly bend of 27.1°. The bearing of the bend must be physically implemented within the existing enclosure location and exactly match to the injection trajectory of the $(g-2)$ storage ring. Figure 7.52 shows the present optimized beamline location in red as determined by a) the ring position, b) the injection alignment requirements, and c) as derived from the bend center to the upstream 1.25° bend center (relative to the ring tangent at the exit of the inflector) to injection center coordinates approximating the fringe-field effect. The green circle represents the upstream end of the inflector. Alignment is discussed in detail in the Final Focus section.

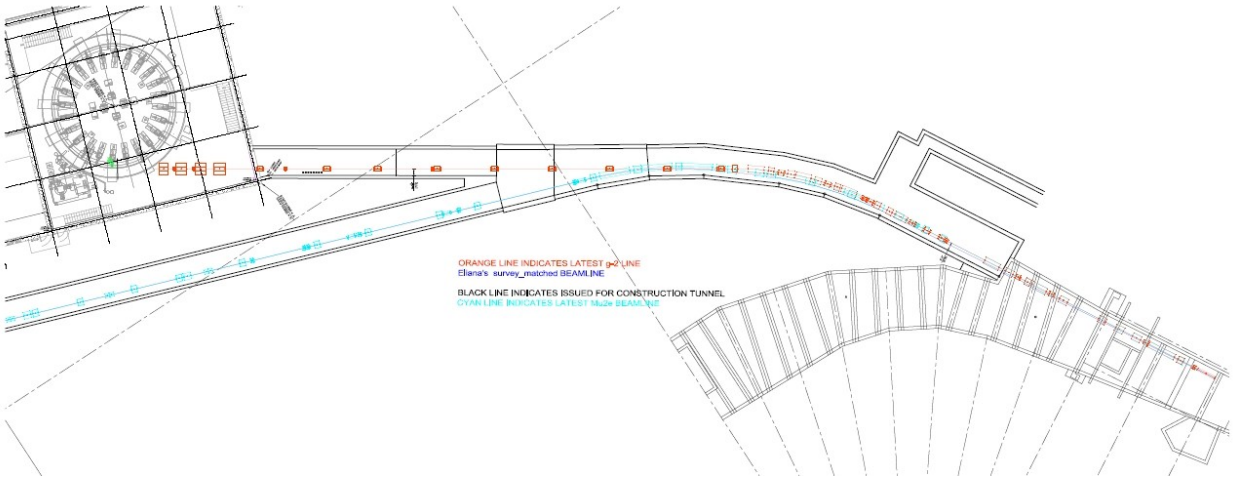

Figure 7.52: Layout of the horizontal bend section showing the horizontal separation of the M4 and M5 lines. The red line represents the optimized upstream-M4 and M5 beamline layout and the green circle the injection point at the upstream end of the inflector. The cyan line shows the beam trajectory through the downstream M4 line to Mu2e.

The horizontal bend design employs a 3-bend module comprised of three MDC dipoles in series as shown in Fig. 7.53 with each MDC delivering 1/3 of the total bend. Quadrupoles in this module supply 120° of phase advance between each dipole, with a symmetry point at the center $(D=0)$ to cancel horizontal dispersion, fulfilling conditions for a linear achromat. Upstream of this module a three-quadrupole matching section connects the optics of the vertical section with the closed optics of the horizontal bend module.

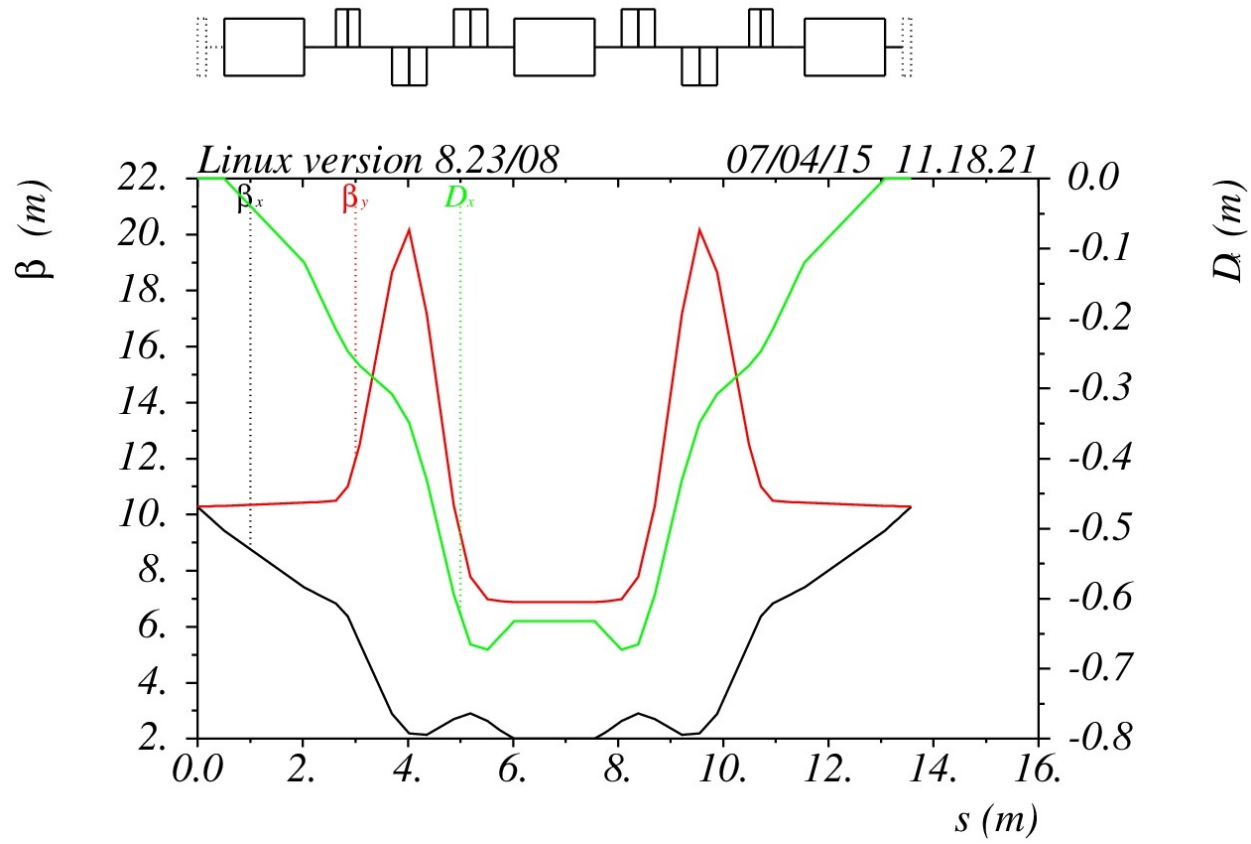

Figure 7.53: The optics of the $(g-2)$ horizontal bend insert.

The FODO-Cell Transport Section

The basic FODO-cell optics transports beam most efficiently with the lowest losses and maximum acceptance. FODO cells are the simplest magnetic lens configuration consisting of alternating horizontally- and vertically-focusing quadrupole elements. Therefore this type of module was implemented to transfer beam from the horizontal bend string to the M5-line final-focus quadrupoles. The FODO cell structure has 90° of phase advance per cell. The current half-cell length (distance between quadrupoles) is 6-7 m and the peak beta value is 22 m, giving a beam size of ±3 cm through this section of the line. What is convenient about this type of interface is that the integrated length of the FODO insertion can be varied by 10-20% without significantly impacting the optics or the matching to upstream and downstream sections. Two consecutive FODO cells are used between the horizontal bend and final-focus modules as shown in Fig. 7.54.

Injection into the $(g-2)$ Ring

The M5 beamline height is set to the $(g-2)$ storage-ring elevation of 49 in above the MC-1 floor elevation of 734.5 ft, or 738.58875 ft (225.1223 m). Horizontally, the bearing of the M5 line and the final-focus optics is dictated by the storage ring Inflector and the steering effect of the strong fringe fields as beam crosses these fields into the main field of the storage ring,

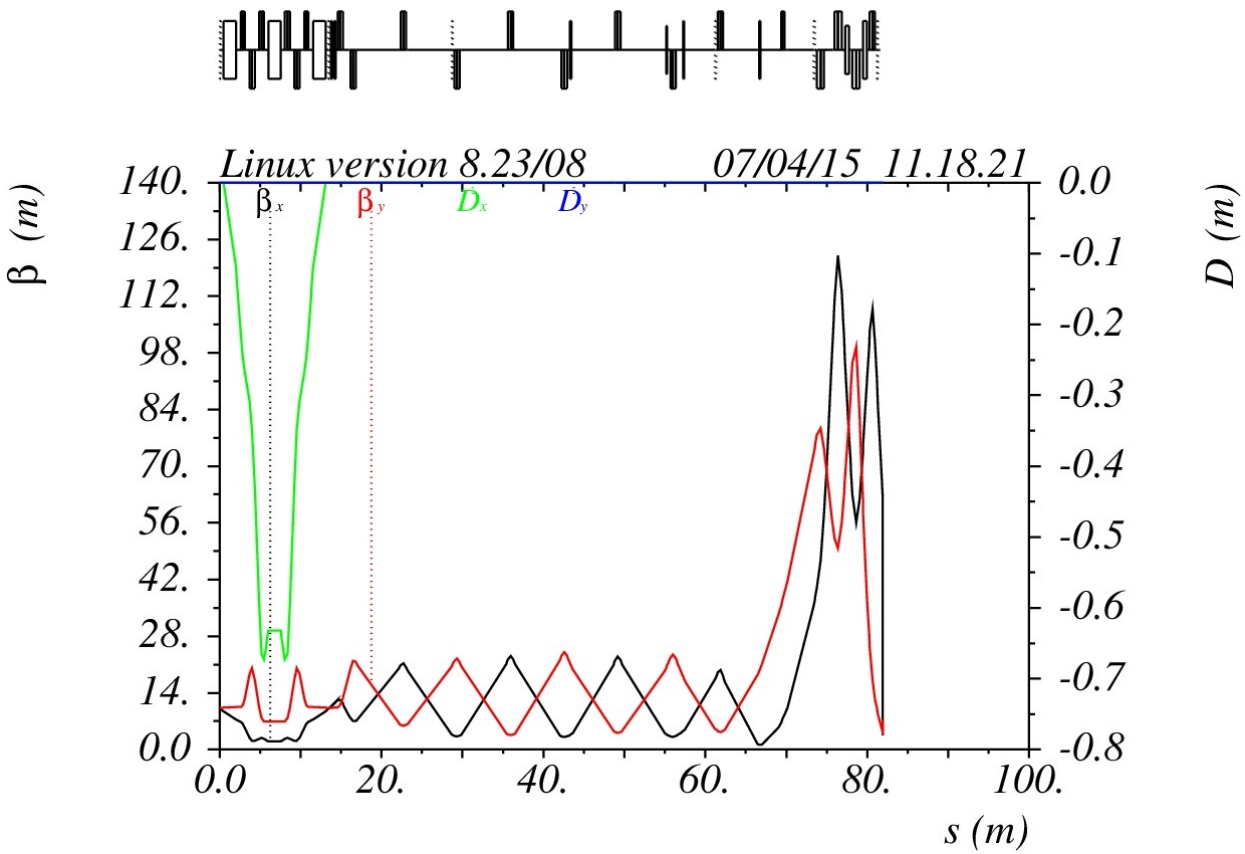

Figure 7.54: The M5 beamline starting at the beginning of the horizontal bend to the point of injection on the right.

77 mm offset tangentially from the reference orbit of the $(g-2)$ ring for 3.1 MeV/c muons as shown in Fig. 7.55 (right). The ring location and rotational orientation within the hall are therefore very critical and completely determine the bearing of the external beamline downstream of the horizontal bend string, as there is insufficient remaining distance to implement another horizontal steering section. The optical matching horizontally is further complicated by the restricted horizontal aperture of the inflector, which is 18 mm at its maximum as shown in Fig. 7.55.

The orientation of the inflector within the ring is given in Fig. 7.56 *(left)*. The linear optical functions of the ring are well established and the exit of the inflector where beam enters the ring is essentially in the center of an "open" section between the electrostatic quadrupoles so that the following are the required matching conditions, with a plot of the $(g-2)$ storage-ring lattice functions in Fig. 7.56.

$$\beta_x \approx 7.9\text{m}$$

$$\alpha_x \approx 0$$

$$\beta_y \approx 18.9\text{m}$$

$$\alpha_y \approx 0$$

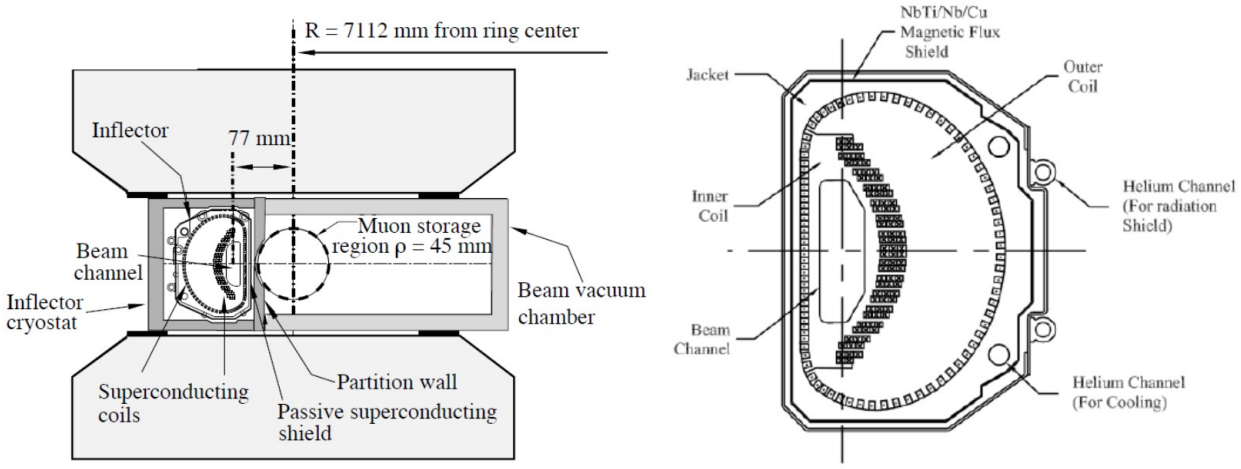

Figure 7.55: The inflector cross section which has a horizontal aperture of ∼9-18 mm and vertical of 36-56 mm.

$$D_x \approx 8.3\text{m}$$

$$D'_x \approx 0$$

However, the restricted horizontal aperture of the inflector means that the horizontal optical functions and dispersion cannot be matched at injection for a 40π-mm-mr geometric emittance without losing a large fraction of the incoming beam – the inflector is the dominant aperture restriction and optical constraint for injection. The largest betatron function that can be transmitted efficiently is only 2 m and is achieved by a waist at the center of the inflector of 1.5 m (The inflector length is 1.715262 m) as in the design of the original experiment at BNL. There is no remaining aperture for increased beam size due to dispersion, so horizontal dispersion is suppressed after the horizontal bend string. This leads to the following requirements for injection:

- $\beta_x \sim 1.5$ m at the center of the inflector leading to an increased mismatched beta function of 2 m and at the point of injection and a mismatched α_x of about -0.6. Vertical functions can be matched with the current inflector.
- No dispersion is possible with efficient transmission through the inflector causing a dispersion wave through the machine shown in Fig. 7.57, cutting the momentum acceptance by a factor of two.

The optical matching and steering of the external beamline is further complicated by the extreme effects of the fringe fields which will be discussed in the following section.

Fringe Field Effects The large fringe fields of the main 1.45 T field depicted in Fig. 7.58 have a major impact on the optics and on the angle of injection. Even the weak field in the yoke has a significant deflection (in the opposite direction as the main fringe field) because of the extended length of the trajectory in this section. For the storage ring, the main field and poletip configuration produce extended fringe fields with a strong vertically focusing

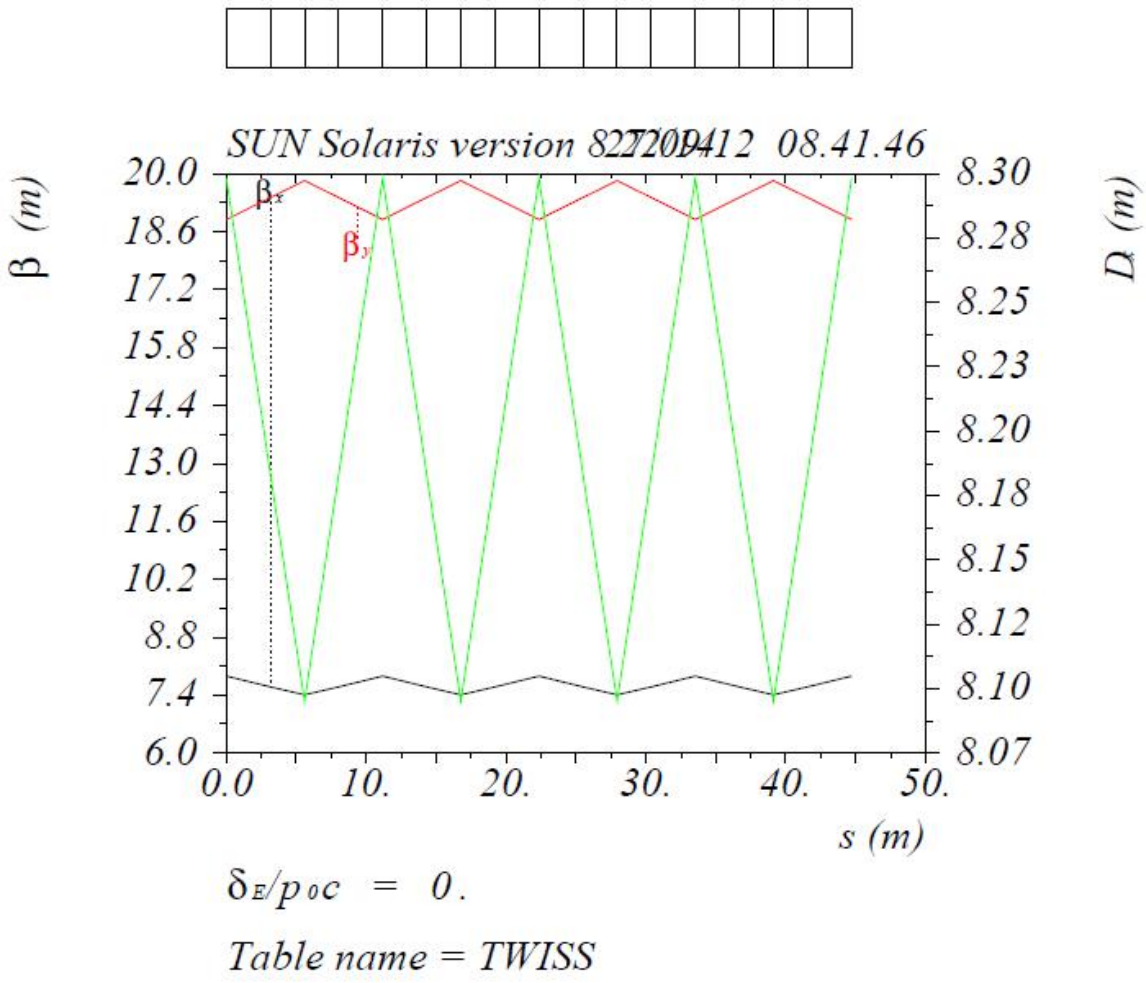

Figure 7.56: The linear ring optical functions.

component due to the tangential crossing of this field (edge focusing effect). A more detailed description of the fringe fields entering the $(g-2)$ storage ring can be found in Ref. [23].

The actual trajectory through this section is complicated by the field-nullifying impact of the inflector. The combined fields [24] have been computed and shown in Fig. 7.59 with the actual trajectory shown. The complicated trajectory was also initially computed for the original experiment [25]. Note that the superconducting inflector has a sharp field fall-off at the ends, but is inserted crossing the fringe fields giving rise to a reversed bend with respect to the main field in the upstream half of the inflector. The deviation from tangential injection is therefore a complicated convolution of the different fields from the yoke, main ring field, and inflector. Since such a complicated trajectory cannot be accommodated in the physical design, only the net effect is compensated for, which is 1.25° from tangential injection.

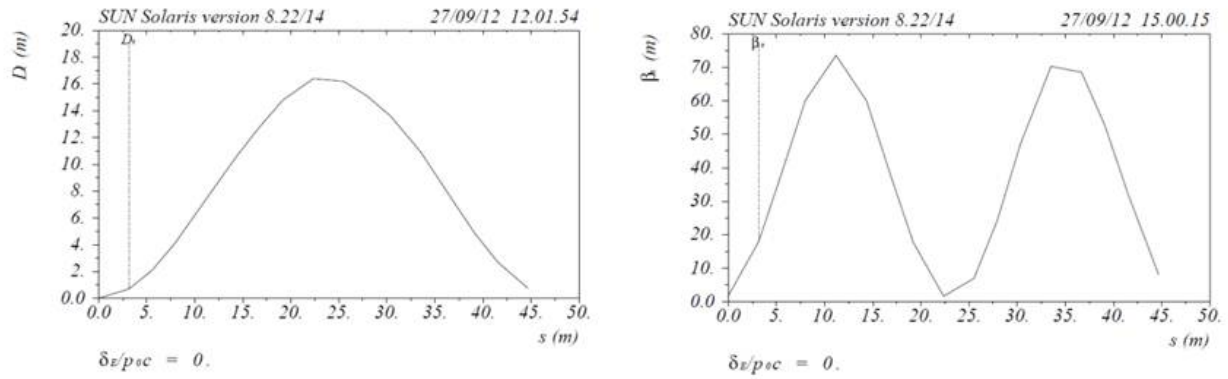

Figure 7.57: The dispersion wave around the ring created by zero dispersion at the inflector and the horizontal betatron mismatch due to the inflector.

Final Focus The strong vertical focusing and horizontal defocusing of the fringe field must be compensated and overcome by a strong final-focus telescope with a focusing quadrupole as close to the iron yoke as possible. Since there are weak but extended fringe fields from the bore through the yoke, a match point is set 30 cm outside of the yoke entrance for optical functions. Final-focus quadrupoles are upstream of this optical matching point to avoid any interfering interaction of the magnet with the fringe field of the yoke. Both matrices were inserted appropriately into the line to test and understand if a single design could accommodate both transfer matrices. The lattice functions at injection are $\beta_x = 2.0$ m, $\alpha_x = -0.6$, and $\beta_y = 2.0$ m, $\alpha_y = 0$. These are back propagated to the 4.3 m upstream match point using both R matrices, which produce very different matching conditions: BNL R matrix: $\beta_x = 2.0$ m, $\alpha_x = -0.6$, $\beta_y = 2.0$ m, $\alpha_y = 0$, and Rubin R matrix $\beta_x = 2.0$ m, $\alpha_x = -0.6$, $\beta_y = 2.0$ m, $\alpha_y = 0$. The differences in the optics of the final focus are shown in Fig. 7.60. Note that steering trims are located within the final-focus quadrupoles. Corresponding trims are located further upstream in 90° phase advance locations in order to implement independent position and angle steering.

The optics of the complete line is shown in Fig. 7.61. Table 7.14 lists magnet types and $(g-2)$ operating currents for the dipoles, quadrupoles and trims in the upstream M4 and M5 lines.

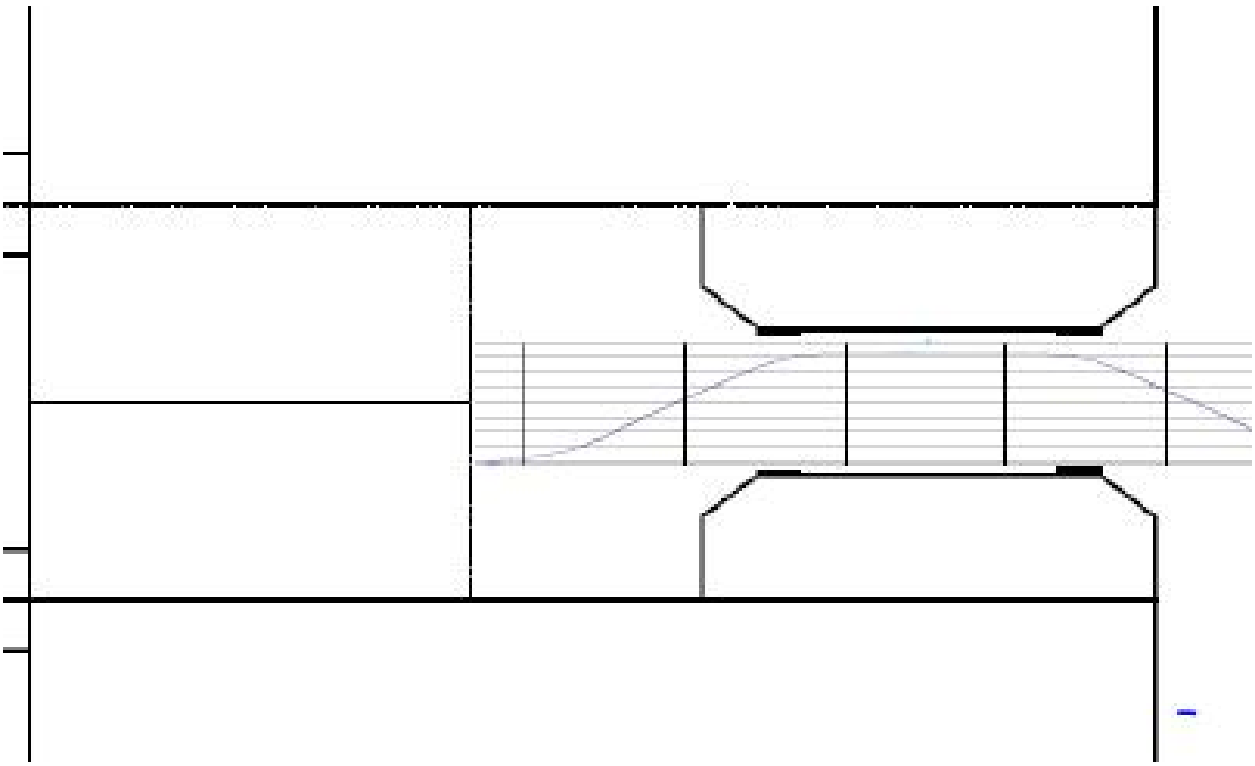

Figure 7.58: Storage ring magnetic field profile superimposed over an outline of the poletip.

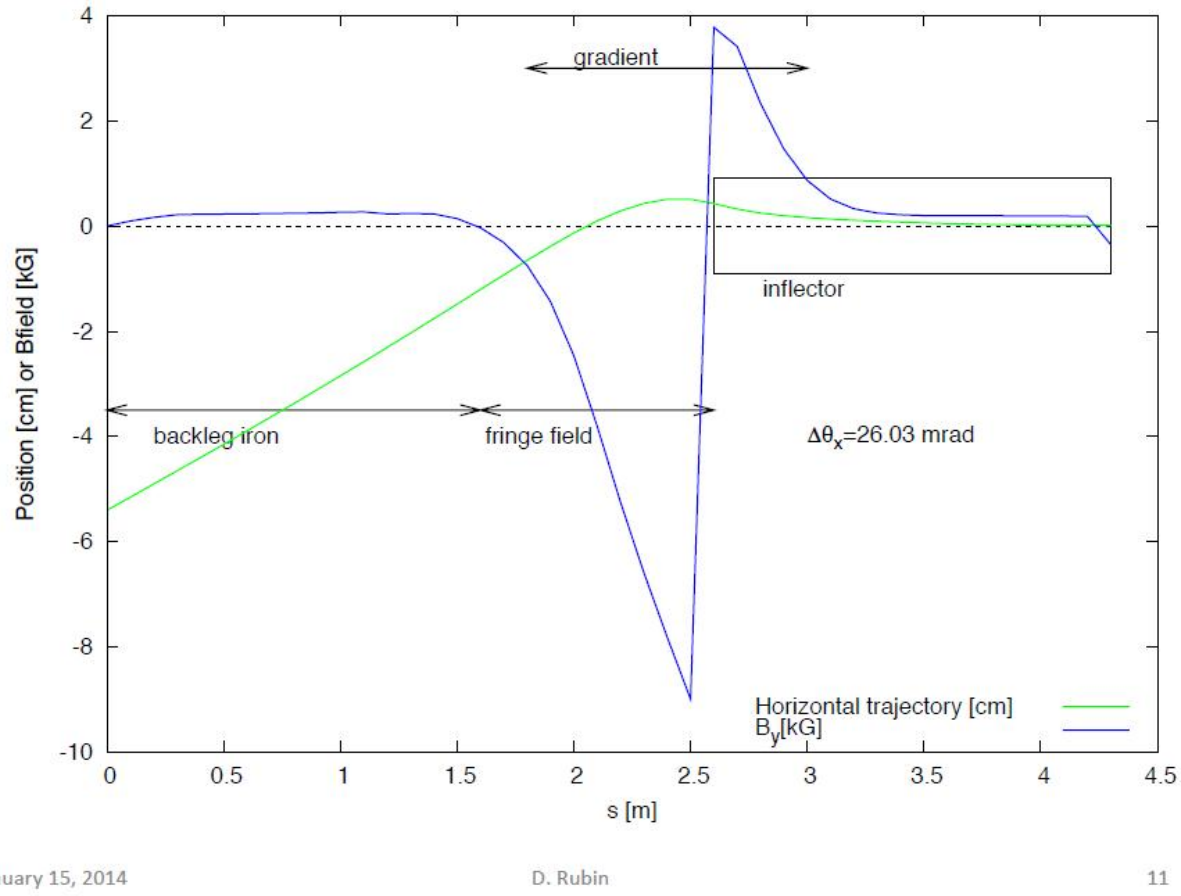

Figure 7.59: Superimposed fields from the yoke, main ring and inflector in blue. The green line is the beam trajectory.

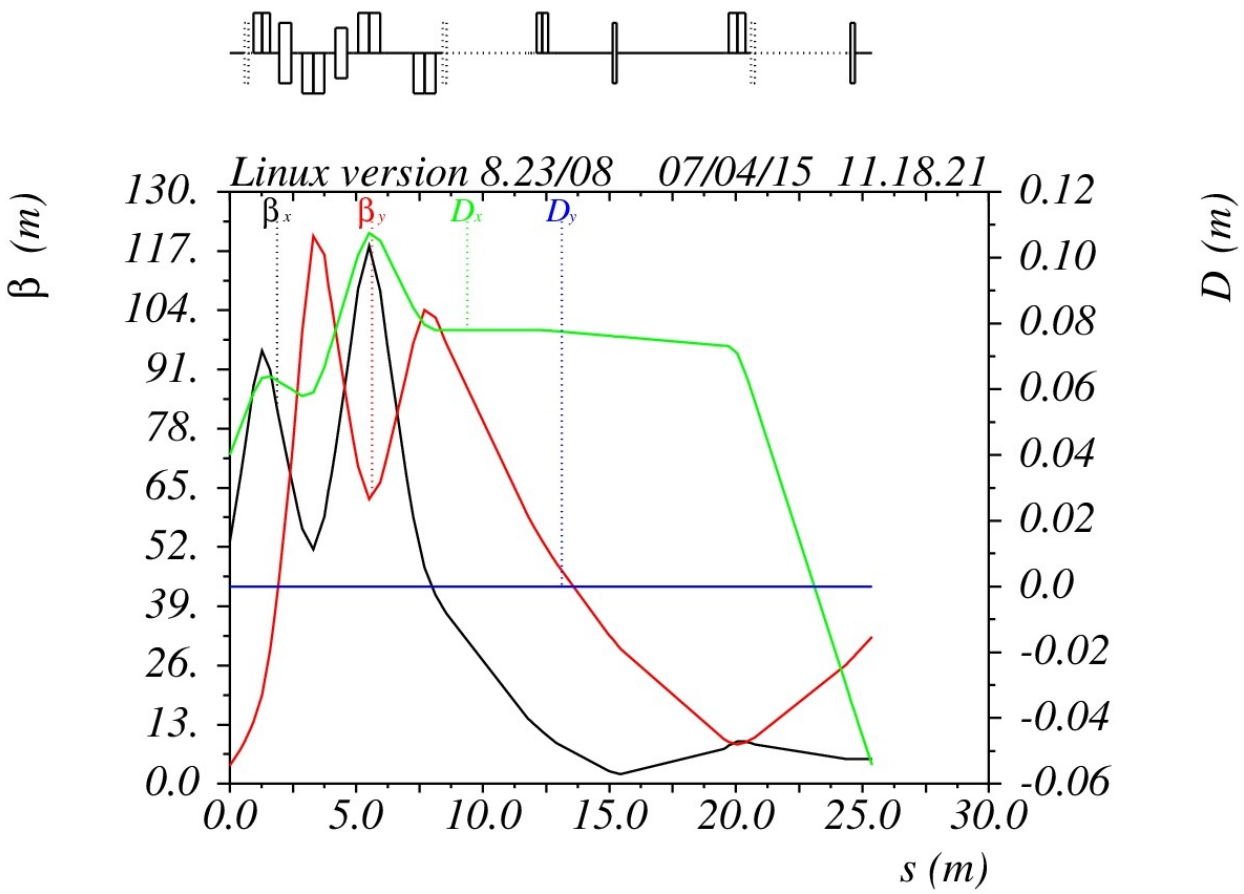

Figure 7.60: Final focus optics with matched injection conditions to the g-2 ring in all but dispersion using the BNL matrix description. The plots are left to right, downstream to upstream with the "4.3 m" match point as the origin.

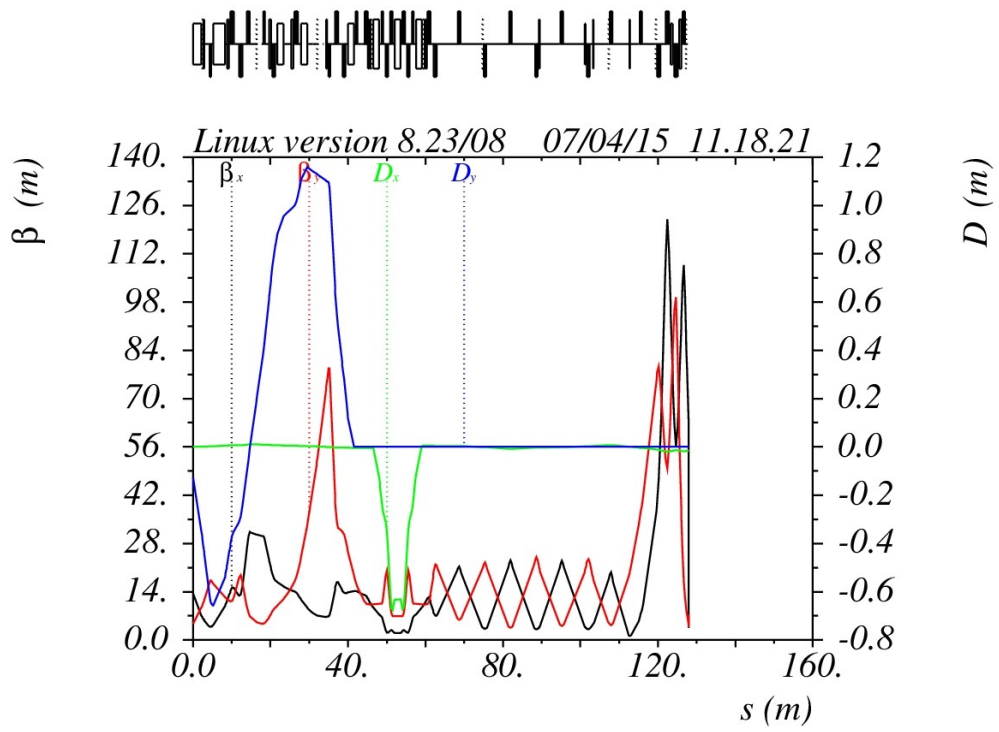

Figure 7.61: Optics of the $(g-2)$ external beamline from the extraction C-magnet to storage-ring injection.

Magnet	Type	Current (A)	Power Supply
ELAM	MLG	487.3	D:ELAM
Q205 (DR)	8Q32	796.0	D:QT205
ECMAG	MSDA	354.6	D:ECMAG
HT900	NDA	25.0	D:HT900
Q901	SQA	90.2	D:Q901
V901	EDWA	173.8	D:V901
HT901	NDB	25.0	D:HT901
Q902	SQD	48.9	D:Q902
Q903	SQD	102.1	D:Q903
Q904	SQD	63.6	D:Q904
Q905	SQA	58.1	D:Q905
HT905	NDB	25.0	D:HT905
Q906	SQC	33.8	D:Q906
HT906	NDB	25.0	D:HT906
V906	MDC	302.4	D:V906
Q907	SQD	16.0	D:Q907
V907	MDC	415.8	D:V907
M4/M5 split			
HT000	NDA	25.0	D:HT000
Q001	SQA	146.7	D:Q001
Q002	4Q24	103.9	D:Q002
Q003	4Q24	23.8	D:Q003
V003	CDC	993.4	D:V003
Q004	SQA	25.7	D:Q004
Q005	4Q24	19.3	D:Q005
VT005	NDA	25.0	D:VT005
HT005	NDA	25.0	D:HT005
H005	MDC	713.3	D:H005
Q006	SQA	132.1	D:Q006
Q007	4Q24	262.9	D:Q007
Q008	SQB	217.1	D:Q008
H008	MDC	713.3	D:H008
Q009	SQB	217.1	D:Q008
Q010	4Q24	262.9	D:Q007
Q011	SQA	132.1	D:Q006
H011	MDC	713.3	D:H005
HT011	NDA	25.0	D:HT011
VT011	NDA	25.0	D:VT011
Q012	4Q24	104.8	D:Q012
Q013	4Q24	116.7	D:Q013
Q014	4Q24	73.9	D:Q014
Q015	4Q24	73.9	D:Q015
Q016	4Q24	89.0	D:Q016
Q017	4Q24	83.0	D:Q017
VT017	NDA	25.0	D:VT017
Q018	4Q24	89.0	D:Q016
VT018	NDA	25.0	D:VT018
Q019	4Q24	83.0	D:Q017
HT019	NDA	25.0	D:HT019
Q020	4Q24	124.0	D:Q020
Q021	SQA	6.0	D:Q021
Q022	LQD	320.0	D:Q022
Q023	LQD	640.0	D:Q023
VT023	NDBW	25.0	D:VT023
Q024	LQD	815.0	D:Q024
HT024	NDBW	25.0	D:HT024
Q025	LQB	840.0	D:Q025

Table 7.14: Magnet locations, type, operating current and power supply configurations for the upstream M4 and M5 lines.

Alignment of the Ring and Injection Beamline

The alignment of the downstream section of the M5 line is critical given the accuracy required to target the inflector correctly and enter the ring tangential to the circulating beam reference orbit. The site coordinates of the MC-1 building were specified initially to place the experimental hall in a location optimal from a shielding and civil-engineering perspective and in consideration of the proximate Mu2e external beamline and experiment. This was further complicated by the fact that the MC-1 service building construction was accelerated to accommodate reassembly and cool down of the $(g-2)$ storage ring. This meant that the storage-ring position and rotation was further constrained because the MC-1 building location was fixed. The rotational orientation of the storage ring is critical given the strict tolerances of the injection system and the fact that a switchyard or injection-bump configuration is not spatially permitted by the external beamline enclosure (at least not without significant cost). The site coordinates now specified for the $(g-2)$ storage ring, and extrapolation of the required incoming injection trajectory and beamline coordinates can be found in Ref. [23] and are shown in Fig. 7.62.

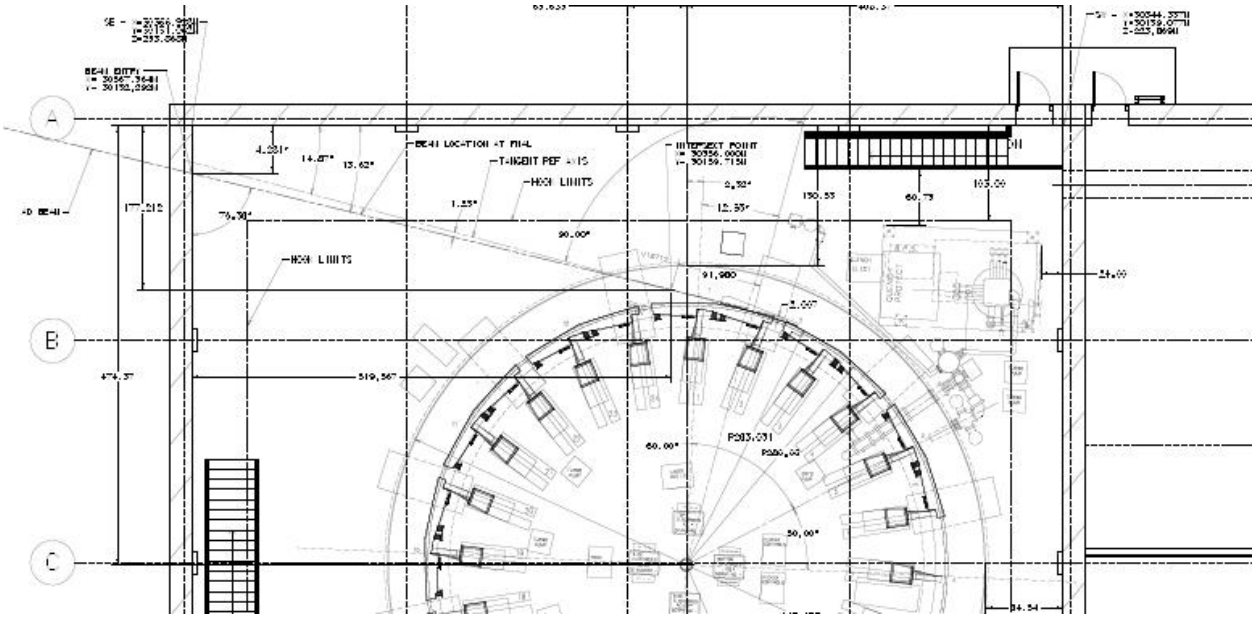

Figure 7.62: Alignment coordinates of the MC-1 hall, beam entry and the preliminary 1.25° point coordinates which have been cross checked or recomputed.

7.5.8 Vacuum Systems

The existing vacuum systems in the rings and transport lines have performed very well during Pbar operation. Typical vacuum readings in the Debuncher and transport lines were approximately 1×10^{-8} Torr. The Debuncher has good ion-pump coverage that should generally be adequate for $(g-2)$ operation. Stochastic cooling tanks, kickers and septa that will be removed during the conversion have built-in ion pumps, so some of these pumps will need to be installed in the vacated spaces. Injection and extraction devices will either have ion pumps integrated into the design, or have additional pumping capacity added to the surrounding area. Vacuum components from the AP2 and AP3 lines should provide most of the needs for the reconfigured M2 and M3 lines. The Accumulator has enough surplus ion pumps available to cover part of the needs for the extraction beamlines. Most of the vacuum pipe for the M4 and M5 lines will need to be purchased. The ion-pump density in the new beamlines will be at least as great as what was used during Pbar operation. Vacuum controls from Pbar will be repurposed for the new beamlines.

The Delivery Ring will retain the present scheme with six vacuum sectors separated by pneumatic isolation valves that can be controlled remotely. The vacuum valves in the D30 straight section will be rearranged slightly to accommodate the new component layout. There will also be manually controlled valves, particularly in the D30 straight section, to allow smaller sections to be isolated. The beamlines will also have isolation valves, both pneumatic and manual, to facilitate repairs and reduce pump-down times.

7.5.9 Infrastructure Improvements

Electrical power for the Antiproton Source is provided by Feeder 24, which operated with a power level of about 4.4 MW during Pbar operation. Although the $(g-2)$ power load is expected to be considerably less than what was used in Pbar by virtue of the reduced beam momentum, the Mu2e experiment must also be able to operate the same magnets at 8.89 GeV/c. For Mu2e, most service buildings are expected to use approximately the same amount of power as they did in Pbar operation. The exception is the AP-30 service building, where there will be an increase in power load from the injection- and extraction-line power supplies. A power test was performed on the individual service building transformers to aid in predicting the power needs for Mu2e [26]. Also, since the Accumulator will no longer be used, approximately 1.4 MW will be available for new loads.

Presently, Pbar magnets and power supplies receive their cooling water from the Pbar 95° Low Conductivity Water (LCW) system. The cooling requirements for $(g-2)$ are expected to be lower than for Pbar operation. However, Mu2e will operate at 8.89 GeV/c and create a substantially larger heat load than $(g-2)$. Fortunately, the removal of the heat load from decommissioning the Accumulator and the D/A line should be enough to offset the increase from the extraction line and other new loads. The M4 and M5 lines will have an LCW branch that will run the length of the new tunnels and connect to the Debuncher header in the D30 straight section. The LCW will also continue into the MC-1 building to be used in the power supply room. If necessary, it is also possible to design smaller closed-loop systems that heat-exchange with the Chilled Water system. This strategy has been used to cool some of the loads in the Target Station. The Chilled Water system has adequate capacity

and is already distributed to the existing Pbar service buildings as well as to the new MC-1 building.

7.5.10 Power Supplies

The magnet power supply systems will provide the necessary current and regulation to transport beam through the Muon Campus beam lines. The transport beam line power supplies will be operated in DC current mode. The power supply system will build on existing power system designs for voltage, current and controls that have been developed by the FNAL Accelerator Division Electrical Engineering Support Department in order to keep the maintenance cost as low as possible.

The Muon Campus beamlines are expected to use two different formats for power supplies. The first type is switch-mode commercial power supplies that can be procured from multiple vendors and operated in voltage mode. Most commercial power supplies are unstable on inductive loads (such as magnets) and do not have built-in compensation correction, which must be added for them to work properly. The switch-mode power supplies have the advantage of being efficient and compact and are more cost effective for lower power applications. The second type of beam line power supplies will be phase-controlled supplies commonly called SCR-type supplies. These supplies will be semi-custom designed and built to FNAL specification. SCR-style supplies will be required to use the AD E/E Support designed voltage regulator and then use a current regulator to close the current loop. New SCR supplies will only be purchased for high-power applications. Some existing Pbar SCR supplies will also be reused in order to save money. For instance, the Delivery Ring power supplies, which are mostly the SCR type, will be reused for Muon Campus operation.

System Layout

AD E/E Support has designed and developed a current regulation and controller system that is used in the DC application. The control portion of the system uses a Programmable Logic Controller (PLC) to manage input power as well as status readback and control through the Accelerator Control NETwork (ACNET) system. A variety of commercial power supplies are used in voltage mode to provide the current to the magnets. This requires an interface circuit to convert the status and control to signal levels that can be provided to the controls system. Two versions of the interface chassis exist and can support 8-16 power supplies.

Each current regulator uses a PC-104 embedded micro controller to provide current regulation for up to four power supplies. This controller also collects the status and control information from the power supplies via the PLC and converts this information into a format that the ACNET controls systems can present to operations.

Current Regulation There are two critical parts of the current regulation system; one is the current-measuring device and the other is the stability of the current reference. Each system will have a total current monitoring DCCT (Direct Current Current Transformer) installed that is used to provide accurate and stable current feedback to the regulator. The current regulation system will be a recent design constructed for the last Main Injector and Linac Ion source upgrades. This system is a Digital/Analog combined regulator built using

a PC-104 embedded processor system that provides the current regulation by providing a total voltage reference to the power supply. This regulator supports four power supplies in a single chassis and provides all of the voltage drive through the power supply for the main current, including any correction needed. The DCCTs used for the feedback will be commercial devices procured at the level that meets the long term stability requirements of the experiment. This regulator system can support operation at the ±4 ppm level as designed but can be improved to the ±0.25 ppm level by procuring a high-performance DCCT. The plan is to use ±300 ppm for the beamline power supplies, which is more economical due to the lower cost current feedback devices. This is a typical regulation specifications for beamlines at FNAL. This system is not intended for fast ramping power supplies and has a dI/dt limiter used during startup. The existing power supplies for the Delivery Ring have much tighter regulation tolerances.

The current regulator has one PC-104 processor that sends an 18-bit digital reference to each of four Sigma Delta DACs in temperature-regulated modules (see Fig. 7.63). Each DAC module receives the analog current from a current output DCCT/HAL probe and converts the current to a voltage using burden resistors in the temperature-regulated module. The reference and current signals are subtracted to generate an error signal, which is then amplified 100 times. This amplified error is then sent to the PC-104 module that adjusts the drive to the power supply to minimize the error signal. The reason for the amplification is to reduce the sensitivity of the PC-104s AD converter. The magnet parameters are loaded into the PC-104 along with the current loop bandwidth and maximum gain limit. It then uses this information to provide the correct correction to each power supply.

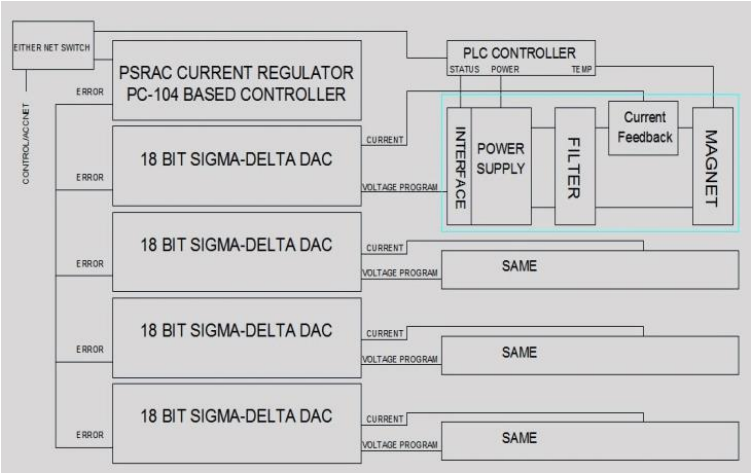

Figure 7.63: Current regulator.

An additional feature of this system is that the PC-104 has a transient recorder built in that will record trip events and provide data for analysis, which is very useful during single-event trips that happen very infrequently. A second option built in this regulator has a window detector that can be set up to monitor current, DAC settings, and the current error signals to ensure that they are within a set range. These limits are set up using an independent path into the processor. The PC-104 monitors and uses four analog signals: current reference, current, voltage, and current error. These signals are stored in the transient

recorder during a trip and can be plotted at 1440 Hz.

PLC Controller All of the control and status read backs are provided through the PC-104 current regulator using a single E-net connection to the ACNET system. The power-supply system uses a PLC to collect data from four power supplies via an E-net connection and passes it through the PC-104 to ACNET. The information is collected in the PC-104 that converts it to ACNET format. The PC-104 also provides the On, Off, and Reset functions to the power supplies through the PLC that manages things that are common to all four supplies. The PLC is a device that allows for the level shifting of signals from the many different types of power supplies that will be used. All of the signals and controls become local to the power supply location with only an E-net cable back to the controls system. This has the benefit of reducing the amount of controls cards needed for collecting data, and the cable that is needed to connect to the cards.

All of the power supplies will need monitoring and control of the 480 VAC input power. The PLC is used to manage the control of this power and to monitor signals common to all supplies: safety system, door interlocks, smoke detectors, and magnet over-temperature. The PLC interfaces the 480 VAC input power to the supplies using a custom-built starter panel that we have chosen to have a limit of 40 kW. Two of these 40 kW starter panels can be installed in a standard relay rack to power two supplies or groups of supplies. This choice to use 40 kW as a power limit to each group of supplies is based on providing reasonable wire for the input power, size of starter on the panel, and a reasonable amount of space for the high-current cables to exit the rack to the magnets. This allows enough room to install up to four 10-kW power supplies in one half of a rack to reduce the amount of floor space needed for racks of power supplies. The starter panel provides a place for this connection; the main contactor on the starter panel uses a +24 VDC coil that can be directly connected to the Electrical Safety System.

Interface Chassis We will be using the PC-104 embedded current-regulation system with many different sizes and manufacturers of power supplies. Some use TTL for status and control, while others use +24 VDC, so the interface chassis and cards provide a place to convert signals to useful levels that can be sent back to the controls system. Using the PLC and interface chassis allows the PC-104 code to be identical for all systems, with the need for only some of the PLC code to be unique.

Switch-Mode Power Supply We plan to group switch-mode (SM) power supplies by size in order to reduce the number of different sizes we need to procure and the number of spares to store. The specification for the SM-style power supplies will define the voltage, current, and power level for each size, as well as a voltage regulation and ripple. The plan is to share a common line voltage for all supplies so that supplies with different power levels can be used in the same rack. There are only three or four manufacturers in the US that can meet all of the Muon Campus needs.

SCR-style power supply The specification for the SCR-style power supplies will be based on the present design of the 75 kW power supplies used in the Main Injector. This

specification requires the use of the FNAL Accelerator Division E/E Support designed voltage regulator. E/E Support will have these voltage regulators constructed, and two copies are provided to the manufacturer to use for testing. The reason for this is to reduce the maintenance load on the engineering staff caused by unique regulation electronics of many different manufacturers. SCR supplies in general support two quadrant operation; this will not be needed for the Muon Campus beamlines. However, to minimize the variety of supplies requiring support in the Accelerator Division, this requirement will be maintained.

Manufacturers of modern SCR power supplies use PLCs internal to the equipment rather than constructing custom circuit boards to provide control connections. The specification for the power supply will include the detailed information needed to ensure that any PLCs used are compatible with maintenance tools we have on hand.

SCR supplies will need LCW cooling for at least the SCRs and possibly the magnetics. The LCW cooling water will be sourced from the M5-line tunnel to the MC-1 power supply room. The power supplies will need 50 kW of cooling with a minimum pressure range of 60-100 psi and a flow of 18 GPM.

Power supply locations

Power Supplies for the Muon Campus will be housed in a combination of existing and newly constructed buildings. Power supply changes for the M1 line are relatively minor and can be incorporated into the existing F23 and AP-0 service buildings. Although the changes to convert the AP2 and AP3 lines into the M2 and M3 lines are significant, there will be enough room in the existing F27, AP0, and AP-30 service buildings to accommodate them. The upstream M4 line will have power supplies located in the AP-30 service building. The M5 line will be powered by supplies located in the MC-1 power supply room. In addition, the MC-1 power supply room will also house supplies for a large part of the downstream M4 line, including the critical A/C Dipole system, which is not needed for $(g-2)$. The sharing of the MC-1 power supply room saved considerable cost for the Mu2e experiment by eliminating the need for an additional service building or a larger power supply area in the Mu2e service building with extremely long cable runs. Figures 7.64 and 7.65 show the power supply layouts in the AP-30 and MC-1 service buildings.

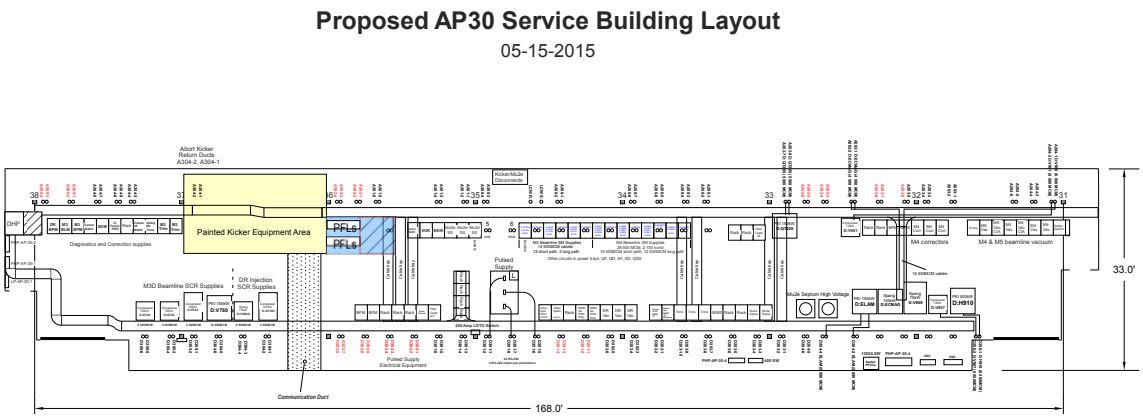

Figure 7.64: Power Supply layout in the AP-30 Service Building.

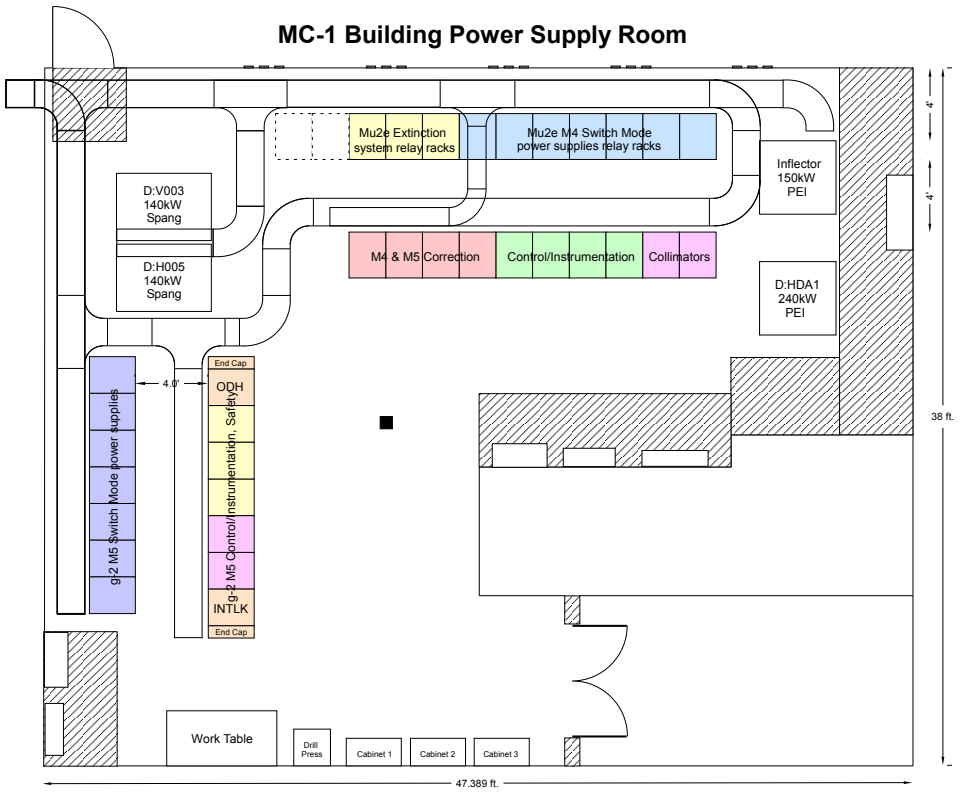

Figure 7.65: Power Supply layout in the MC-1 Power Supply Room.

7.6 Controls and beam monitoring

7.6.1 Accelerator controls

A well-established controls system allows devices in the former Antiproton-Source ("Pbar"), now Muon, service buildings and tunnel enclosures to receive information such as synchronization signals and to communicate back to other accelerator systems. A map of the service buildings, labeled "AP" for former Antiproton-Source buildings, and "F" for buildings which are part of the F-sector of the Tevatron, is shown in Fig. 7.66. Devices in the new extraction beamlines and MC-1 building will also need to be connected to the controls system.

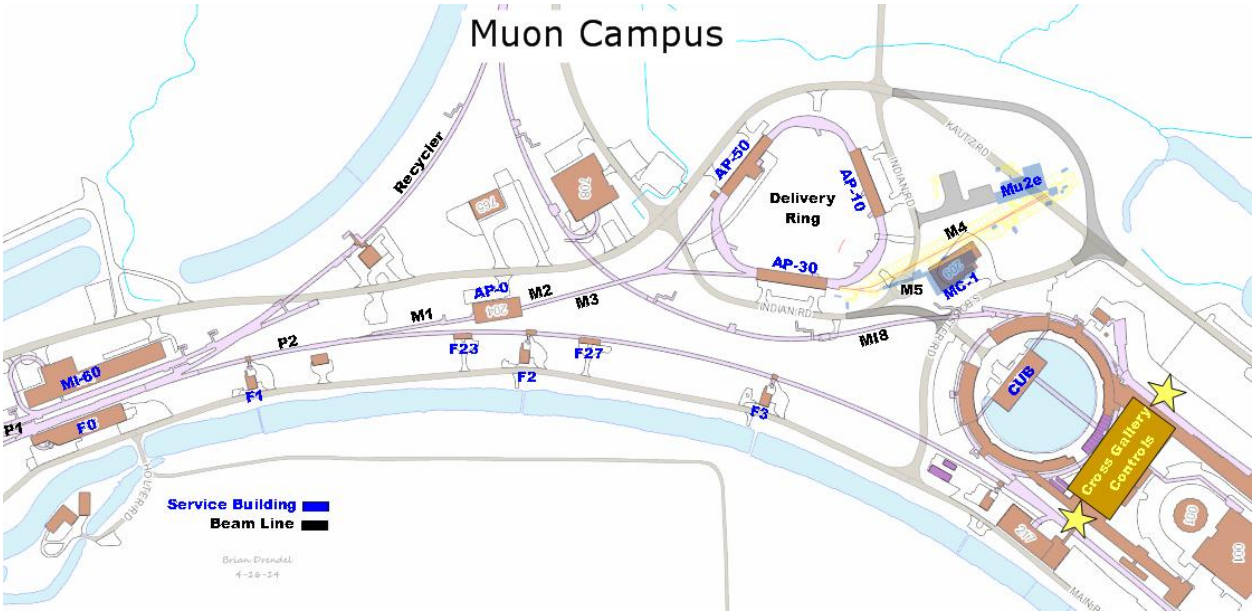

Figure 7.66: Muon Campus service buildings.

For completeness, all changes to the controls system needed for the Muon Campus are described here. The re-routing of controls in the Delivery Ring is covered by the Delivery Ring AIP, and work required only for Mu2e is covered by the Mu2e project. Cable pulls to the MC-1 building and work required to establish network, phone, and the Fire and Utility System in the MC-1 building is covered by the MC-1 Building GPP. Other work related to establishing accelerator controls in the MC-1 building is on the $(g-2)$ project.

CAMAC and links

The existing accelerator service buildings will continue to use the existing legacy controls infrastructure. These service buildings include all of the Main Injector service buildings, as well as F0, F1, F2, F23, F27, AP0, AP10, AP30 and AP50. Future Muon Campus service buildings, including MC-1, will be upgraded to a more modern controls infrastructure which will be discussed later in this document.

CAMAC Computer Automated Measurement and Control (CAMAC) crates exist in each service building and communicate with the control system through a VME-style front-end computer over a 10 MHz serial link as shown in Fig. 7.67. Both digital and analog status and control of many accelerator devices occur through the CAMAC front ends. There should be ample CAMAC-crate coverage for $(g-2)$ operation in the existing Muon service buildings, as there is excess capacity in most of the existing crates, and very few crates will need to be added or moved.

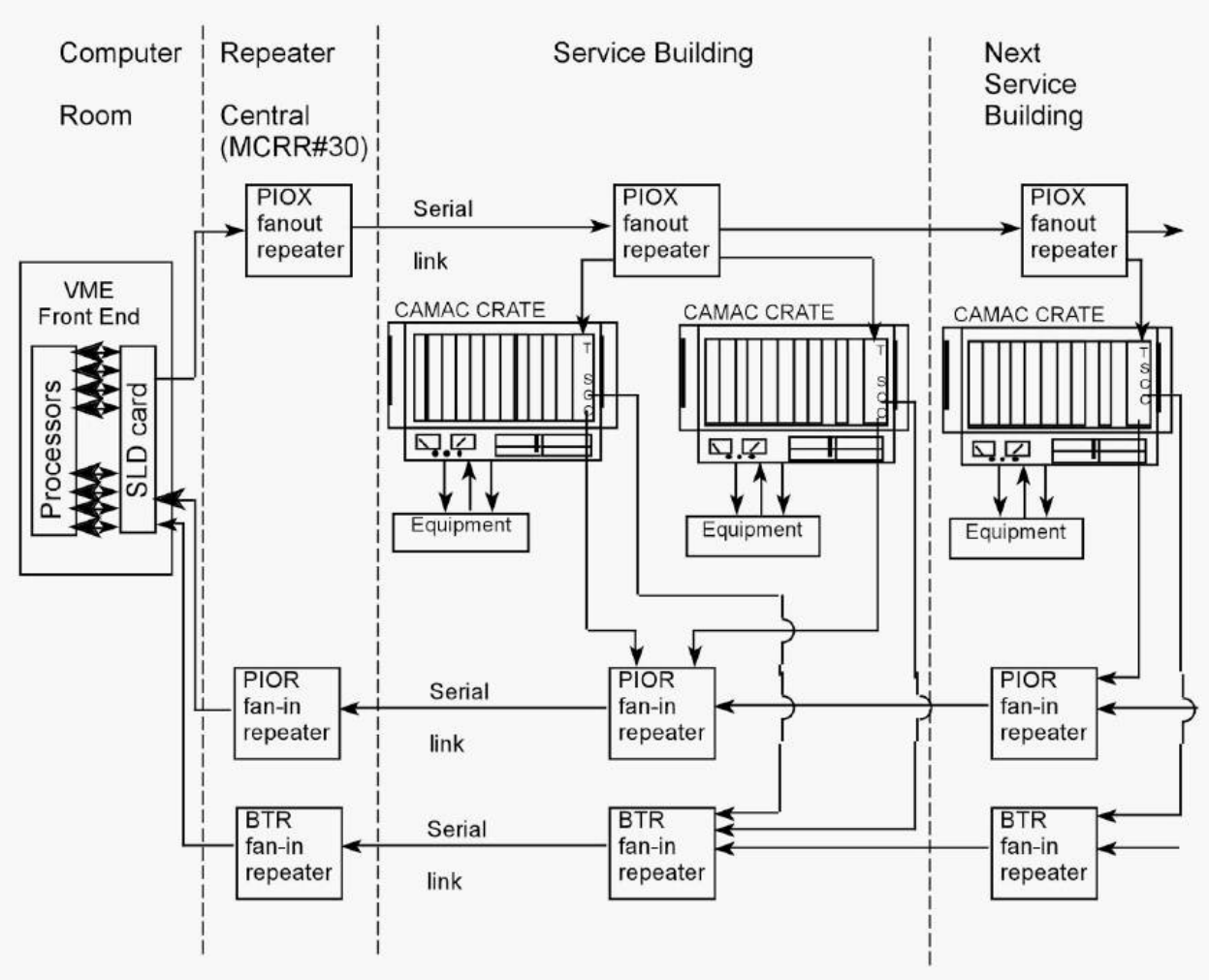

Figure 7.67: Legacy CAMAC crates interfacing VME front ends via serial links provide both analog and digital status and control of accelerator devices, and will continue to be used in existing Muon service buildings [27]. Drawing courtesy of the AD Operations Controls Rookie Book [28].

Serial Links There are serial links that are distributed through and between the service buildings via the accelerator enclosures that provide the necessary communications paths for CAMAC as well as other necessary signals such as clock signals, the beam permit loop, and the Fire and Utilities System (FIRUS). Controls serial links can be run over multimode

fiber-optic cable or copper Heliax cable. Most Muon links that run through accelerator enclosures are run over Heliax, which should function normally in the radiation environment expected for $(g-2)$ operations [29].

TCLK Accelerator device timing that does not require synchronization to the RF buckets will remain on the existing 10 MHz Tevatron Clock (TCLK) system. The existing TCLK infrastructure will remain in existing service buildings and new TCLK link feeds will be run via multimode fiber optic cable from the Mac Room to the MC-1 service building [29].

Beam Synch Accelerator device timing for devices that require synchronization to the RF buckets will continue to be handled through the Beam Synch Clocks; however, a few changes will be required to maintain functionality. The F0, F1 and F2 service buildings will need both 53-MHz Main Injector beam synch (MIBS) for SY120 operations and 2.5-MHz Recycler beam synch (RRBS) for $(g-2)$ and Mu2e operations. These buildings already support multiple beam synch clocks, so the addition of RRBS will require minimal effort. An obsolete 53-MHz Tevatron beam synch (TVBS) feed in the MI60 control room will be replaced with a 2.5-MHz RRBS feed in order to provide the necessary functionality. The remaining Muon service buildings currently use 53-MHz MIBS, but will require 2.5-MHz RRBS for $(g-2)$ and Mu2e operations. This functionality can be obtained by replacing the MIBS feed at F0 with RRBS and using the existing infrastructure. Further upgrades and cable pulls will only be required if it is later determined that both MIBS and RRBS are required in these service buildings. New beam synch feeds to the MC-1 building were run via multimode fiber-optic cable from the Mac Room as part of the MC-1 Building GPP [29].

Beam Permit The Delivery-Ring permit loop provides a means of inhibiting incoming beam when there is a problem with the beam delivery system. The Pbar beam permit infrastructure will be used in the existing buildings. The CAMAC 201 and 479 cards, which provide the 50-MHz abort loop signal and monitor timing, will need to be moved from the Mac Room to AP50 to accommodate the addition of the abort kicker at AP50. Existing CAMAC 200 modules in each CAMAC crate can accommodate up to eight abort inputs each. If additional abort inputs are required, spare CAMAC 200 modules will be repurposed from the Tevatron and will only require a minor modification. The permit loop will be extended to the MC-1 building via multimode fiber-optic cable from the Mac Room. Implementation of a Hot-Link Rack Monitor abort card is not expected to be completed by the time of $(g-2)$ operations. As a result the abort inputs from devices in the MC-1 building will be transported to existing CAMAC 200 modules in the AP-30 service building via a Heliax cable that will be pulled through the accelerator enclosures [29].

Operational and permit scenarios are under development. The capability of running beam to the Delivery-Ring dump when Mu2e and $(g-2)$ are down will be needed, as well as the ability to run to either experiment while the other is down.

Hot-Link Rack Monitor

New controls installations will use Hot-Link Rack Monitors (HRMs) in place of CAMAC. A HRM runs on a VME platform that communicates with the control system over Ethernet

as shown in Fig. 7.68. Unlike CAMAC, no external serial link is required, minimizing the need for cable pulls between buildings. Each HRM installation provides 64 analog input channels, 8 analog output channels, 8 TCLK timer channels, and 8 bytes of digital I/O. This incorporates the features of multiple CAMAC cards into a single, compact chassis. Like CAMAC, when additional functionality or controls channels are needed, additional units can be added. Two HRMs will be installed in the MC-1 building and should provide ample controls coverage for both accelerator and experimental devices.

Figure 7.68: A Hot-Link Rack Monitor is a flexible data acquisition system composed of a remote unit and a PCI Mezzanine card that resides in a VME crate. Each HRM provides provides sixty-four 16-bit analog input channels, 8 analog output channels, 8 TCLK timer channels and 8 bytes of digital I/O. HRMs will eventually replace all of the functionality of CAMAC [30].

Ethernet

Many modern devices have some form of Ethernet user-interface. In addition, many devices and remote front-ends use Ethernet to interface with the control system, instead of using the traditional CAMAC. The results are an increasing demand on the Controls Ethernet. Figure 7.69 is a map of the Muon Controls network. All of the current Muon Ring service buildings have Gigabit fiber-optic connections from the Cross-Gallery computer room to Cisco network switches centrally located in each service building. These will provide ample network bandwidth and connections after the reconfiguration for $(g-2)$ and Mu2e. A central Ethernet switch that fans out to the other Muon buildings is currently located in AP10, but will need to be moved to AP30, as will be discussed later in this document [31].

Ethernet connects between the Muon-Ring service buildings via multimode fiber-optic cable paths that traverse the Rings enclosure on the Accumulator side. The multimode fiber currently in place will be replaced by single-mode fiber under the Delivery Ring AIP as needed for the high-radiation environment of Mu2e.

Most beamline service buildings have gigabit fiber connected to centrally located network switches that provide ample network bandwidth and connections. AP0, F23, and F27 are the only three buildings that do not have this functionality. AP0 runs off a 10 Mbps hub that connects to 10Base5 “Thicknet” that runs through the Transport and Rings enclosures

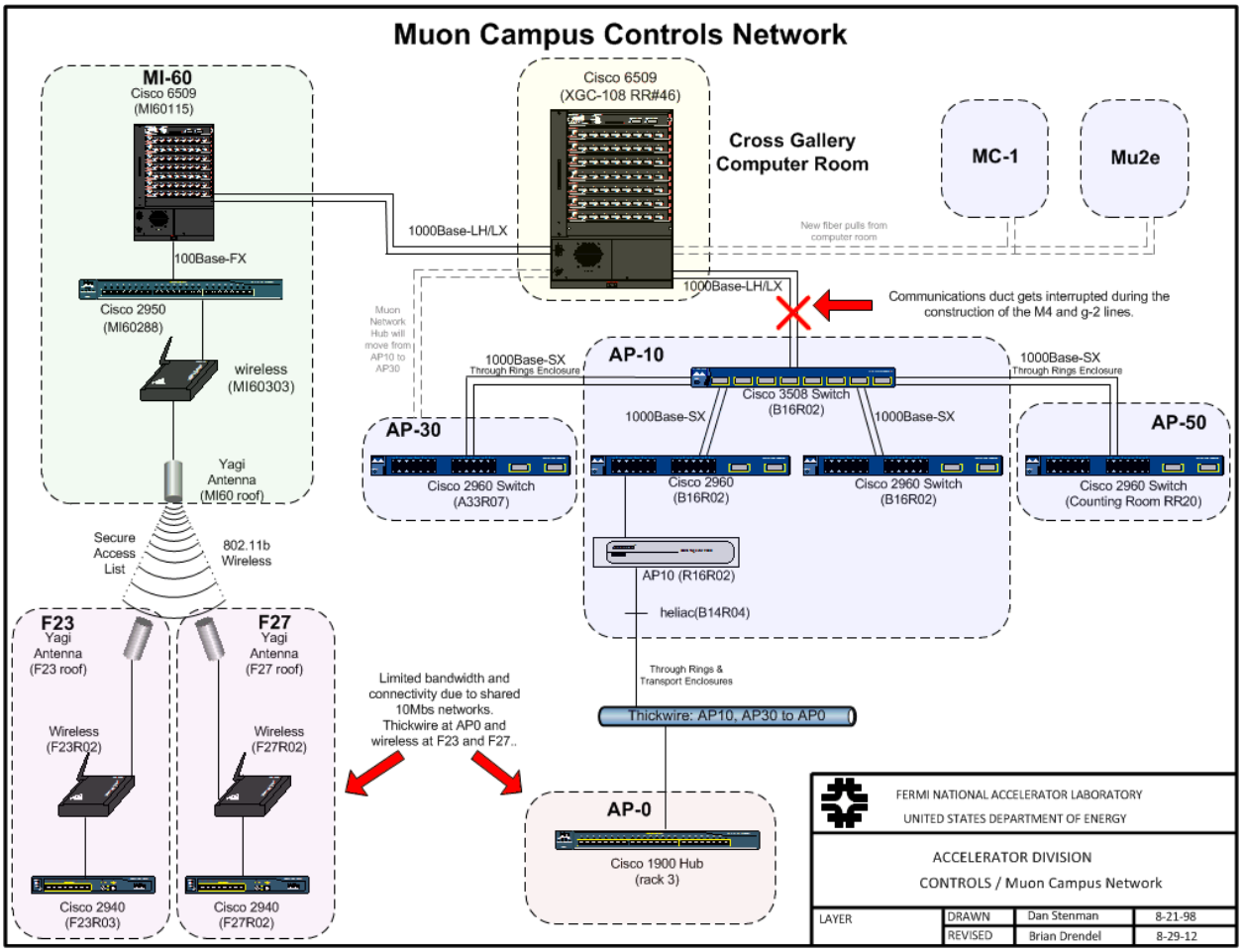

Figure 7.69: Controls Ethernet to the Muon service buildings is expected to be adequate for $(g-2)$ operations. The central switch at AP10 will be moved to AP30. Legacy networks at AP0, F23, and F27 have limited bandwidth and connectivity, but should be sufficient for $(g-2)$ operations.

back to AP10, while F23 and F27 run off 802.11b wireless from MI60. Both are 10 Mbps shared networks with limited bandwidth and connectivity. It is anticipated that the network in these three buildings will be sufficient for $(g-2)$ operations.

Controls connectivity

Civil construction of the M4 and M5 beamline enclosures will result in the removal of the underground controls communication duct that provides the connectivity between the Accelerator Controls NETwork (ACNET) and the Muon Campus [32]. Included in this communication duct is the fiber-optic cable that provides Ethernet connectivity, as well as 18 Heliax cables that provide the controls serial links and other signals including the FIRUS [29]. These cables currently connect from this communications duct to the center of the 20 location in the Rings enclosure, and travel through cable trays on the Delivery Ring side to the AP10 service building. New communications ducts from the existing manholes are being constructed as part of a General Plant Project. These communications ducts go directly to AP30, MC-1 and Mu2e service buildings without going through accelerator enclosures. See Fig. 7.70 for drawings of the current and future controls connectivity paths.

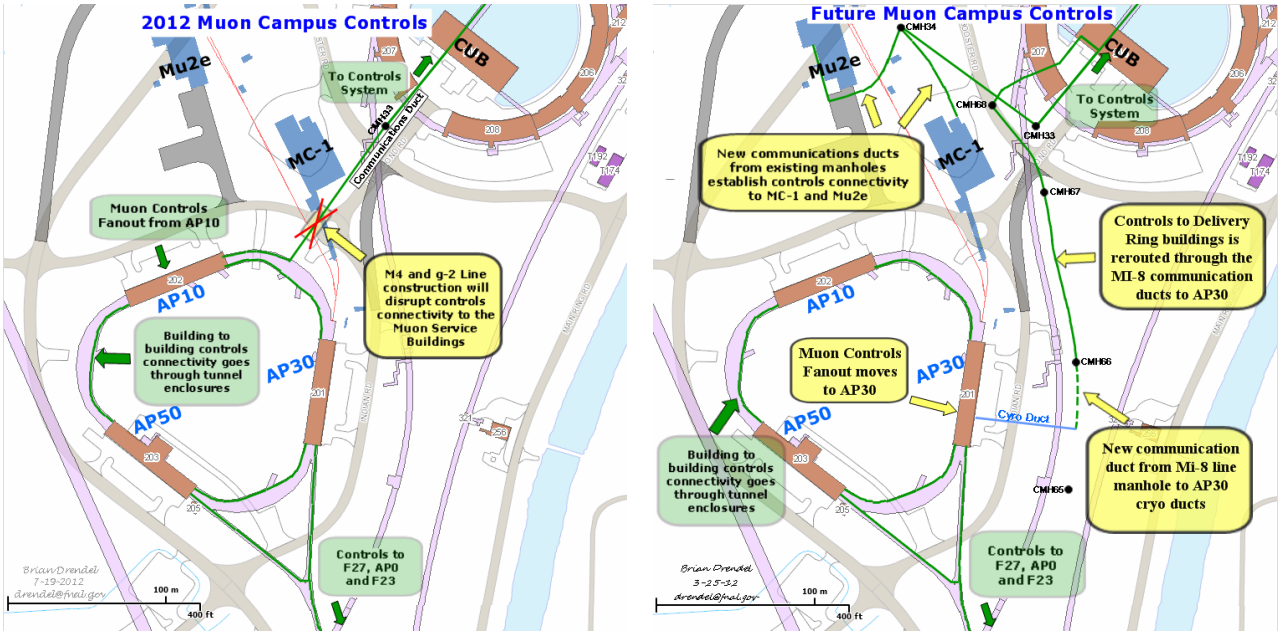

Figure 7.70: *(left)* Communication paths prior to Muon Campus operations. During construction of the M4 and M5 beam line enclosures, the communications duct that provides controls connectivity to the Muon Campus will be interrupted and controls will need to be restored via a different path. *(right)* Controls signals will be rerouted through the MI-8 manholes to a newly constructed manhole near AP30. From this manhole, communication ducts will connect to existing and unused cryo duct work to get to the AP30 service building. New controls will need to be established at the MC-1 and Mu2e building via new communications ducts that connect to an existing manhole [33].

Restoring connectivity When the Heliax and fiber-optic cables are cut during the removal of the above-mentioned communications duct, controls connectivity will be lost. New fiber optic cable has been pulled from the cross gallery, through the MI-8 line communications ducts to AP30. As a result, the Ethernet and controls links will fan out from AP30 instead of AP10. This will require some additional controls hardware configuration and labor. Efforts will be made to minimize the disruption by staging the new hardware at AP30 before the communication duct is cut. This is especially important for FIRUS which is necessary for monitoring building protection. This work is being done as part of the Delivery Ring AIP. More details can be found in Refs. [33] and [34].

Establish connectivity to MC-1 New fiber-optic cable will be pulled from the Cross Gallery to the MC-1 service building. Single-mode fiber is needed for Ethernet and FIRUS, and multimode fiber is needed for the timing links and the abort-permit loop. A bundle of 96-count single-mode and a bundle of 36-count multimode fiber-optic cable will be pulled to MC-1. The fiber bundles will share a common path with the fiber bundles headed toward Mu2e from the Cross Gallery to the manhole by Booster West Tower. Both fiber bundles will travel through a single inner duct to the manhole. The Mu2e and MC-1 fiber bundles will then branch off to a second manhole inside a common inner duct, and then separate into the new communication ducts to the Mu2e and MC-1 service buildings. The fiber bundles to the MC-1 building were pulled by the MC-1 Building GPP, and will be pulled to the Mu2e building by the Mu2e project. The fiber will provide ample connectivity for all Ethernet and controls signals for both the accelerator and experiment. The $(g-2)$ experiment anticipates requiring network rates approaching 100 MB/s during production data taking which can be handled easily with the proposed infrastructure.

Safety system

The existing safety system enclosure interlock hardware installed in the Pre-Target, Pre-Vault, Vault, Transport and Delivery Rings will remain in place. The tunnel egress between the Delivery Ring and Transport enclosures on the AP2 side will be blocked as a result of the new beam abort dump. A safety system mini loop will be created on each side of the abort dump to satisfy ES&H requirements. Reset boxes will be repurposed from the Tevatron for these mini loop areas [35].

The Delivery Ring enclosure will be separated from the new extraction line enclosure under AP30 using a gate. The Delivery Ring side of the gate will use a reset box repurposed from the Tevatron. The Extraction enclosures area will be defined using interlocked gates. One gate is the Delivery Ring / Extraction Enclosure gate; a second gate will separate the Extraction Enclosure from the M4 Enclosure (beam to Mu2e). The third gate separates the Extraction Enclosure from the MC-1 experimental hall. The Extraction Enclosure and the MC-1 experimental hall will each use the Rack Mounted Safety System (RMSS) chassis for their safety system interlocks. These chassis will be mounted in a rack dedicated for safety system equipment. The Extraction Enclosure RMSS will be located in the AP-30 service buildings safety system relay rack and the MC-1 RMSS will be located in the MC-1 buildings safety system relay rack which is located in the power supply room. The RMSS chassis uses a reset box similar to the Main Injector [35].

The three existing Pbar area Critical Device Controllers (CDCs) will function much as they presently do, with one to bring beam into the AP-0 area, one to bring the beam on target for $(g-2)$ operation, and one to take the beam around the AP0 target for Mu2e operation. These three CDCs will remain in the existing AP0 safety-system relay rack. Three new CDCs will be installed in the AP30 safety system relay rack to accommodate Delivery Ring extraction for $(g-2)$ and Mu2e beam operations. One CDC will be called the Extraction CDC to bring beam out of the Delivery Ring and into the Extraction Enclosure. This CDC will be repurposed from the Recycler CDC. The second CDC will bring beam from the Extraction Enclosure to the MC-1 Experimental Hall and is named the MC-1 CDC. This CDC will be repurposed from the Tevatron CDC. The third CDC will bring beam from the Extraction Enclosure to the M4 Enclosure for Mu2e operation and will be named the M4 CDC. The M4 CDC will be repurposed from the Pelletron CDC. The Extraction CDC can only be permitted when the MC-1 CDC or the M4 CDC is permitted. A Safety System Logic Module will be installed in the AP30 safety system relay rack to accommodate the "OR" function needed for the Extraction CDC. This Logic Module will be repurposed from the Tevatron Logic Module. Existing interlocked radiation detectors may be moved if needed and the system modified to include Total Loss Monitors (TLMs). The key trees from Pre-Vault, Pre-Target, and Transport will remain in the Main Control Room (MCR), while the remote AP10 key tree will likely be moved from AP10 to the MCR [35].

Cryogenics will be used in the MC-1 Refrigerator Room and the experimental hall, so an Oxygen Deficiency Hazard (ODH) system will be implemented using a safety-rated PLC system. This PLC will be located in the MC-1 buildings Power Supply Room in a dedicated relay rack.

Cable Path Copper safety system cables will be pulled to AP30, MC-1 and Mu2e. The existing Safety System signal trunk lines, which consist of seven 20-conductor #18 AWG cables that run from the safety system vault room XGC-005, through the Central Utility Building (CUB) to AP10, will be interrupted due to the Muon Campus installation. These trunk lines will need to be spliced at CUB and replaced with new cables from CUB to the AP30 building. These cables will be pulled at the same time the Control System fiber in order to minimize contract electrician costs. Below we will outline how we will establish the Safety System signals for the Transport and Delivery Rings, as well as the new MC-1 and Mu2e areas. Figure 7.71 gives a pictorial representation of each of the required cable pulls [35] [33].

Interlocks The safety system will need to be reestablished to the existing Muon Campus areas when the seven 20-conductor cables are interrupted. New junction boxes will be installed at CUB and at AP30, new cables will be pulled as shown in Fig. 7.71, and a new safety-system end rack will be installed on the existing safety system relay rack at AP30 to accommodate three critical device controllers and a Logic Module for $(g-2)$ and Mu2e operations [35] [33].

Radmux The Multiplexed Radiation Monitoring Data Collection System (MUX) is operated by the ESH&Q / Radiation Protection / Instrumentation Team. The MUX system

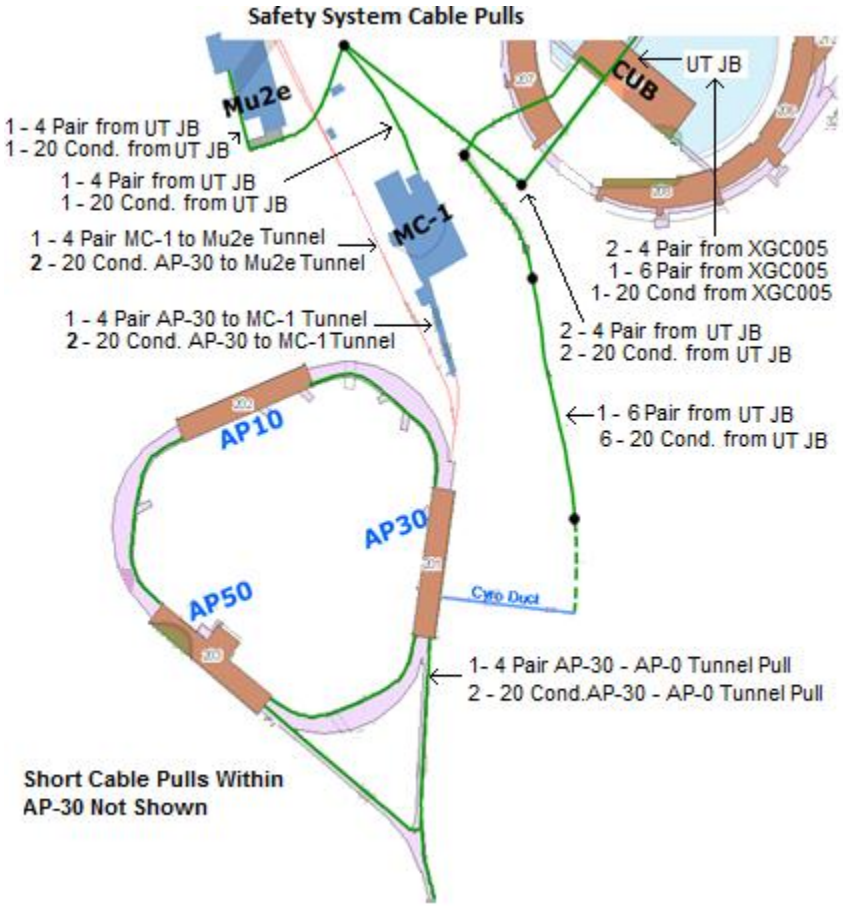

Figure 7.71: Safety system interlock cable pulls [35] [33].

is used to collect data from connected radiation monitors throughout the accelerator areas, beamline areas, and test areas at the Laboratory. The system provides an interface between the radiation monitors and the hardware network, provides real-time data for its various users, logs the raw data, and processes the data into formatted reports for users and for archive purposes. Additionally the archived data serves as the legal record of radiation levels throughout the laboratory [36]. Radmux connectivity will be restored to the existing muon buildings and established to the MC-1 Experimental Hall via new cable pulls [33].

Phone Phone connections to the existing Muon service buildings will be reestablished by splicing into the 400-pair cable in the MI-8 communications duct. A new section of 100-pair cable will be run from the splice via a new communications duct path established by the Delivery Ring AIP to the AP30 service building. Phone connections to the MC-1 Experimental Hall will be established by splicing into 400-conductor pair phone line in the CMH33 Manhole and running new 100-conductor pair phone line to the MC-1 and Mu2e Experimental Halls [37].

Site Emergency Warning System The Site Emergency Warning System (SEW) currently runs to the Muon Rings buildings over the CATV system. When the communications

duct is cut, the CATV system will not be reestablished to the Muon Rings buildings. Instead, the SEWs will be run over single mode fiber optic cable to AP30 and then through the Muon Rings enclosure to AP10, where a connection will be made to the existing system. The fiber will be fusion-spliced to make one continuous fiber path all of the way to AP10. No cabling infrastructure will be needed for the SEWs in the Mu2e and MC-1 service buildings. A paging system will be internal to each building and will be tied to a radio receiver (called a TAR) which receives the SEWS radio broadcast system. The messages will be broadcast over the paging system [38].

7.6.2 Accelerator instrumentation

Beam monitoring can be divided into distinct zones: primary protons, mixed secondaries, proton secondaries, and muons. The locations of each of these areas are shown in Fig. 7.72. The expected beam properties in each of these areas are shown in Table 7.15.

Beam Type	Particle Species	Beam Momentum (GeV/c)	Number of Particles per pulse	RF Bucket (MHz)	Bunch Length (ns)	Transverse Emittance (mm-mr)
Primary protons	p	8.9	10^{12}	2.515	120	18π
Mixed secondaries	μ^+, π^+, p, e^+	3.1	10^7 to 2×10^8	2.515	120	40π
Proton secondaries	p	3.1	10^7	2.515	120	40π
Muons	μ^+	3.1	$< 10^5$	2.515	120	40π

Table 7.15: Expected properties of primary proton beam, secondary beam off the target, and muon beam from pion decay relevant to instrumentation designed to measure beam. Transverse emittances are 95% normalized.

Primary proton beam

Instrumentation for the primary proton beam in the Recycler, P1 stub, P1, P2 and M1 lines is covered by the Beam Transport AIP. Much of the instrumentation needed to measure the primary proton beam during $(g-2)$ operation already exists, but needs to be modified for use with the faster cycle times and 2.5-MHz RF beam structure. The overall beam intensity is similar to that seen in Pbar stacking operations, and in many cases requires only small calibration changes be made to the instrumentation. Toroids will be used to monitor beam intensity and will be used in conjunction with Beam Loss Monitors (BLMs) to maintain good transmission efficiency in the beamlines. Multiwires and Secondary Emission Monitors (SEMs) will provide beam profiles in both transverse planes. Beam Position Monitors (BPMs) will provide real-time orbit information and will be used by auto-steering software to maintain desired beam positions in the beamlines.

Mixed secondaries

Mixed-secondary beam will traverse the M2 and M3 lines, as well as the Delivery Ring. Changes to existing instrumentation are required in these areas as a result of the secondary beam being approximately two orders of magnitude lower in intensity than it was during

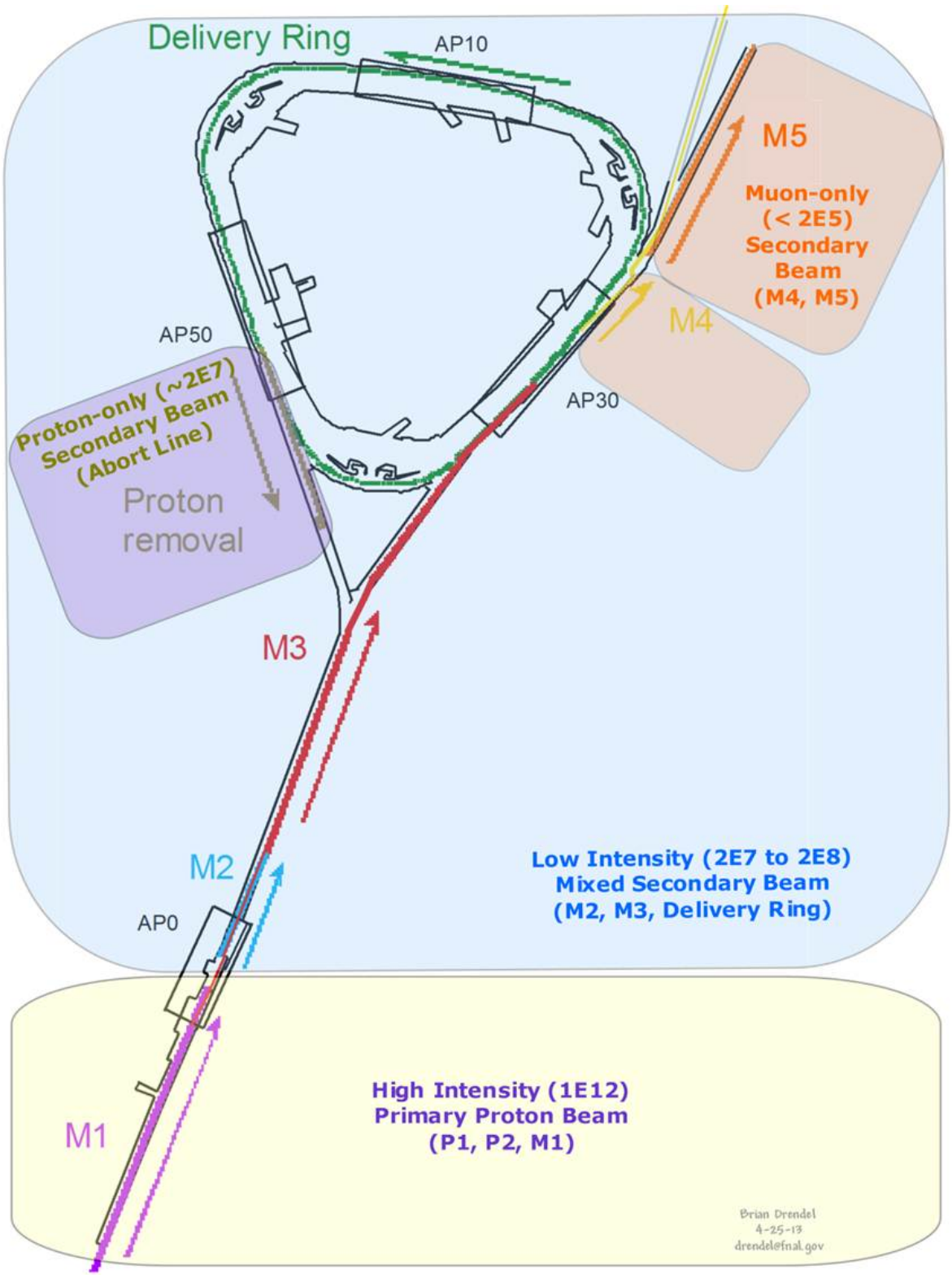

Figure 7.72: Beam monitoring can be divided into four different zones, each with different instrumentation schemes. High-intensity proton beam will be monitored with Toroids, BPMs and BLMs. Low-intensity secondary and proton-only secondary beam will be monitored with Ion Chambers, BLMs and SEMs. Muon-only beam will be monitored with Ion Chambers and PWCs.

the former Antiproton-stacking operations. In addition, 2.515 MHz bunch structure and a faster pulse rate must be taken into consideration. Mu2e beam will have beam intensities four to five orders of magnitude higher than $(g-2)$ operations in the M3 line and Delivery Ring, so design upgrades take into account the vastly different beam intensities required for both experiments. Beam studies have been conducted in order to help determine what instrumentation best suits the low-intensity secondaries of $(g-2)$ operations [2].

Toroids Four toroids are available for use in the secondary beamlines and were the primary intensity-measurement device in these lines during Antiproton operations. These will be used for Mu2e operations; however, beam studies show that even with high gain and careful filtering, they are not able to measure beam at $(g-2)$ operational intensities [2]. As a result, toroids will not be used during normal $(g-2)$ operations, but will still be used with higher-intensity beams during commissioning and studies periods.

Ion chambers Ion chambers will become the primary beam-intensity measurement device for mixed-secondary beam. They are relatively inexpensive devices that can measure beam intensities with an accuracy of $\pm 5\%$ with as little as 10^5 particles. Ion chambers were used in the AP2 line in the past, and work was done during beam studies to recommission the ion chamber that used to be operational near the end of the AP2 line [2]. For $(g-2)$ operations, ion chambers will be implemented in the M2 line, M3 line, and the Delivery Ring; these ion chambers will be installed in a vacuum can with motor controls to allow them to be pulled out of the beam. Figure 7.73 shows the ion chamber design. The vacuum can with motor controls that the ion chamber sits in will be described in the PWC section below.

Each ion chamber consists of one signal foil interleaved between 24 high-voltage foils. The foils are sealed in an aluminum chamber continuously purged with an 80% argon - 20% carbon dioxide gas mix. The standard ion chamber is shown in Fig. 7.73. Protons passing through the $ArCO_2$ gas generate 96 e/ion pairs or about 1.6×10^{-17} charges/cm which equals about 1.6 pC for 10^5 protons [39].

The ion chambers are made retractable because the beam going through those ion chambers and the vacuum windows required to separate beam tube vacuum from the $ArCO_2 2$ gas required for the chamber would result in excessive Coulomb scattering during high-intensity Mu2e operations [40]. The solution is to make the ion chamber retractable much like what will be discussed in more detail in the Proportional Wire Chamber section below. The ion chamber will be installed inside of an anti-vacuum chamber with two titanium vacuum windows to provide a barrier between the gas needed for the ion chamber and the beamline vacuum. The entire anti-vacuum chamber would be mounted inside of a vacuum can that is common to beam tube vacuum. The ion chamber will be on a motorized drive that would allow it to be moved in or out of the path of beam [39].

Beam studies were completed to check the effectiveness of using ion chambers in the range of intensities expected during $(g-2)$ operation [2]. One ion chamber was installed in the upstream portion of the AP2 beam line at the 704 location, while the other ion chamber was located at the downstream portion of the AP2 line at the 728 location (Fig. 7.8. Both ion chambers were shown to integrate beam charge as expected over the normal range of $(g-2)$ operational intensities for the M2 and M3 lines as can be seen in Fig. 7.74.

Wall Current Monitors Wall Current Monitors (WCMs) are non-destructive intensity-measurement devices that could be used for the mixed-secondary beam. These devices have the advantage of being completely passive and not requiring a break in the vacuum, which may make them a better fit in the M3 line where we need to minimize beam losses during the higher intensities of Mu2e operations, and in the Delivery Ring where beam circulates multiple times for $(g-2)$ operations and for approximately 56 ms during Mu2e operations. A new WCM design has been developed that would provide accurate intensity measurements for secondary beam during $(g-2)$ operations. The design is based on that of a WCM for Mu2e extraction. Each slice of the slow-spilled Mu2e beam is approximately 2×10^7, which is consistent with the intensity that we would expect in the M3 line and Delivery Ring during $(g-2)$ operations. The prototype WCM is currently installed in the Delivery Ring and will remain in place during $(g-2)$ operations. If additional funding becomes available, additional WCMs could be built for other areas.

Secondary Emission Monitors SEMs will be used to measure beam profiles in the M2 and M3 lines. There are 24 SEMs in the former Antiproton-source beamlines available for use. SEM tunnel hardware will require some maintenance, and locations where SEMs are moved will require new cable pulls. Beam studies showed that special high-gain preamps are required to measure the low-intensity secondary beam during $(g-2)$ operations [2]; the design is described below.

SEMs will provide profile information via Fermilab generation-3 profile-monitor scanners and Fermilab standard profile-monitor software. Each scanner connects to one SEM and communicates to the control system via an Ethernet connection. The scanner is at the center of all profile monitor installations. It collects the charge from each of the detector wires and converts the values of the charges to a set of digital numbers. The data are transferred to the Accelerator Control System for analysis and display. Example profiles are shown in Fig. 7.75.

The scanner consists of five printed circuit boards, one controller board and four analog integrator boards. It has a set of 96 integrator circuits, 48 for horizontal and 48 for vertical. The integrators collect the charge from each of the detector titanium strips and converts it to a voltage value proportional to the total charge collected. The basic integration capacitor value for most scanners is 100 pf; this value provides the most sensitivity. Larger capacitors are used in higher-intensity beams to minimize the possibility of overloading the integrators. The integrators collect charge until they reach the end of the integration duration set by the user or until at least one wire reaches the preset threshold voltage. At the end of the integration period, the integrators are switched from the sample mode to the hold mode. The integrated voltages on each channel are measured one by one and converted to digital values.

The third-generation scanner (Fig. 7.76) is an evolution of the previous design. The SEM interfaces to the scanner through the integrator boards as in the previous version. The control board centers around an Altera Cyclone III FPGA, which handles sequence control, ADC conversion, TCLK decoding, and timing. Communications and data handling are performed by a Rabbit Semiconductor RCM3209 module. The Rabbit module includes the microprocessor and Ethernet interface. New features include Ethernet communications,

advance triggering options, and background subtraction [41].

A new high-gain preamp has been designed to enable the existing SEMs to measure the low-intensity secondary beam [41]. The new preamp consists of two amplification stages. The first stage is a transimpedence amplifier with a gain of approximately 2×10^7 and an integration capacitor to slow down and widen the incoming pulse. The second stage reduces the DC offset of the first stage by a factor of about 100, then amplifies the remaining signal by about 100, with a low-pass roll-off of about 16 kHz. There is a DC blocking capacitor at the output of the amplifier to prevent any offset voltage of the amplifier from washing out our signal. The 1.5 kΩ resistance of the integrator in the scanner is accounted for in the gain equation (R_{INT} in Fig 7.77). After integration in the scanner, the integrator output can be amplified by another factor of 10 or 100 if necessary.

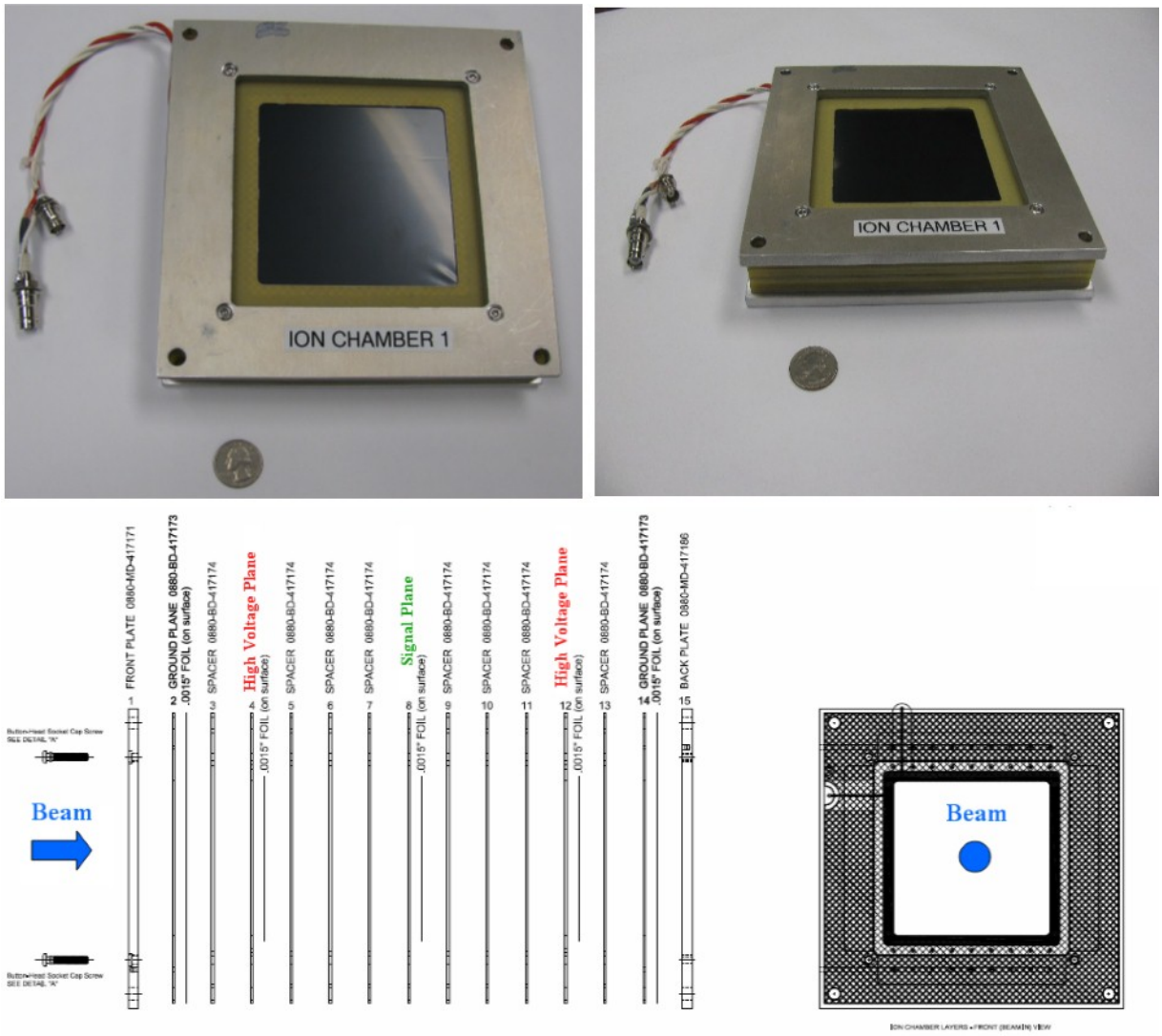

Figure 7.73: Finished ion chamber assembly (top). Ion Chamber layout (bottom). Ion Chamber assembly is made up of a single signal plane sandwiched between two high voltage foils with a ground plane and end plate on each end.

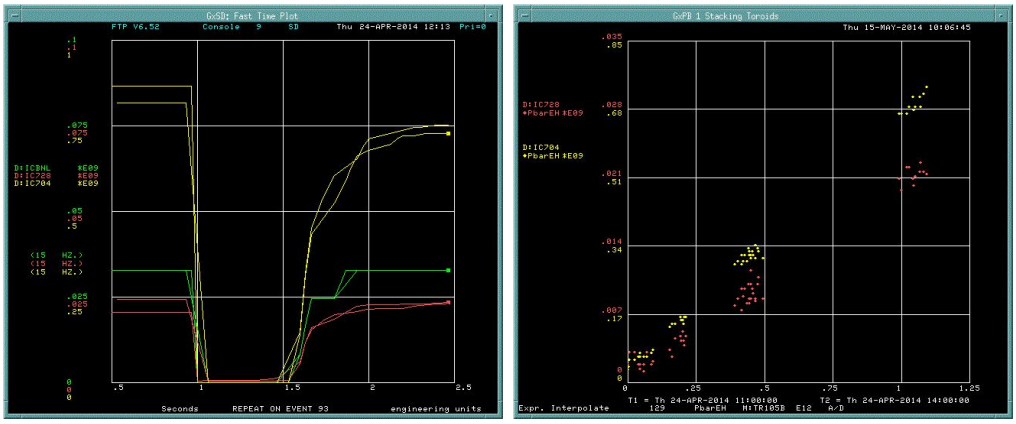

Figure 7.74: AP2 ion chamber performance was measured during beam studies. *(left)* Ion chamber integration over time. The signal is reset at 1.0 s and samples at beam time just after 1.5 s. The yellow trace is the intensity reported by the ion chamber at the 704 location and the red trace is that from the ion chamber at the 728 location. This plot was taken with 1×10^{12} protons on target and shows an intensity of 7.5×10^{8} particles at the 704 location and 2.5×10^{7} at the 728 location. *(right)* The output of the same two ion chambers over varied intensities of beam on target. The response is linear through a wide range of beam intensities.

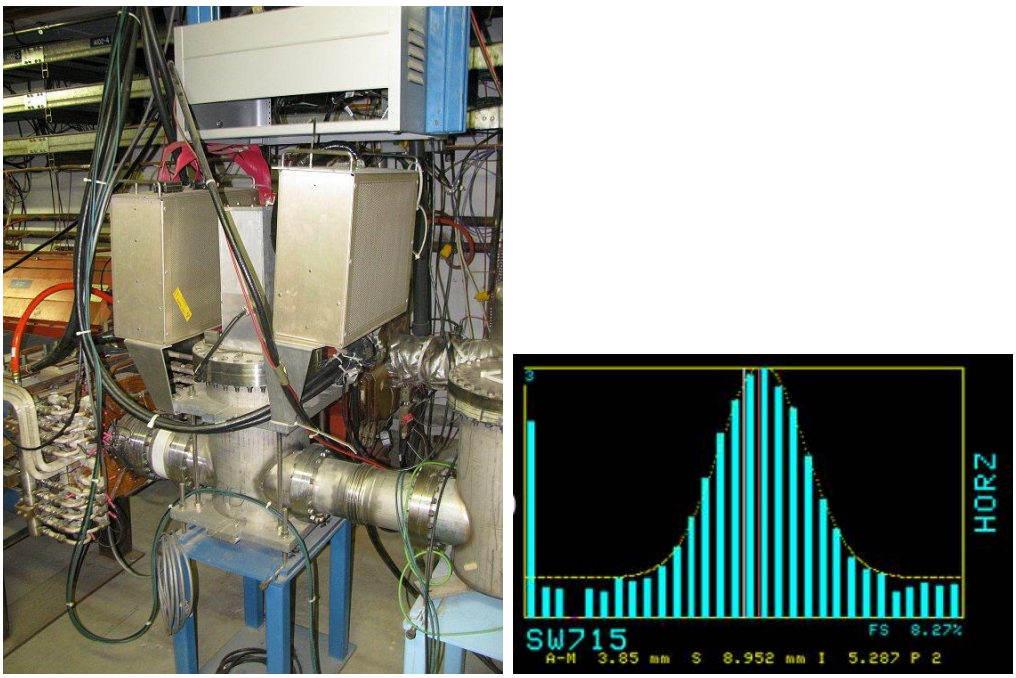

Figure 7.75: SEMs will be used to measure mixed secondary beam profiles. SEM tunnel hardware (left) is pictured. Preamp boxes are mounted next to the vacuum can. The SEM wires can be pulled out of the beam when not in use. SEMs can be used to measure beam profiles, positions and intensities (right).

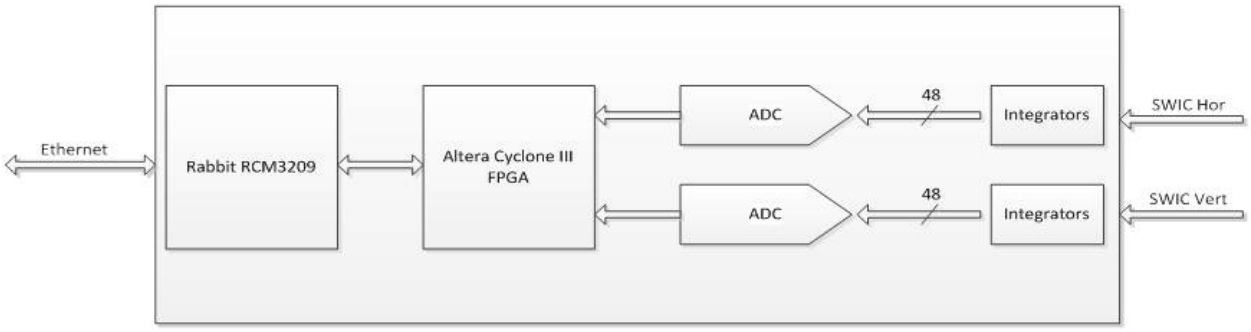

Figure 7.76: Scanner block diagram [41].

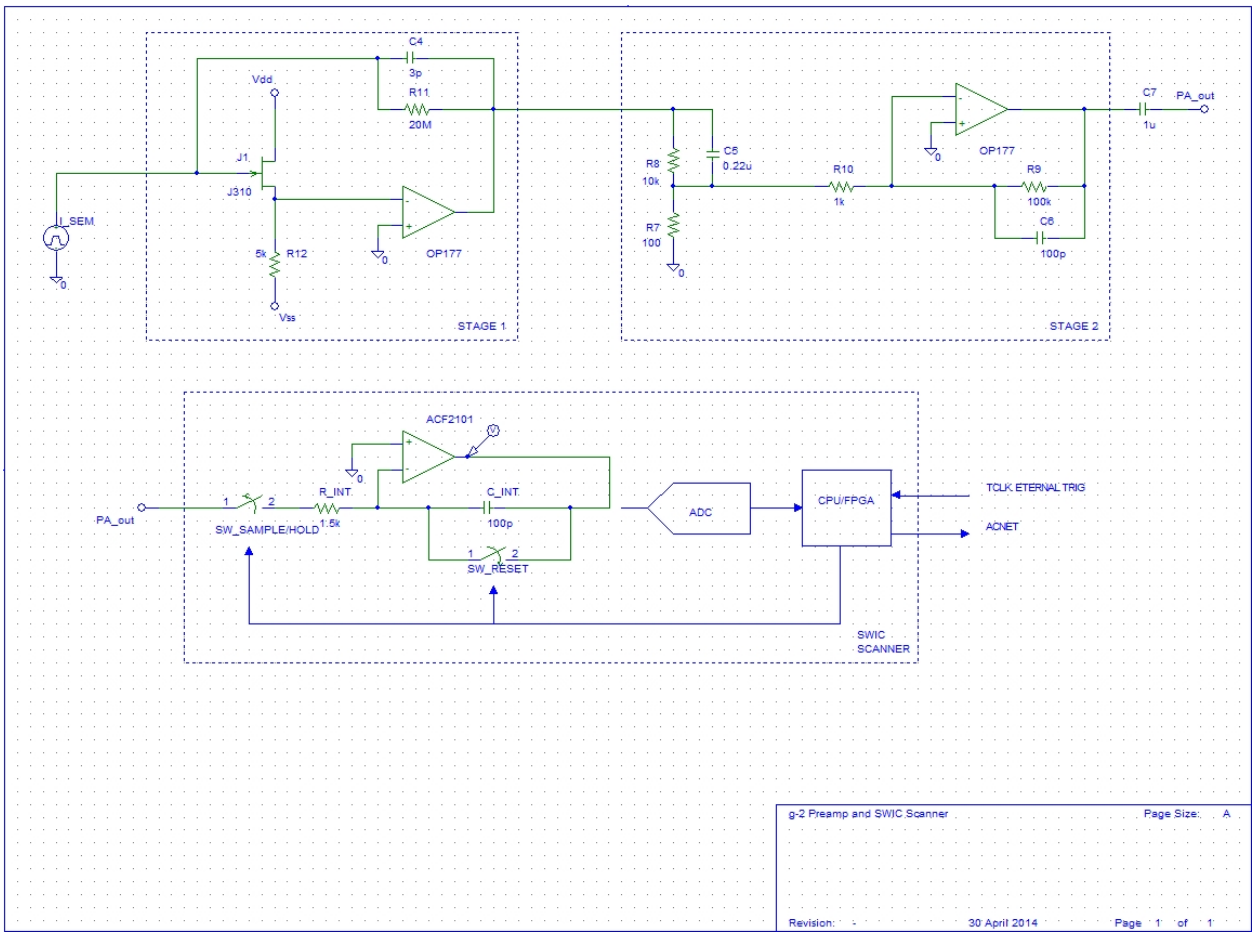

Figure 7.77: Profile monitor preamp design [41].

Prototype high-gain preamps were tested during beam studies in the AP2 line with 8-GeV beam on target and 3.1-GeV secondary beam with positive charge. Beam intensities were varied through the range expected for $(g-2)$ operations. Figure 7.78 shows SEM profiles at two locations in the AP2 line using the new high-gain preamps with the nominal $(g-2)$ intensity of 10^{12} protons on target.

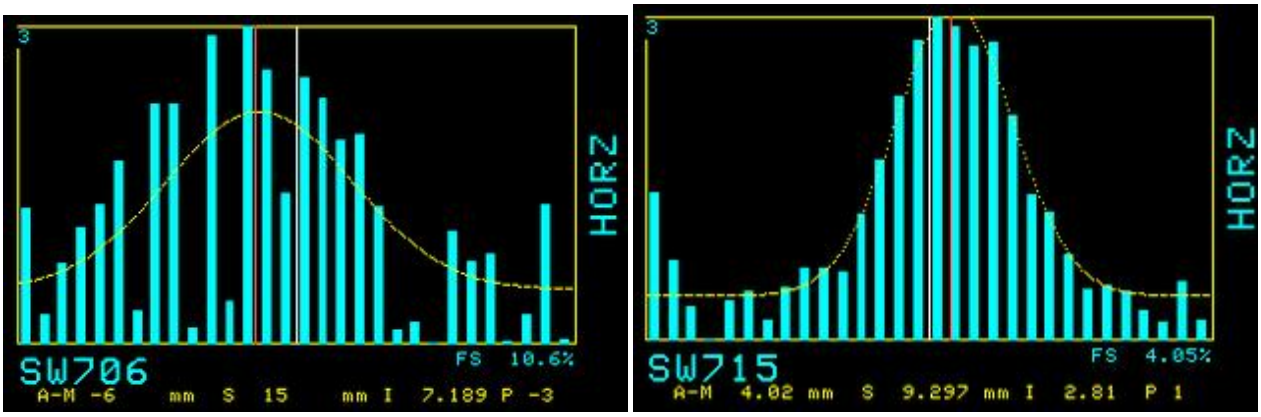

Figure 7.78: Demonstration that SEM wire profiles can be obtained at $(g-2)$ operational intensities and energies. Shown are profiles of low-intensity secondary beam collected with 10^{12} protons on target and an intensity of 10^9 mixed secondary beam as measured by the ion chamber at the 704 location. The SEM at the 706 location has some bad wires which will be repaired during maintenance periods.

Figure 7.79 shows profiles with 10^{11} protons on target so that intensity at the 706 location approximates that expected at the end of the M3 line during $(g-2)$ operations in order to test the range of the SEM high-gain preamp.

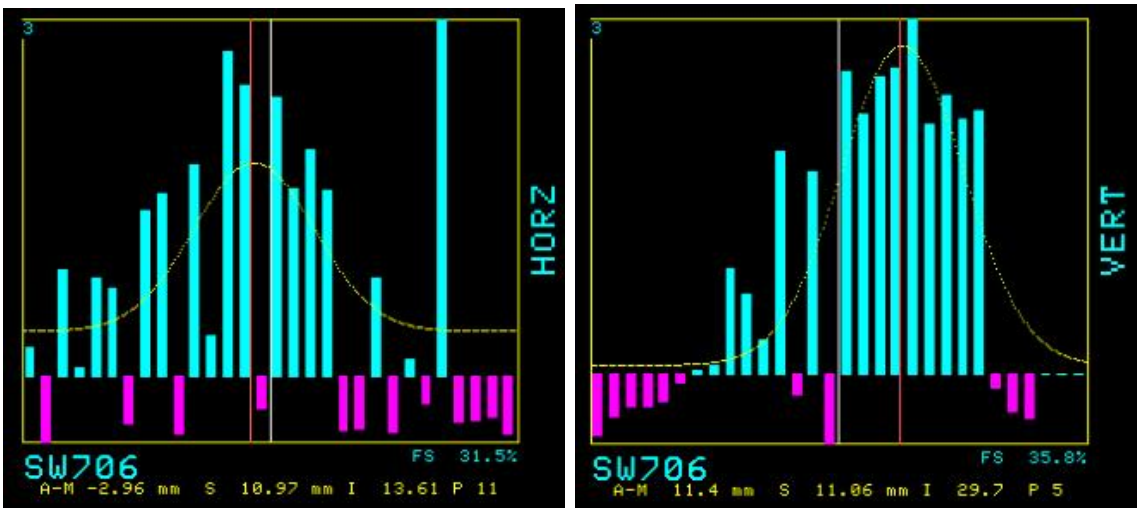

Figure 7.79: Profiles are still visible on SEM706 with 10^{11} protons on target and an intensity of 5×10^7 mixed secondary beam as measured by the ion chamber at the 704 location.

Large pulse-to-pulse noise variation was observed with the AP2-line SEMs, so a third-

generation scanner was tested during beam studies. This scanner implements a hardware pulse-by-pulse background noise subtraction. For each beam cycle, the background noise is subtracted before the beam pulse arrives, and that signal is subtracted from a second sample taken at beam time. The results were very promising, giving us clean-looking profiles, as seen in Fig. 7.80.

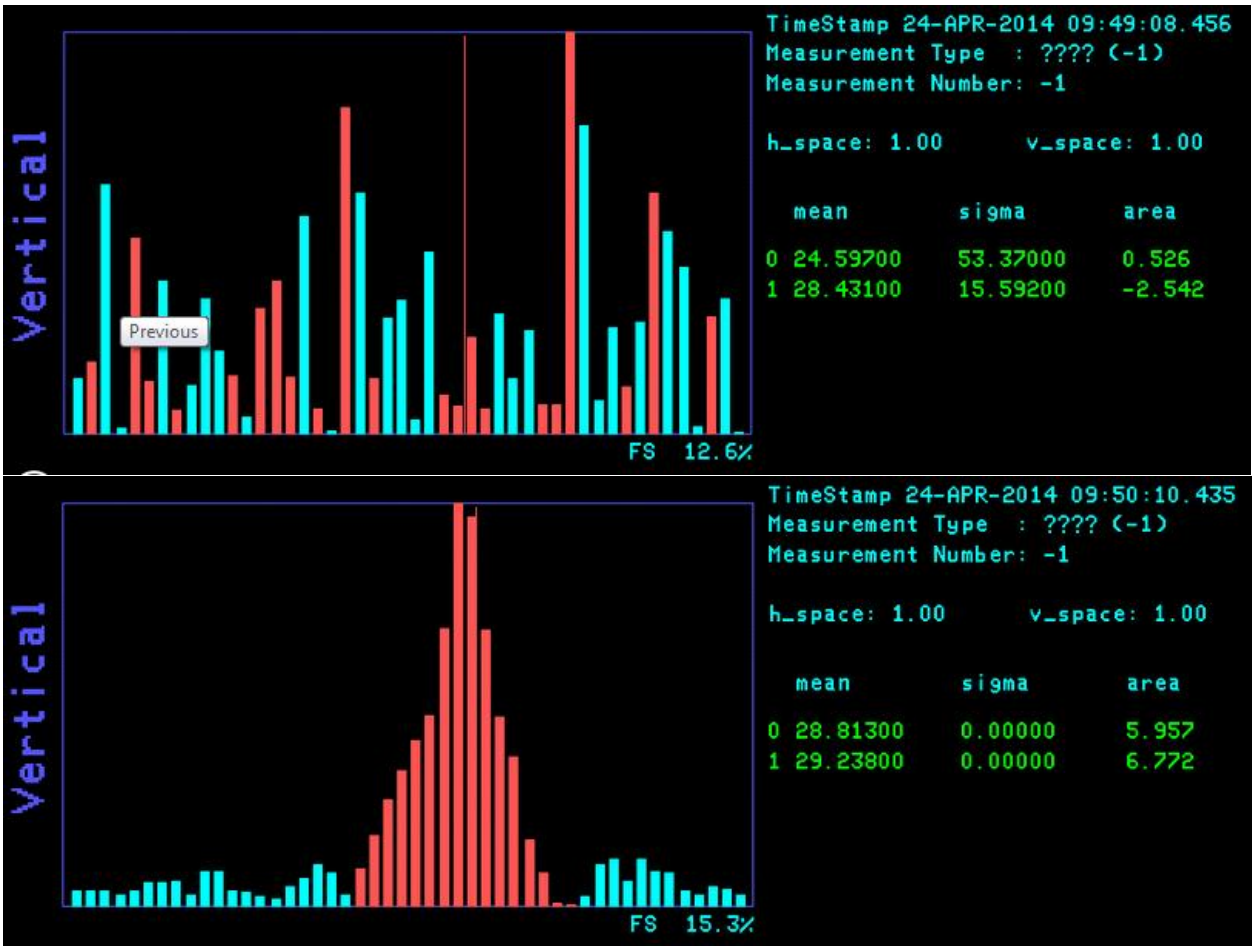

Figure 7.80: Wire profile at the 728 location for 10^{11} 120-GeV protons on target with 2.5×10^{8} low-intensity secondary beam measured using an ion chamber at at 728. The top plot is the noise sample and the bottom plot shows the results of subtracting the noise sample from the raw beam signal.

Beam Loss Monitors BLMs (Fig. 7.81) will be used to help maintain good transmission efficiency through the beamlines. Both Delivery-Ring and AP3 loss monitors will use the existing hardware and electronics for $(g-2)$ operations, but will be replaced for the higher-intensity Mu2e operations. The BLM design allows for switching back and forth between the two separate BLM systems with minimal effort.

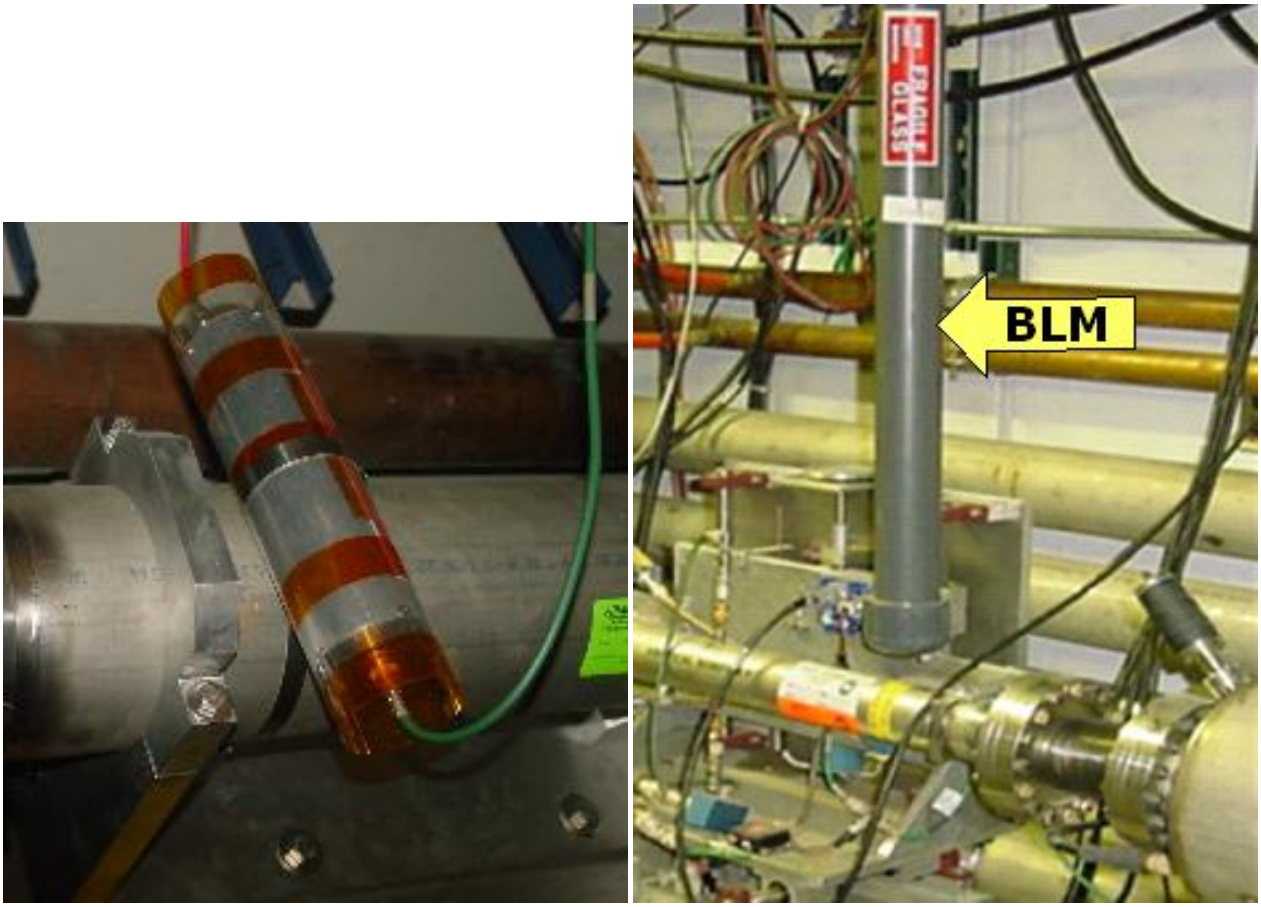

Figure 7.81: Two styles of BLMs will be used. Tevatron-style ion chamber loss monitors (left) will be used in areas of primary beam, and also in the Delivery Ring for Mu2e operations. The Pbar-style ion chamber, which consists of a plastic scintillator and a long light guide connected to a photomultiplier tube shielded from light in PVC, will be used in the Delivery Ring during $(g-2)$ operations.

The plastic-scintillator type BLM is sensitive to a small number of particles, making it ideal for Delivery Ring $(g-2)$ operations. The loss monitors are made up of a 4 in $\times$ 2 in $\times$ 1/2 in piece of plastic scintillator glued to a 36-in long Lucite light guide (see Fig. 7.82). At the end of the light guide, a small Lucite coupling attaches it to an RCA 4552 photomultiplier tube (PMT). The intent of the light guide is to keep the scintillator near the magnets but to extend the phototubes up and away from the region of beam loss. This assembly is mounted in a housing made up of PVC pipe and has feed-throughs for the high voltage and signal cables, as shown in Fig. 7.82.

The BLM output is processed through a series of three cards located in one or more

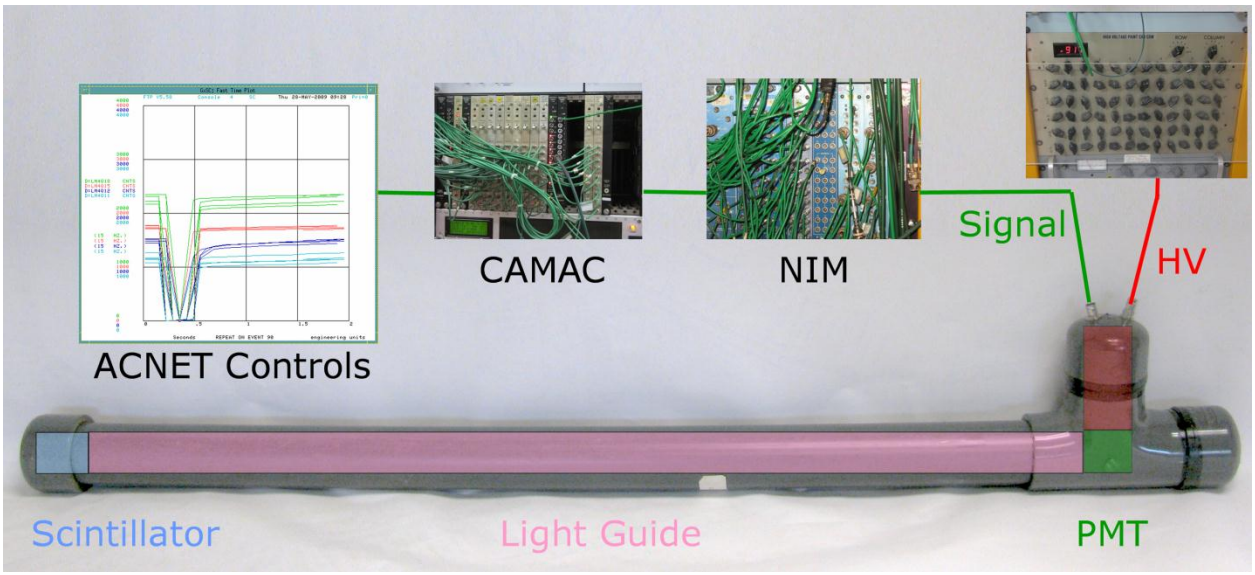

Figure 7.82: Delivery-Ring PMT BLM system.

NIM crates. Each service building has a single BLM rack to process loss signals for two sectors. The signals are passed from card to card via LIMO connections in the front panels of the cards. The BLM output first goes to an amplifier card, which handles twelve BLMs and amplifies each BLM signal by a factor of ~ 10. Each amplified signal is next sent to a quad or octal discriminator, which handles four or eight BLMs, respectively. This card levels the signal spike from the PMT caused by the lost particle and sends a NIM-level pulse to a Jorway quad scalar which handles four BLMs. The quad scalar is really a pulse counter that counts pulses during the gated period defined by the gate module. A CAMAC 377 card provides start, stop and clear times to the gate module for the gate pulse. Output from the Jorway quad scalar card is sent to the control system.

Mixed Secondaries Instrumentation Summary Table 7.16 summarizes the instrumentation installation locations in the M2 beamline, M3 beamline, and Delivery Ring.

Name	Device	Beam Line	Specific Location
SEM804	SEM	M2	Use existing SEM704 location
Tor804	Toroid	M2	Use existing Tor704 location
IC804	Ion Chamber	M2	Use existing IC704 location
SEM810	SEM	M2	Immediately downstream of Q811
SEM702	SEM	M3	Use existing SEM926 location
SEM703	SEM	M3	Immediately downstream of H703
SEM706	SEM	M3	Immediately downstream of Q706
SEM711	SEM	M3	Immediately downstream of Q711
SEM719	SEM	M3	Immediately downstream of Q719
SEM726	SEM	M3	Immediately downstream of Q725
SEM729	SEM	M3	Immediately downstream of Q730
SEM740	SEM	M3	Immediately downstream of Q740
IC740	Ion Chamber	M3	Immediately downstream of SEM740
SEM744	PWC	M3	Immediately downstream of Q744
SEM748	PWC	M3	Immediately downstream of Q749
SEM204	PWC	DR	Immediately upstream of ELAM
SEM302	PWC	DR	Immediately downstream of ISEP
IC209	Ion Chamber	DR	Immediately downstream of D2Q9
SEM607	PWC	DR	Use existing SEM607 location
SEM105	PWC	DR	Near D1Q5
IC102	Ion Chamber	DR	Immediately upstream of D1Q2
SEM403	PWC	DR	Use existing SEM403 location
SEM506	PWC	DR	Near D5Q6
WCM503	WCM	DR	Between D5Q3 and D5Q4. Use WCM until needed for Mu2e in M4 and then replace with ion chamber or another WCM.

Table 7.16: Mixed secondary beam instrumentation in the M2 beamline, M3 beamline, and Delivery Ring [42].

Proton Secondaries

Proton secondaries will extracted to the Delivery-Ring abort line and will have a similar beam intensity to that of the Delivery Ring. Instrumentation already located in that region will be used. A toroid will be used to measure beam intensity for Mu2e operations, but will be out of its operational range for $(g-2)$. Ion chambers, SEMs and BLMs will be used for $(g-2)$ in the same way they are for the mixed secondary lines.

Muon Secondaries

Muons will traverse the upstream portion of the M4 line and the M5 line. The largest technical challenge will be measuring the low-intensity muon beam, which models show should be on the order of 10^5 muons per pulse. This is two to three orders of magnitude smaller than the upstream mixed-secondary beam. Most of our standard diagnostics will not work at these beam intensities.

Ion Chambers Beam intensity will be measured with ion chambers as described in the ion chamber section above. This design will allow beam intensity measurements down to 10^5 particles. The ion chamber in the M4 line will need to be retractable in order to be compatible with Mu2e operations, while the M5-line ion chambers can be permanently in the beam path.

Proportional Wire Chambers Beam profiles in the upstream M4 and M5 beamlines will be measured using Proportional Wire Chambers (PWCs). Other proposed solutions, such as the BNL Segmented Wire Ion Chambers (SWICs), would have required design of vacuum bypass systems as well as permanent vacuum windows in the path of the beam that would create significant losses due to Coulomb scattering effects [40]. PWCs are more sensitive than SWICs, with the capability of measuring beam intensities down to the 10^3 particle range. When mounted inside refurbished Switchyard bayonet vacuum cans, the PWCs can be pulled out of the beam path when not in use. This eliminates the need for permanent vacuum windows and vacuum bypasses. A new design that will be used for the Switchyard beamlines was recently developed and provides the measuring capabilities needed to measure low-intensity muon-only beam for the $(g-2)$ experiment [43]. Using this existing design makes using PWCs even more cost effective.

The PWC has two planes of signal wires, one plane for horizontal and one for vertical. There are 48 signal wires in each plane which are 10-μm diameter gold-plated tungsten and can be configured with either 1 mm or 2 mm spacing. The wire planes are sandwiched between Aluminum high-voltage bias foils where negative voltage is applied. In addition to the bias foils, there are two more grounded foils on the outermost surfaces over the outer bias foils. These grounded foils balance the electrostatic field on the bias foil and prevent the bias foil from deflecting towards the sense wires. They also provide a degree of safety by covering the bias foils with a grounded conductive shield. Two end plates hold the entire assembly together. See Fig. 7.83 for a detailed view of the assembly.

The PWC assembly is filled with an 80% Argon and 20% Carbon Dioxide gas mixture. Ions are created when beam passes through the gas in the chamber. The positive ions are

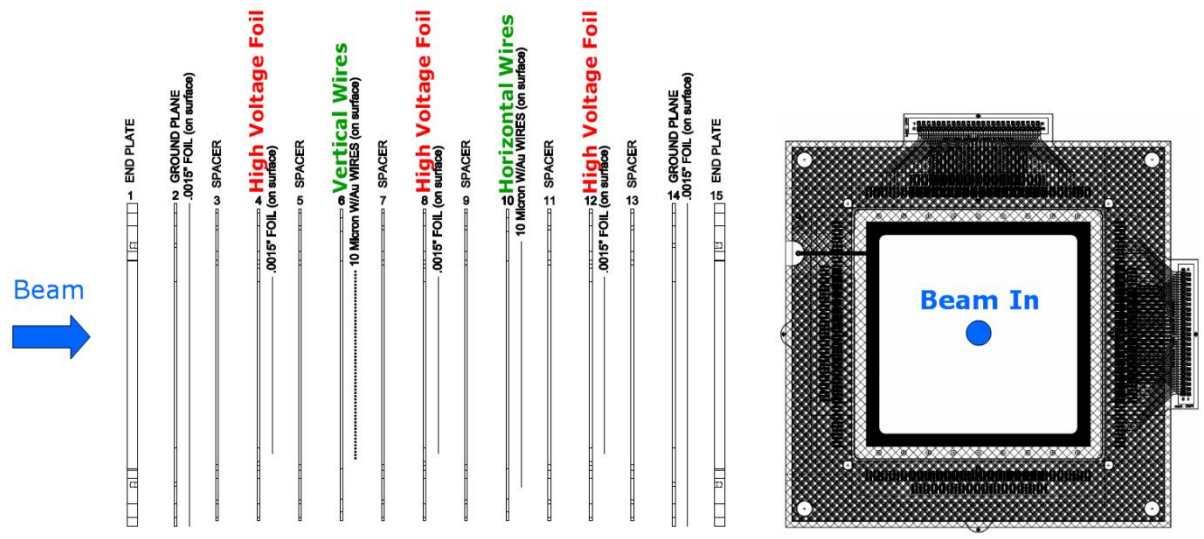

Figure 7.83: The Proportional Wire Chamber (PWC) assembly is made up of horizontal and vertical signal planes separated by high-voltage foils with a ground plane and end plate on each end. On the left is a side-view showing each layer of the assembly and on the right is a front (beam in) view showing the entire assembly.

drawn toward the negatively charged high voltage foils, where they are neutralized. The electrons are drawn toward the signal wires. As the electrons get within close proximity of the sense wires the electrostatic field around the wires causes the electrons to accelerate, creating an electron cascade in the gas. The collected negative charge on the wires is then processed by the same type scanner as is used for the SEMs.

As with the previously mentioned ion chambers, the gas filled PWCs must be isolated from beam tube vacuum. The PWCs will be packaged in an anti-vacuum box. The anti-vacuum box is a sturdy machined aluminum shell with a 0.003-in thick titanium foil window mounted on each side for the beam to pass through. The anti-vacuum box allows the detector to be mounted in a beamline vacuum chamber while the PWC inside the box remains at atmospheric pressure. A vacuum-tight duct attached to the box allows the gas tubing, signal and high-voltage cables to be routed from the PWC to outside the vacuum chamber.

In order to save engineering and assembly costs, the anti-vacuum boxes will be installed inside of bayonet vacuum vessels that are being repurposed from Switchyard. The bayonet-type drive slides the PWC linearly into and out of the beam with a screw drive system. Bayonet drives use a 72-RPM Superior Electric Slo-Syn AC synchronous stepping motor coupled directly to the screw shaft. The detector linear drive shaft is housed in a collapsible bellows that seals it from atmosphere. Figure 7.84 shows the PWC assembly, the anti-vacuum box, and the bayonet vacuum can. The same configuration is being used for the earlier-mentioned retractable ion chambers. In that case, the PWC assembly is modified to hold a single foil plane.

Figure 7.84: The first completed PWC prototype (top left). The signal connection is at the top and the high voltage connection comes out the left side. The PWC is installed in an anti-vacuum box (lower left). ArCO2 gas is pumped into this chamber, and there is a vacuum window on both front and back of this module. The anti-vacuum chamber is installed inside of the bayonet can (right) which is pumped down to beam tube vacuum. The PWC wires can be lowered into the beam or raised out of the beam via a motor drive.

Cerenkov Counter The BNL experiment E821 used a Cerenkov counter to measure the particle composition entering the $(g-2)$ ring. The detector was used to distinguish the relative particle compositions of $\pi+$, $e+$, and $\mu+$, but could not be used to measure protons [44].

The E821 Cerenkov detector was shipped to FNAL in 2012. The tank was refurbished and brought up to current ESH&Q standards [45] before being installed in the AP2 beamline for studies in 2014 (Fig. 7.85). The flammable isobutane gas was replaced by nonflammable Octafluorotetrahydrofuran (C_4F_8O), which simplified ESH&Q requirements. C_4F_8O has been used in other Cerenkov detectors at FNAL, and calculations showed that the Cerenkov light angle θ_c and pressure thresholds were compatible with repeating the E821 particle composition measurements in the AP2 line [2].

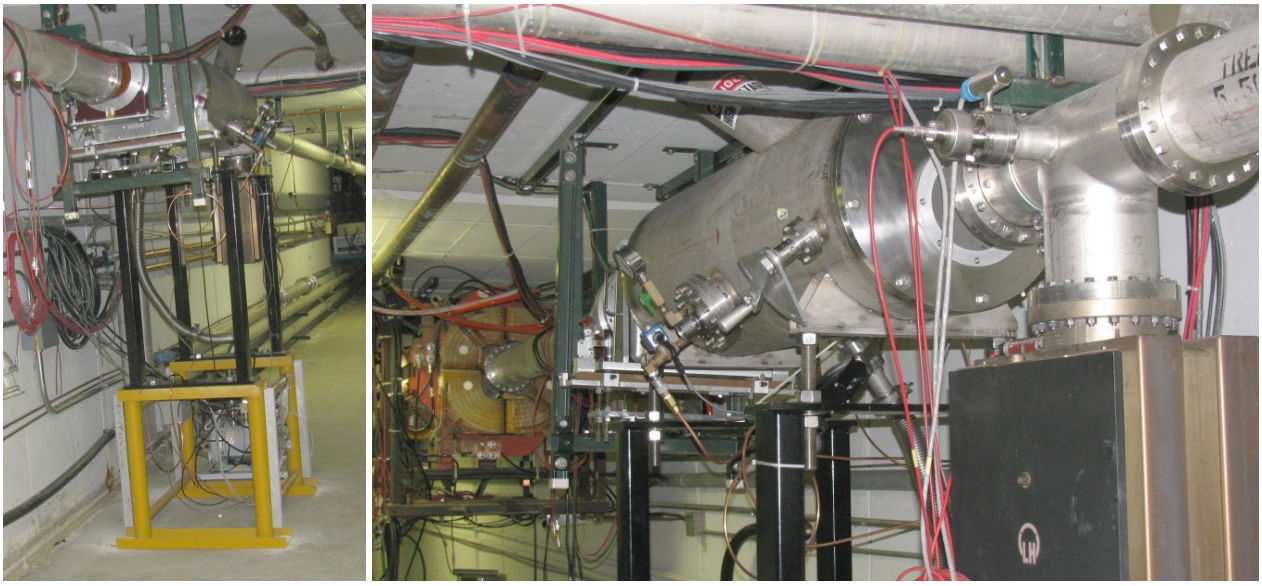

Figure 7.85: Cerenkov detector installed in the AP2 line.

A new controls system interface was designed and is shown in Fig. 7.86 [46], [2]. An Automation Direct DL405 series Programmable Logic Controller (PLC) in the AP50 service building handles most of the control and monitoring for the Cerenkov detector. The PLC has input and output capability for 24 VDC signals, relay contacts, and 0-10 V analog signals used by the pump cart and valves.

Monitoring and controls are through ACNET, with status bits for pumps and valves, analog readings for turbo pump speed and tank pressure, and control bits for pumps, valves and the test LED. The gate valve connects the pumps to the chamber. The solenoid valve allows the introduction of gas to the chamber. PLC logic prevents the gate valve from moving from the closed position to the open position if the turbo pump speed is above 10% in order to prevent damage to the turbo if there is gas in the chamber.

A small additional microcontroller board is used to communicate over a serial link with the Setra chamber pressure gauge. The microcontroller queries the gauge once per second, parses the response and writes the value into the PLC memory for presentation to ACNET [46].

Data were collected from the Cerenkov detector during the spring 2014 beam studies.

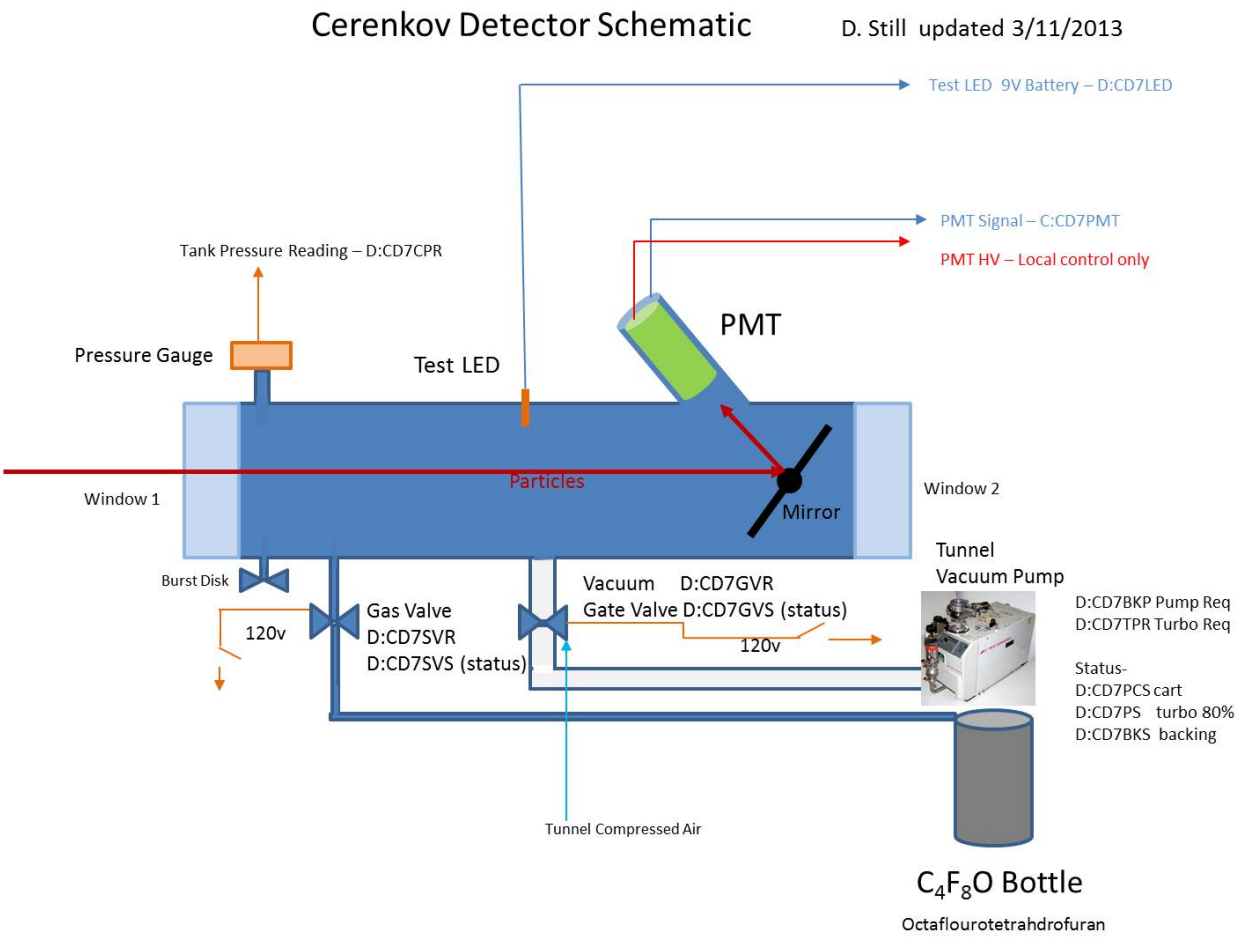

Figure 7.86: Cerenkov detector schematic showing basic PLC controls [2]

Beamlines were configured with 8 GeV beam on target and 3.1 GeV positive secondary beam in the AP2 line. Figure 7.87 shows the results of these studies with pulses of 2.7×10^{12} protons on target. The intensity of secondary beam in the upstream AP2 line was approximately 2×10^9, while the beam intensity in the downstream portion of the line near the Cerenkov detector was approximately 6×10^7. Detector response was measured as the gas pressure was slowly raised to about 14 psi and again as gas pressure was lowered. As expected, Fig. 7.87 shows three distinct slopes representing the positrons, muons and pions [2].

With the successful implementation of the Cerenkov Detector in the AP2 line, the next step will be to move the electronics and controls to the MC-1 service building and the detector to the M5 beamline for commissioning. The Cerenkov detector will be installed between Q023 and Q024 in the M5 line as shown in Fig. 7.88, and modifications will be made to the detector stand to match the beampipe elevation. The Cerenkov detector is a significant source of Compton scattering, so during normal $(g-2)$ operations, the detector and vacuum windows will be replaced with a spool piece.

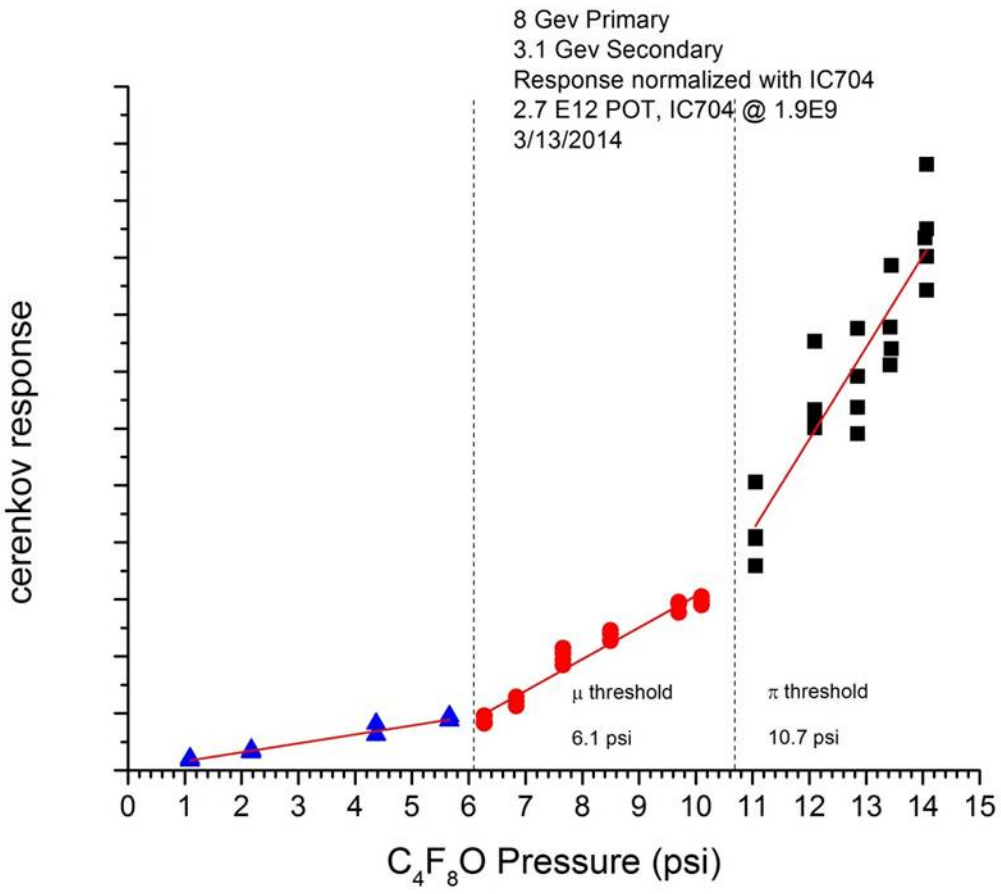

Figure 7.87: Cerenkov detector response (in arbitrary units) as a function of gas pressure. The three distinct slopes represent positrons, muons and pions [2].

Figure 7.88:

Muon Instrumentation Summary There will be one retractable ion chamber and two PWCs in the M4 beam line before the split. There will be an additional ion chamber and six PWCs in the M5 beam line. In addition, there will be a Cerenkov detector in the M5 line during beamline commissioning. Specific locations of these devices are outlined in Table 7.17.

Name	Device	Beam Line	Specific Location
PC900	PWC	M4	Immediately downstream of c-magnet
IC901	Ion Chamber	M4	Immediately upstream of Q902
PC903	PWC	M4	Immediately downstream of Q903
PC000	PWC	M5	Half-way between V907 and Q001
PC006	PWC	M5	Immediately upstream of H006
PC012	PWC	M5	Immediately downstream of H012
PC020	PWC	M5	Immediately downstream of Q020
CD024	Cerenkov	M5	Immediately upstream of Q024 (commissioning only)
PC026	PWC	M5	Immediately downstream of Q026
PC027	PWC	M5	Immediately downstream of Q027
IC027	Ion Chamber	M5	Immediately downstream of PWC027

Table 7.17: Muon beam instrumentation in the M4 and M5 beamlines [47].

Accelerator instrumentation summary

A summary of instrumentation devices which will potentially be used for $(g-2)$ is shown in Table 7.18.

Beamline	Beam type	Intensity	Position	Profile	Loss
Primary protons	P1, P2, M1	toroids	BPMs	multiwires, SEMs	BLMs
Mixed secondaries	M2, M3, DR	ion chambers	SEMs/PWCs	SEMs/PWCs	BLMs
Proton secondaries	DR abort	ion chambers	SEMs	SEMs	BLMs
Muons	M4, M5	ion chambers	PWCs		

Table 7.18: Instrumentation to be used in the beamlines for $(g-2)$ operations.

7.7 ES&H, Quality Assurance, Value Management, Risk

7.7.1 ES&H

The Accelerator Division ES&H Department has the responsibility for providing Environmental, Safety, and Health coordination and oversight of ES&H for all accelerator work on the project. As with all Fermilab projects, attention to ES&H concerns will be part of the project management, and Integrated Safety Management will be incorporated into all processes. Line management responsibility for ES&H will be maintained on this project. Safe coordination of installation activities will be accomplished through the Project Management team, Project ES&H Coordinator, Project Engineer, and Task Manager. During installation, the Subcontractors, T&M Crafts, and all Fermilab personnel will utilize Job Hazard Analyzes to plan all work and to mitigate hazards. The Project Manager and Project ES&H Coordinator will audit compliance with all applicable ES&H requirements.

The handling and installation of magnets, vacuum systems, power supplies, and other accelerator components are common tasks within the Accelerator Division, and standard safety practices will be used. If any work falls outside of common practices, job hazard analyses will be conducted in order to ensure that the tasks are performed safely. Detailed procedures exist for handling components in the radioactive target vault, and the activation will be lower after years of not running beam than it was during antiproton production.

7.7.2 Quality Assurance

All aspects of the accelerator work will be periodically reviewed with regard to Quality Assurance issues from Conceptual Design through completion. The following elements will be included in the design and construction effort: an identification of staff assigned to each task with clear definition of responsibility levels and limit of authority as well as delineated lines of communication for exchange of information; requirements for control of design criteria and criteria changes and recording of standards and codes used in the development of the criteria; periodic review of the design process, drawings, and specifications to insure compliance with accepted design criteria.

7.7.3 Value Management

Significant cost savings have been incorporated into the $(g-2)$ accelerator design by utilizing the existing infrastructure from the Antiproton Source. This includes 1 km of tunnel complete with electrical infrastructure, cable trays, a cooling water distribution system, and safety interlocks. Service buildings with HVAC, cooling water, controls communication infrastructure, extensive electrical infrastructure, electronics racks, access roads and parking lots are also already in place.

The existing Target Station and its components will be reused: target, lens, collimator, momentum-selection magnet, target vault, cooling systems, a "hot" work cell, and tunnel access points with overhead crane coverage. A new target-station dump to replace the current one which has an internal water leak will be constructed using the existing design.

As many existing components as possible will be reused for the beamlines, including approximately 250 Antiproton-Source magnets plus about 30 beamline magnets from the previous $(g-2)$ experiment at BNL. New magnets will be based on existing designs, where practical. Power supplies will also be repurposed where practical, although modern switch-mode power supplies will be purchased which have high efficiency and power factor near unity, which will save operating costs, and which are also smaller in size and save substantial building space.

Much of the beamline instrumentation will also be recycled, including Secondary Emission Monitors and Beam Loss Monitors, with upgraded readout electronics where necessary to see the low-intensity $(g-2)$ secondary beam.

7.7.4 Risk

The largest risks to the cost and schedule of the accelerator work are delays of funding and lack of engineering support when it is needed.

Another large risk depends on Mu2e shielding needs in the Delivery-Ring D30 straight section, which have not yet been fully determined. Shielding may need to be placed in areas which would obstruct current plans for reconfiguration of beamlines and cable trays. Magnets may need to be made radiation-hard.

The external beamline depends on a new tunnel enclosure being built under a General Plant Project. If that project is delayed or if construction costs rise, there may be a burden on $(g-2)$.

Conflicts and difficulty of work in the congested area of the D30 straight section and the M3 line which joins the DR in that area are a schedule risk on the order of a month or two.

There is also an opportunity that the M2/M3 crossover design may be simplified and be made to cost up to \$500k less.

Magnets which need to be built new and those which have been taken from the BNL beamline carry a risk on the order of \$200k.

The possibility that existing accelerator controls infrastructure is not able to support $(g-2)$ is low, but carries risks on the order of \$100-200k. The risk that various types of instrumentation cannot be refurbished or upgraded to see the low-intensity $(g-2)$ secondary beam would require new instrumentation to be built at a cost of roughly \$200-400k and a 4-month delay.

The biggest technical risk was that the lithium lens used for focusing secondaries off the target would not be able to pulse at the $(g-2)$ rate. However, a lens has been pulsed in a test stand at the average 12-Hz rate for 80 million pulses without any sign of lens failure, confirming ANSYS simulations which predicted that mechanical fatigue should be less than it was during antiproton production.

There is an opportunity to save \$100k if a new transformer will not be required in order to support the lens power supply.

The risk that the Target Station does not provide the desired yield may be handled by running the experiment for a longer period, or additional cooling may be needed for the final focus system, or a new target may be designed and constructed.

References

[1] W. Pellico *et al.*, "Proton Source Task Force Report", Beams-doc-3660 (2010); F. G. Garcia *et al.*, "Fermilab Proton Improvement Plan Design Handbook", Beams-doc-4053 (2012).

[2] D. Still *et al.*, "$g-2$ Yield Beam Study Results – April 2012", G2M-doc-430 (2012); D. Still *et al.*, g-2 Yield Beam Study Results, GM2-doc-1607, March 2014.

[3] I. Kourbanis, "Bunch Formation for $g-2$ experiment", G2M-doc-335 (2012).

[4] V. Tishchenko, "AP2 MARS Simulations and G4beamline for Beam Studies", G2M-doc-1885.

[5] Muons, Inc., http://www.muonsinc.com/muons3/G4beamline.

[6] N.V. Mokhov, "The Mars Code System User's Guide", Fermilab-FN-628 (1995); O.E. Krivosheev, N.V. Mokhov, "MARS Code Status", Proc. Monte Carlo 2000 Conf., p. 943, Lisbon, October 23-26, 2000; Fermilab-Conf-00/181 (2000); N.V. Mokhov, "Status of MARS Code", Fermilab-Conf-03/053 (2003); N.V. Mokhov, K.K. Gudima, C.C. James et al, "Recent Enhancements to the MARS15 Code", Fermilab-Conf-04/053 (2004); http://www-ap.fnal.gov/MARS/.

[7] ANSYS®, http://www.ansys.com.

[8] R. Shultz, "ANSYS Mechanical Simulation for Lithium Lens", Fermilab Doc GM2-doc-362.

[9] R. Schultz, "Estimate for Increasing $g-2$ Rep Rate due to NOVA not Running", G2M-doc-472 (2014).

[10] V. Tishchenko, "Update of Li-Lens Optimization", $g-2$ Doc 1789 (2014).

[11] B. Drendel *et al.*, "Antiproton Source Rookie Book", Beams-doc-2872, (2010).

[12] T. Leveling, "An Estimation of Antiproton Source Target Station Performance for Muon $g-2$", G2M-doc-536.

[13] K. Bourkland, "Lens and PMAG Power Supply Design", G2M-doc-1706 (2014).

[14] C. Hojvat *et al.*, "The Fermilab Tevatron I Project Target Station For Antiproton Production", Fermilab TM-1175 (1983).

[15] A. Leveling, "Pbar Target Vault Beam Dump Residual Activity", G2M-doc-1691 (2014).

[16] D.C. Carey, K.L. Brown, F. Rothacker, FERMILAB-Pub-98/310 (1998).

[17] J.P. Morgan and M. Xiao, "Details about the Design of the RR to P1 Stub Line", G2M-doc-484 (2012).

[18] V. Lebedev, "Modifications to g-2 Target System with Increased Production", G2M-doc-171 (2012).

[19] J.P. Morgan, "Delivery Ring Extraction Devices and Specifications", GM2-doc-1484 (2014).

[20] W. Morse, "Debuncher Lost Muon and Differential Decay Systematic Errors", G2M-doc-252 (2012).

[21] C. Johnstone and J.P. Morgan, "M4 and M5 Line Magnet Names, Currents and Lattice", GM2-doc-1568 (2014).

[22] W. Meng and K. Woodle, "Inflector Fringe Field Study on a Wire Model", BNL $(g-2)$ Note 195; "BNL Test Results on $g-2$ Superconducting Inflector Prototype", BNL $(g-2)$ Note 209; "Superconducting Shield Test on $g-2$ Inflector Prototype", BNL $(g-2)$ Note 210.

[23] C. Johnstone, "Injection into the $g-2$ Storage Ring", G2M-doc-1928 (2014).

[24] D. Rubin, "Beam Transport and Focusing into Storage Ring", GM2-doc-1575.

[25] BNL $(g-2)$ Note 76.

[26] J.P. Morgan, "Power Tests for Pbar Service Buildings", Mu2e-doc-2117 (2012).

[27] B. Drendel *et al.*, "Muon Campus Controls Costing", Mu2e-doc-1611 (2012).

[28] Controls Rookie Book, http://www-bdnew.fnal.gov/operations/rookie_books/Controls_V2.pdf (2009).

[29] Al Franck and G. Vogel, FNAL/AD, private communication.

[30] A. R. Franck *et al.*, "HOTLink Rack Monitor", FERMILAB-Conf-01/342/E.

[31] Brown, FNAL/AD, private communication.

[32] B. Drendel *et al.*, "Controls to Mu2e/g-2/Muon and Communications Duct Issues", Mu2e-doc-2069 (2012).

[33] B. Drendel *et al.*, "Muon Campus Controls Cost Overview", Beams-doc-4327 (2013).

[34] B. Drendel, "Muon Campus Controls Update Talk", Beams-doc-4422 (2013).

[35] R. Zifko, C. Worel, J. Anderson, FNAL/AD, private communication.

[36] S. Hawke, FNAL/ESH&Q, private communication.

[37] N. Larson, FNAL/BSS Telecommunications, private communication.

[38] T. Cunneen, FNAL/PPD, private communication.

[39] G. Tassotto, D. Schoo, FNAL/AD, private communication.

[40] B Drendel, "M5 Line Scattering Through BNL SWICs, Ion Chambers and Vacuum Windows", GM2-doc-1443 (2013).

[41] D. McArthur, FNAL/AD, private communication.

[42] J. Johnstone *et al.*, M2 and M3 Line Optics, Magnets, Instrumentation and Operating Currents, GM2-doc-1440 (2014).

[43] D. Schoo, "Fermilab Profile Monitor Systems", Internal Documentation (2010).

[44] R.M. Carey *et al.*, "The New $g-2$ Experiment: A Proposal to Measure the Muon Anomalous Magnetic Moment to ± 0.14 ppm Precision", GM2-doc-1, p. 75 (2010).

[45] Fermilab ES&H Manual, http://esh.fnal.gov/xms/ESHQ-Manuals/FESHM.

[46] D. Peterson, FNAL/AD, private communication.

[47] C. Johnstone *et al.*, M5 Line magnet names, currents and lattice, G2M-doc-1568 (2014).